The Effect of Decoupled Low-level Flow on Winter Orographic Clouds in Northern Colorado

by
Thomas Carl Peterson

Department of Atmospheric Science
Colorado State University
Fort Collins, Colorado

NSF ATM 8109590, 8704776, & 8813345

Colorado State University

Department of Atmospheric Science

Paper No. 442

THE EFFECT OF DECOUPLED LOW-LEVEL FLOW ON WINTER OROGRAPHIC CLOUDS IN NORTHERN COLORADO

By

Thomas Carl Peterson

This report was prepared with support provided by
National Science Foundation Grants ATM-8109590, ATM-8704776,
ATM-8813345, and the Colorado Experiment Station.

Department of Atmospheric Science
Colorado State University
Fort Collins, Colorado

May 1989

Atmospheric Science Paper No. 442

ABSTRACT

THE EFFECT OF DECOUPLED LOW-LEVEL FLOW ON WINTER OROGRAPHIC CLOUDS IN NORTHERN COLORADO

In stably stratified conditions, mountains often act as barriers to low-level flow creating regions of stagnant, decoupled flow. Since cloud conditions in winter orographic storms are directly related to lift over the cross section of the mountain barrier and a region of low-level decoupled flow is connected to the base of the mountain barrier, the question arises: does a region of stagnant, low-level decoupled flow affect the orographic cloud because it too may present a barrier that must be risen over?

Three different methodologies were used to examine this problem. The first method involved analysis of 1½ months of precipitation and wind data from a 24 station mesonetwork located in the Yampa River valley and surrounding mountains during the winter of '81-'82 as part of the third Colorado Orographic Seeding Experiment (COSE III). The second method was a case study analysis of two orographic storms using data from an instrumented cloud physics aircraft to supplement the data from the mesonetwork. The third method involved 2-D numerical simulations using Colorado State University's Regional Atmospheric Modelling System (RAMS).

The results indicate that the presence of extensive low-level decoupled flow does indeed cause part of the orographic lift of the mountain barrier to be experienced upstream of the barrier. This changes

the location of condensate production which in turn shifts precipitation upstream.

Thomas Carl Peterson
Atmospheric Science Department
Colorado State University
Fort Collins, CO 80523
Summer 1989

Acknowledgements

Many people generously contributed their aid and guidance to me during the course of this research. Here are some of the people I would like to publicly thank along with just some of the reasons I am grateful to them.

I would like to thank my advisor, Professor Lewis O. Grant, for his support and guidance; my co-advisor, Professor William R. Cotton, for his many specific helpful suggestions; Dr. David Rogers, for his day to day aid and advice; committee member Professor Graeme Stephens for his basic but insightful questions and advice on how to write a thesis; committee member Professor Paul Mielke for his strong and appreciated words of encouragement; Robert Rilling for his work in collecting and insuring the quality of the PROBE data; Paul DeMott for compiling and correcting aircraft data used in the case studies; Mike Meyers for his help with modeling; and Lucy McCall for drafting some of the figures.

Funding for this research was provided by National Science Foundation grants ATM-8109590, ATM-8704776, and ATM-8813345, and the Colorado Agricultural Experiment Station. Computations were performed at the National Center for Atmospheric Research. NCAR is supported by the National Science Foundation.

Table of Contents

1. Introduction

During winter orographic storms, the surface layer upwind of the barrier can flow up and over the barrier, it can be stagnant, it can flow parallel to the mountain barrier, or it can even flow back 180 degrees to the ridge top winds. Any time the low-level air is not flowing over the barrier with the synoptic scale winds, the low-level flow can be considered decoupled.

The physics involved in the creation of low-level decoupled flow can vary since the definition of low-level decoupled flow used in this research is strictly observational. For instance, low-level drainage flow may be created by radiative cooling of the surface air on the mountain sides which produces down valley flow. Or low-level blocked flow may be created when stably stratified oncoming flow cools as it experiences adiabatic ascent which creates a positive pressure perturbation and a negative pressure gradient directed upstream of the barrier which in turn produces down valley flow.

> "The blocking of low-level flow described above is likely to be an essential feature of flow in the vicinity of steep mountains. As such it would participate in virtually all other important orographic effects, including lee cyclogenesis, gravity wave generation and frontal distortion." Pierrehumbert and Wyman, 1985.

The research presented here examines what effect the extent of low-level decoupled flow has on the overlying winter orographic clouds. Three methods were used in this analysis. The first method examined precipitation and wind data from a mesonetwork to see how precipitation intensity and location varied with the length of decoupled flow. The

second method was a case study analysis that used data from an instrumented aircraft to examine cloud conditions over 2 very different degrees of low-level decoupled flow upwind of the barrier. The third method used numerical simulations of orographic clouds with conditions that produced two very different magnitudes of low-level decoupled flows.

The working hypothesis used during this research was that low-level decoupled flow acts as an extension of the mountain for purposes of orographic lift. Therefore, parcels of air moving towards the mountain will first have to rise over the layer of denser low-level decoupled flow -whether it is a large layer of decoupled flow or very small- before it rises over the mountain. Large extents of low-level decoupled flow would therefore cause parcel lift well upstream of the barrier which in turn would be reflected in condensate formation farther upstream from the barrier than would otherwise occur. The change in location of condensate formation would tend to shift precipitation upwind.

The results strongly support a modified version of this working hypothesis. A noticeable upstream shift in precipitation was found when the magnitude of low-level decoupled flow was large. Case study analysis indicated that parcel lift occurred well upstream of the barrier when the magnitude of low-level decoupled flow was large versus major lift right at the barrier when the extent of low-level decoupled flow was small. The numerical simulations exhibited these same features. In addition, the model results indicated that the region of lift was over the upwind edge of the low-level decoupled flow. However, this lift was not confined to a small area as if the region of low-level decoupled flow formed a solid extension of the mountain. Instead, the area of lift was large and

diffuse as the oncoming flow decelerated into the region of decoupled flow which resulted in convergence and vertical motion.

The shift in location of condensate formation should have a major effect on precipitation efficiency since it gives ice crystals a longer trajectory in which to grow and indeed the model results indicated significantly greater precipitation efficiency occurred when there was a large layer low-level decoupled flow than no decoupled flow. Therefore the length of decoupled flow could be an important criteria in determining the need for cloud seeding and in analyzing the effectiveness of cloud seeding. Furthermore, the understanding that the extent of low-level decoupled flow changes parcel trajectories over the same cross section of a mountain barrier may effect research on other orographic phenomena, such as lee wave activity, that are sensitive to parcel trajectories over mountain barriers and the pressure perturbations that alter parcel trajectories.

2. COSE III Topography and PROBE Stations

The data used in this research were collected during the third Colorado Orographic Seeding Experiment (COSE III) during the winter of 1981-82. COSE III was a large multipurpose experiment located near Steamboat Springs Colorado. The topography of the COSE III research area is shown in Figure 1. The four prime topographic features of this area are:

1. The Yampa River valley runs almost due west. This is readily apparent on Figure 1.

2. The valley sides increase in height towards the east. Figure 2 illustrates how the valley gets wider and the sides lower as it opens to the west.

3. The east end of the valley is blocked by the sharp rise of the Park Range which runs almost due north/south. The magnitude of the barrier is readily apparent in the averaged west/east cross section of the research area shown in Figure 3.

4. Also present in the valley are many smaller mountains and hills. Notable among these are Quarry Mountain southwest of Steamboat Springs and the ridges that form a constriction in the valley west of Milner, both visible in Figure 1. The extent and variety of the topographic variations are shown in Figure 4.

COSE III instrumentation included research aircraft, rawinsondes released upstream at Craig and down stream at Hebron (see Figure 1), and a mesonetwork called PROBE. The Portable Remote Observation Equipment

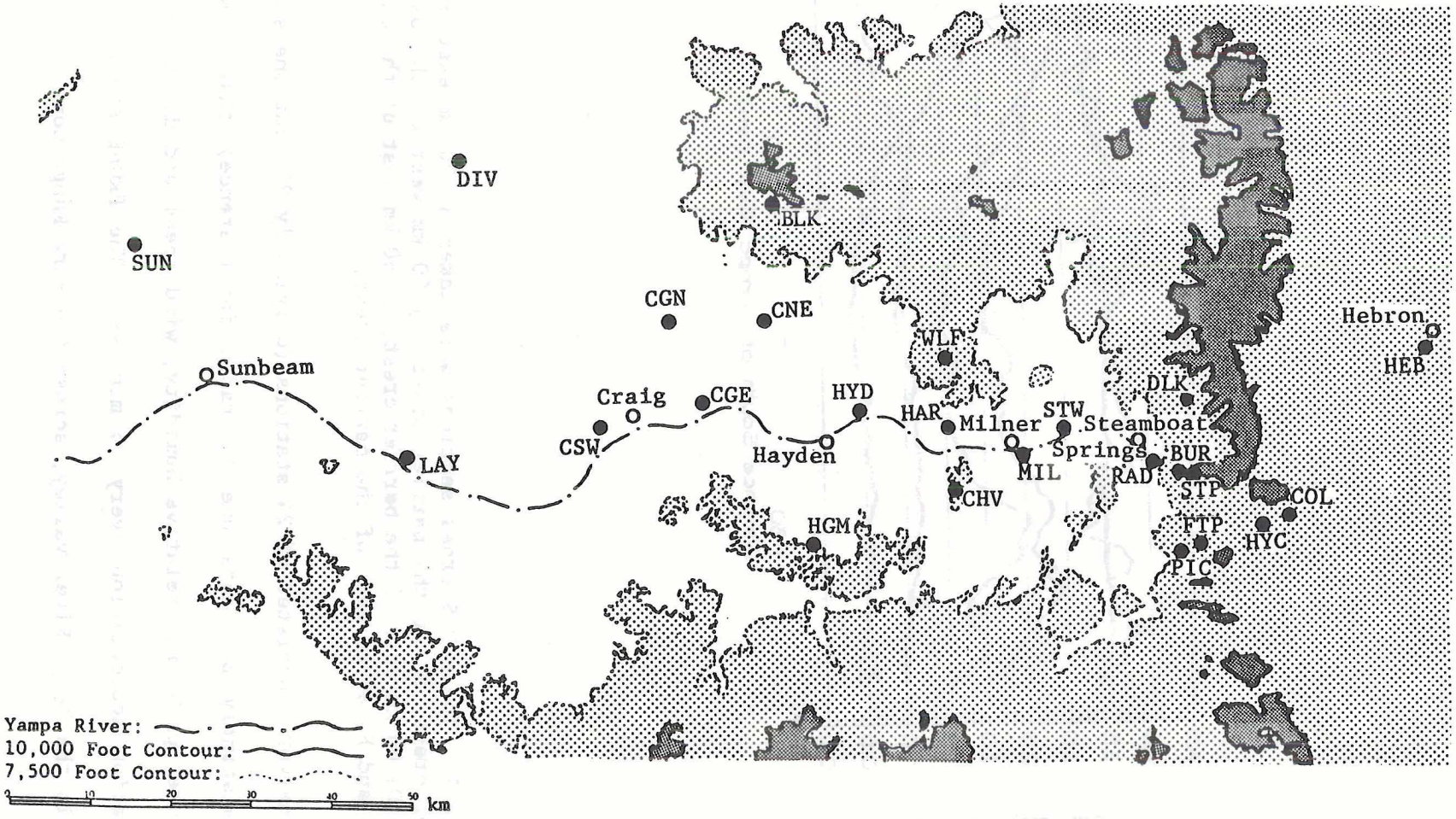

Figure 1. A map of the COSE III research area showing towns and PROBE station names and elevations. Lightly stippled area represents elevations between 7,500 feet and 10,000 feet MSL. Darker stippling represents elevations greater than 10,000 feet.

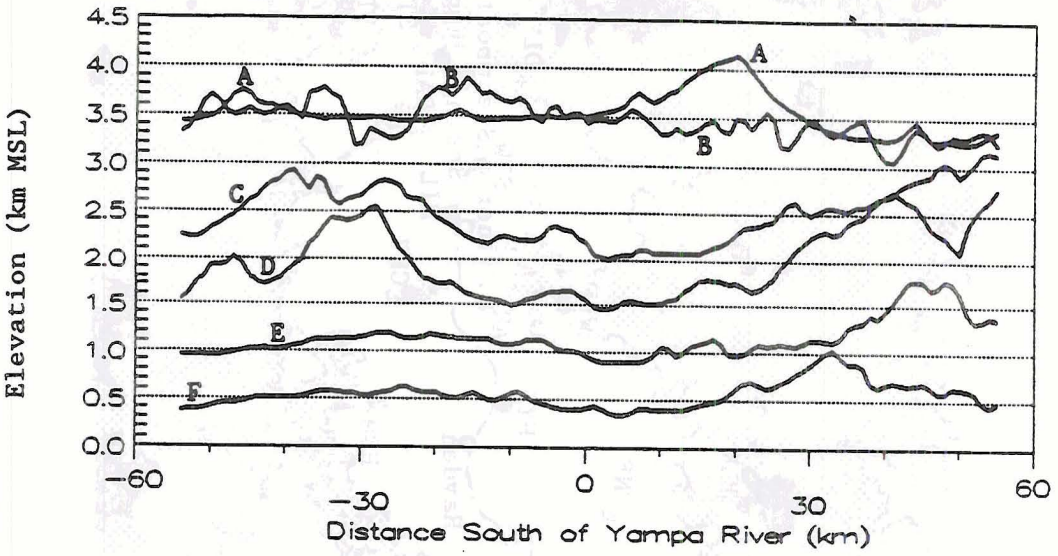

Figure 2. These N-S cross sections were taken A) 20 km east of the barrier crest, B) at the barrier crest, C) 20 km west of the barrier crest, D) 40 km west of the barrier crest, E) 60 km west of the barrier crest, and F) 80 km west of the barrier crest.

(PROBE) network consisted of 24 stations (originally 25, but one station had consistently bad data due to radio interference) that reported temperature, pressure, relative humidity, wind speed and direction, and precipitation accumulation every 15 minutes. The PROBE stations were located in the Yampa River valley, across the Park Range Continental

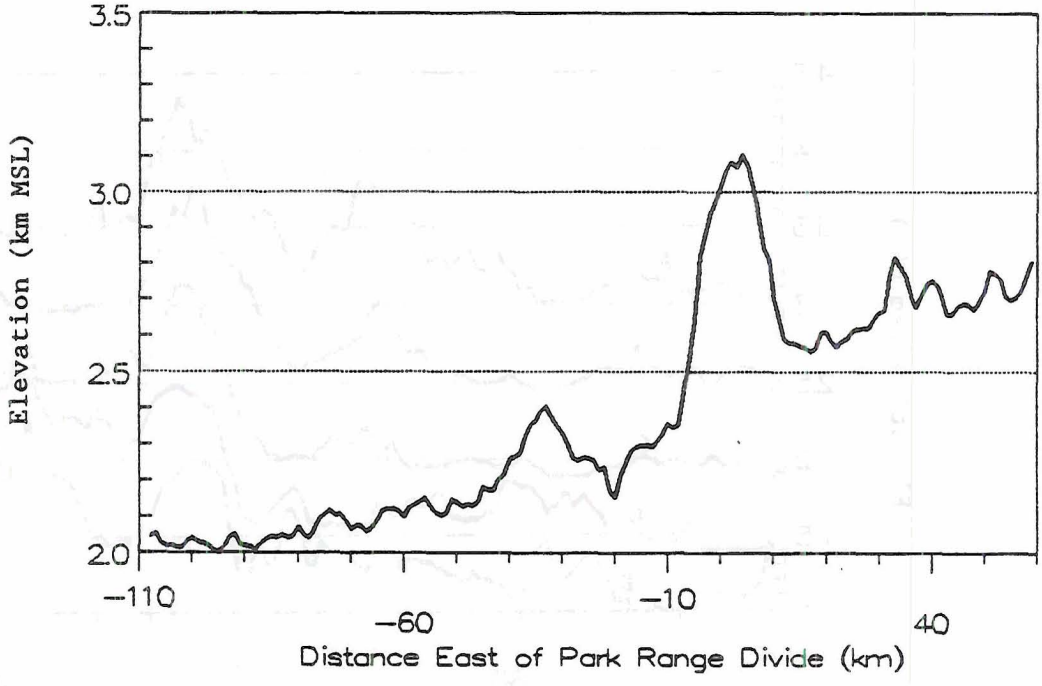

Figure 3. Average of 5 west-east cross sections taken along the Yampa River valley axis, 20 km north of the axis, 10 km north of the axis, 10 km south, and 20 km south of the Yampa River valley axis.

Divide and down the east side of the Park Range. They cover an area with an east/west length of 160 km and a north/south extent of about 50 km. The locations of PROBE stations are indicated in Figure 1. The PROBE stations covered a wide range of elevations, as indicated in Figure 5 which displays the PROBE station elevations. Figure 6 is a west/east cross section that shows the location of the PROBE stations in relation to the valley floor (Yampa River) elevation.

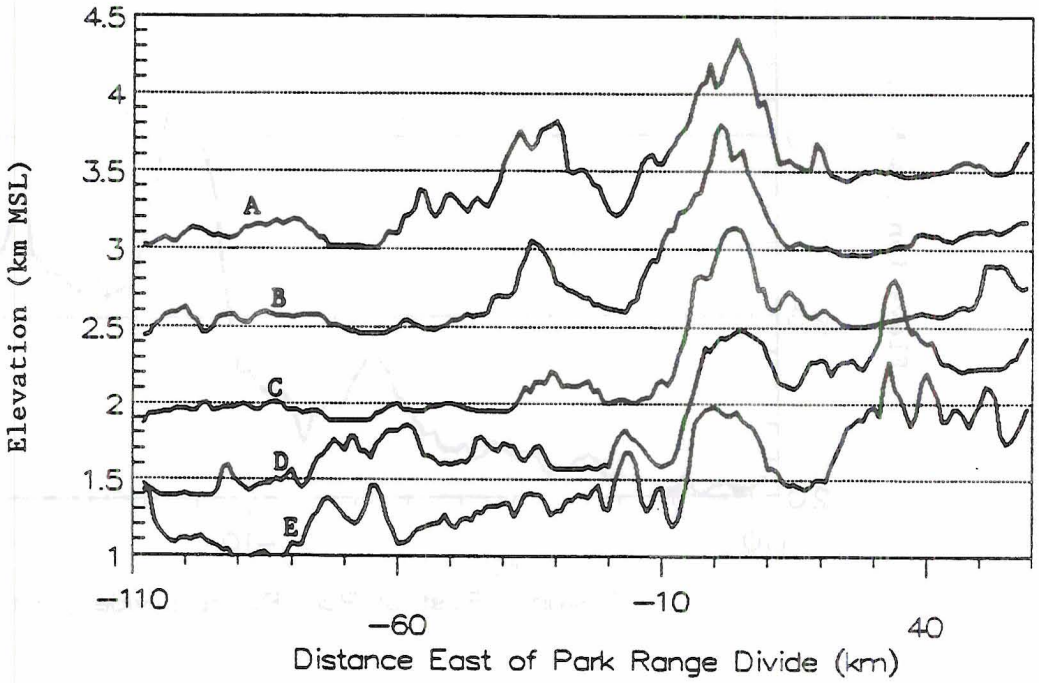

Figure 4. A) 20 km north of the Yampa River valley axis and displayed offset +1.0 km, B) 10 km north and offset +0.5 km, C) along the valley axis with no offset, D) 10 km south and offset -0.5 km, E) 20 km south and displayed with a -1.0 km offset.

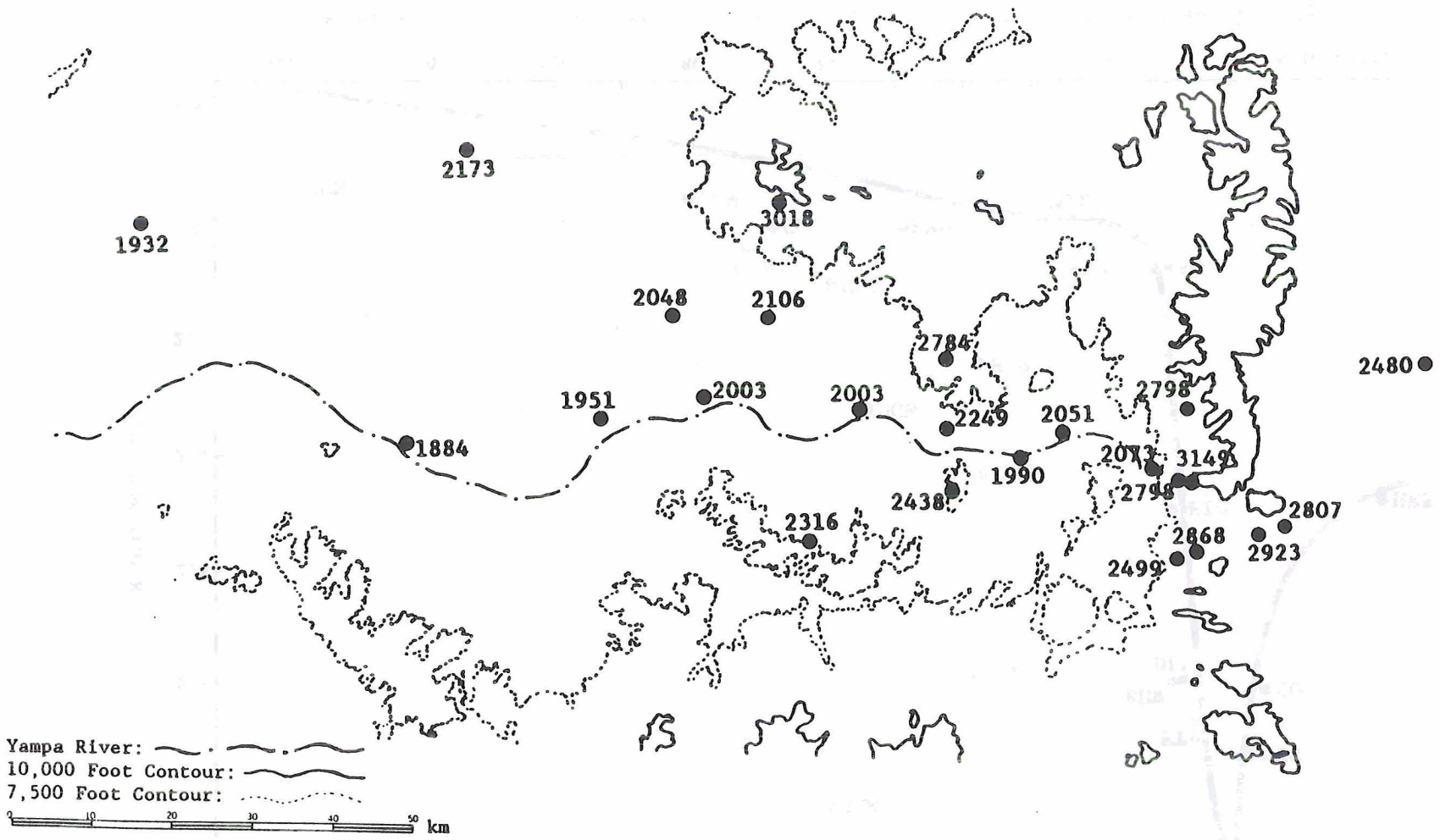

Figure 5. A map of the COSE III research area showing the PROBE station elevations in meters.

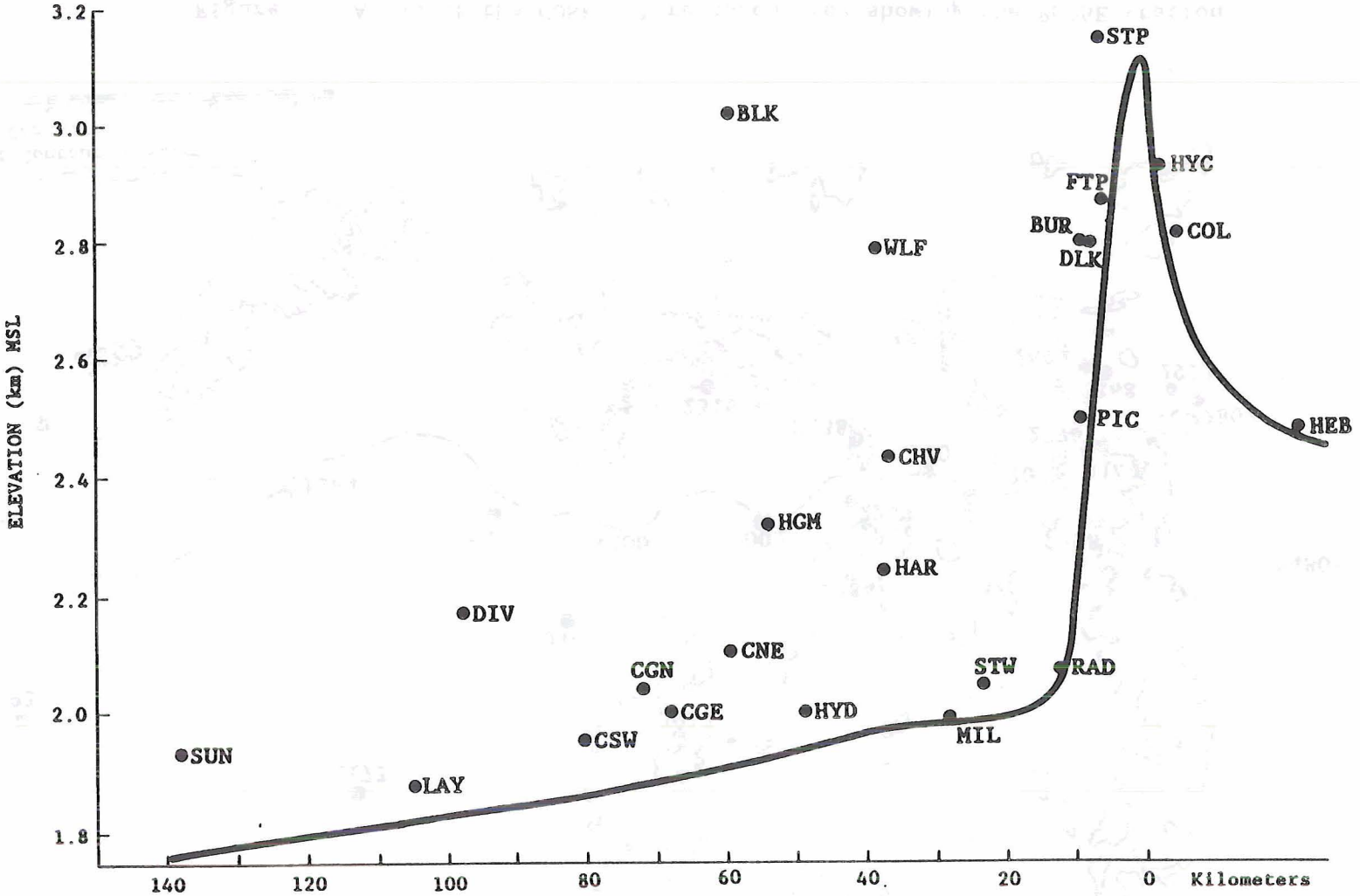

Figure 6. West-east cross section of the COSE III research area showing the name and location of PROBE stations in relation to the Yampa River valley floor elevation.

3. Variations in Precipitation with Extent of Decoupled Flow

3.1. Introduction

The one cloud physics parameter recorded at all 24 PROBE stations 24 hours a day was precipitation. Utilizing this data source to examine the effect of low-level decoupled flow on the overlying cloud, this section will present the results of an investigation of precipitation intensity and location and how they vary depending on the magnitude of low-level decoupled flow. This analysis takes a climatological approach by analyzing all the good PROBE data collected during the winter of '81-'82.

Other researchers have indicated that there are changes in precipitation intensity and location due to different degrees of decoupled flow, but they don't agree on what the changes are. Grossman and Durran, 1984, indicate that low-level blocking upstream of the Western Ghat mountains in India causes rising of moist air over the ocean resulting in convection well upstream of the barrier. Marwitz, 1980, and Lee, 1981, interpret the effect of low-level blocking quite differently. They suggest that upstream blocking acts to decrease the effective height of the barrier. Decreasing the effective height of the barrier could decrease the precipitation.

3.2. Methods

3.2.1. Synoptic Scale Winds

The dominant synoptic scale winds during the two months of COSE III were westerlies. Eighty-seven soundings were taken during COSE III,

mostly during storm periods. All but one of these soundings showed westerlies above 700 hPa. The sounding taken west of the barrier at Craig on January 29, 1982 at 1800 GMT showed light winds from the northeast from ridge-top height to a height of 8 km above ground level. Since this occasion of easterly synoptic flow is completely different than the bulk of the data, this event is excluded from this analysis. Therefore, the results will pertain only to the more common events with synoptic scale westerlies.

3.2.2. Low-level Decoupled Flow

3.2.2.1. Definition of Decoupled Flow

For purposes of this research, low-level decoupled flow is a term applied to air below mountain top level which is not moving up and across the barrier with the synoptic scale flow. This includes low-level flow which turns parallel with the barrier. It includes cold pooling and down valley drainage flow. And it includes low-level air which becomes stagnant upstream of the barrier due to an inversion layer. Basically, the definition of low-level decoupled flow used here does not depend on the source of the low-level air, only its destination: namely that it is not flowing over the barrier with the synoptic scale winds.

3.2.2.2. Identifying Low-Level Decoupled Flow

If the low-level flow is not directed over the barrier with the synoptic scale winds, it must be decoupled from the synoptic scale winds. However, to be accurate in determing what could be considered decoupled flow, the data set would have to include hourly soundings to determine when the flow is decoupled. Such data is not available for COSE III.

However, a threshold value for the cross-barrier component of the wind could be chosen to discriminate the decoupled flow.

Lee (1981) uses the value of 2.0 ms^{-1} for the cross-barrier component to be the cutoff point for decoupled flow and Graw (1988) uses 1.0 ms^{-1} for the threshold. Clearly if the synoptic scale winds are strong, there can be a positive cross-barrier component of surface flow even when the surface winds are effectively decoupled. But if the synoptic winds are weak, a high threshold value may inappropriately describe the low-level flow as decoupled flow.

Rather than confront this problem directly, a somewhat different approach has been used in this study. First the Yampa Valley was divided into nine different sections, eight of these corresponding to a section east of the eight valley floor PROBE stations with the ninth farther west than the westernmost PROBE station. Then values of the cross-barrier wind component that could best divide the observed cases into meaningful sized groups were sought. For example, if the value for determining whether decoupled flow extends past a given station puts 40% of the hours into one of the nine divisions and gives three of the divisions only one or two percent of the hours, the information would not provide much resolution. The 40% case would blur the finer details together and the one and two percent cases would allow single event anomalies to distort the results.

It was discovered that since the valley floor PROBE stations varied considerably in their individual exposure to winds from the west, one value for all stations did not divide the data set very well. So taking the varied individual locations into account, a different threshold value was chosen for the u-wind (cross-barrier) component at each of the eight

valley floor stations. A value was sought that would cut off another 10-11% of the data set, and as shown in Table 1, the required u-wind value varied considerably. To indicate the need for a variable u-wind threshold

Table I

Station	U-Wind Threshold for Decoupled Flow in ms^{-1}
RAD	2.4
STW	3.2
MIL	1.4
HYD	2.9
CGE	1.0
CSW	1.6
LAY	0.3
SUN	0.1

for determing decoupled flow, Figure 7 shows a cross section of the COSE III research area with one particular example where the cross-barrier wind component varied considerably from station to station even in a region that clearly had decoupled low-level flow.

3.2.2.3. Processing the Data

For the climatological type analysis described in this chapter and the 2 following chapters, hourly PROBE data for the months of December 1981 and January 1982 were used. The reasons for limiting this analysis to two months of hourly data were practical ones. Bob Rilling, a former CSU graduate student, set up the PROBE mesonetwork, collected its data, and laboriously hand corrected the precipitation data on an hourly basis. Hence the limitation to hourly data. Though there are some PROBE data available for February, efforts towards data quality assurance for wind

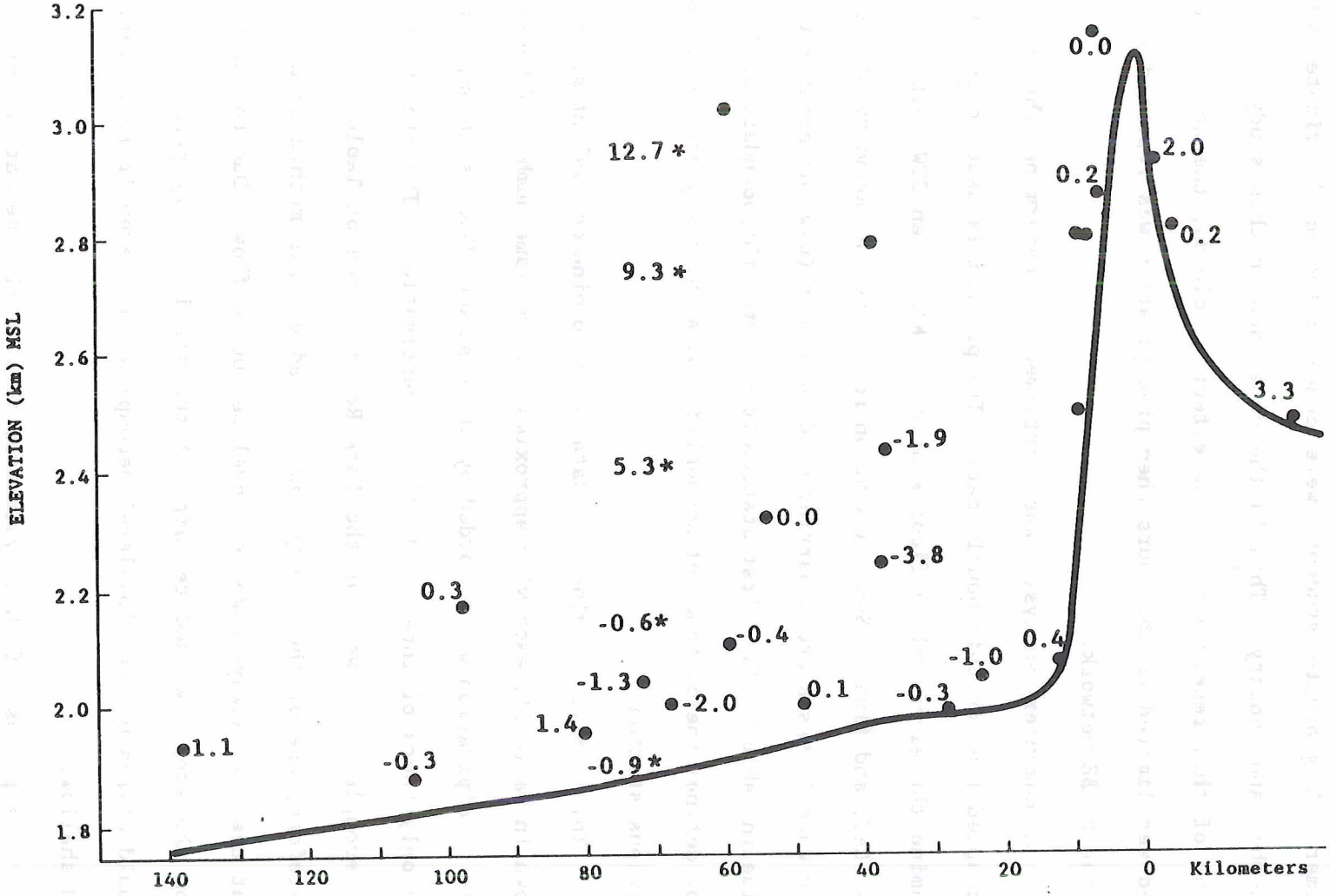

Figure 7. XZ cross section of COSE III research area with the cross-barrier wind component in m^{-1} recorded by PROBE stations (dots) and by a rawinsonde (stars) on January 5, 1982 15:00 GMT.

and other non-precipitation data by Bob Rilling and Richard Graw, another former CSU graduate student, were concentrated on 15 minute data for December and January. This is the data used in this study. Since the focus of this research is on the effect on clouds, the actual data set used was limited to the hours when precipitation was reported somewhere in the PROBE network.

A computer analysis was performed to determine the length of decoupled flow on this hourly data. The program is used to sequentially examine the eight valley floor stations: RAD, then STW, MIL, HYD, CGE, CSW, LAY, and finally SUN. A station registers the boundary of decoupled flow when it has a cross-barrier wind component (u-wind) greater than the value in Table I. The first station to register the boundary of decoupled flow defines the distance of decoupled flow as half way between it and the previous station.

This analysis divides the data set into nine equivalent sized groups shown in Table II, each with approximately the same number of hours where some precipitation was recorded by at least one PROBE station, which are the only hours of interest to this investigation. The minimum distance of decoupled flow west of the Park Range listed on Table II is 10 km. Therefore, one of the assumptions implied by this method of division is that there is always some low-level decoupled flow. Due to the friction from the steep, wooded terrain, if the air is stably stratified, there should always be some low-level decoupled flow, even if it is very small and shallow.

The purpose of this system was to stratify the data according to a decoupled flow related parameter, not to exactly represent the distance

Table II

Decoupled Flow Divisions

Extent of blocked flow Station	km	Number of hours with Precipitation	Percent
<RAD	10	79	11.2
>RAD & <STW	18	80	11.3
>STW & <MIL	26	78	11.0
>MIL & <HYD	38	77	10.9
>HYD & <CGE	58	80	11.3
>CGE & <CSW	74	77	10.9
>CSW & <LAY	92	79	11.2
>LAY & <SUN	120	74	10.5
>SUN	140	83	11.7
TOTAL		707	100.0

a tongue of low-level decoupled air extends west of the Park Range. Yet the system of division used does both very well. Over 60 comparisons were made between where a meteorological analyst would mark the length of decoupled flow on plots of the entire PROBE wind field and the computer program's calculated extent of decoupled flow, and the two agree very well. Figures 8 through 16 provide examples of wind fields and the magnitude of decoupled flow as determined by this computer program.

Figure 11 shows the length of low-level decoupled flow just to the west of a fairly strong upvalley wind 1½ barb from Station HAR located near the center of the valley. HAR is situated 275 meters above the valley floor, though it is very near the center of the valley. Stations such as HAR provide an opportunity to examine the depth of low-level decoupled flow. The cross-barrier wind component at three elevated stations, CNE which was 200 meters above the valley floor, HAR which was 275 meters above the valley floor, and CHV which was 450 meters above the

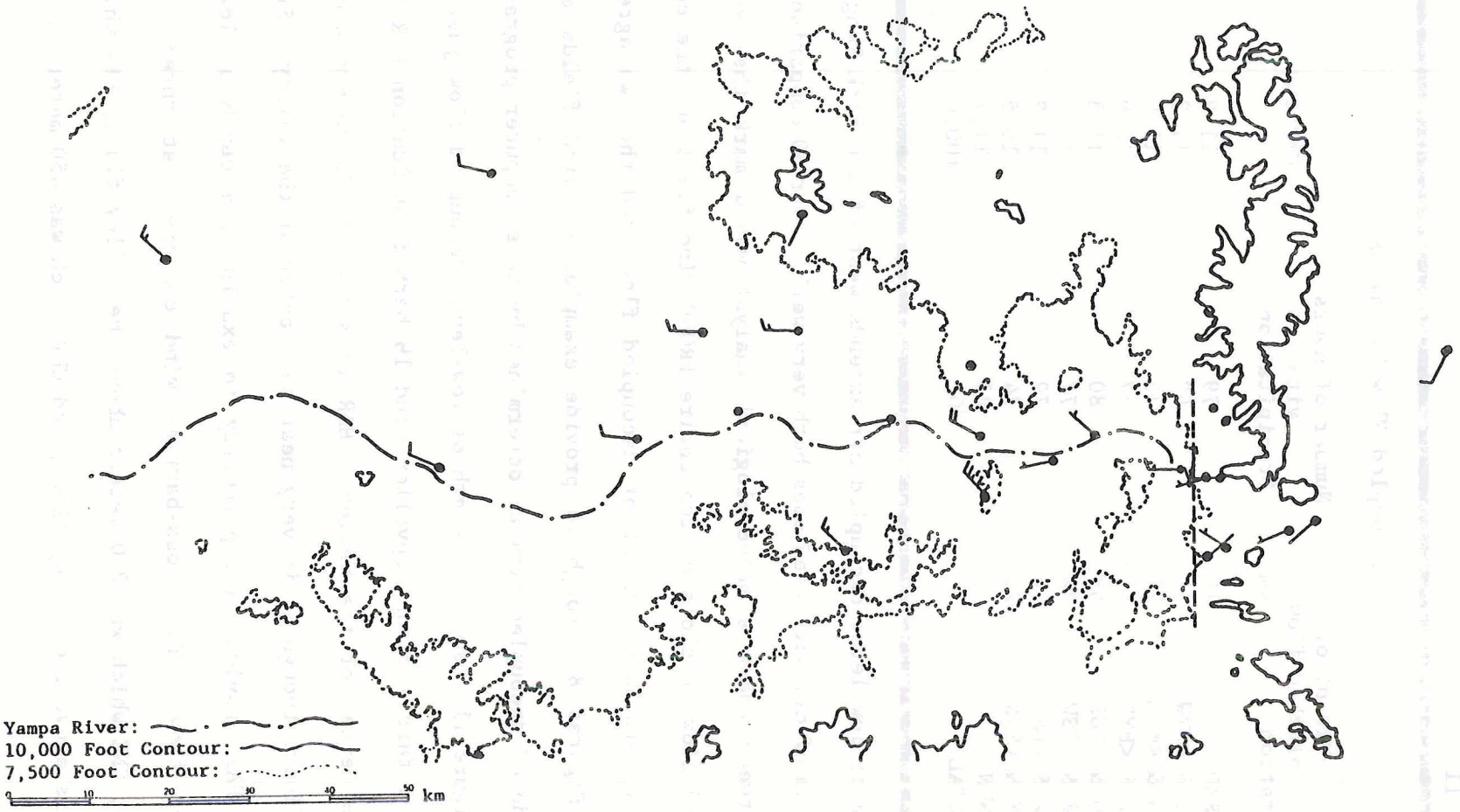

Figure 8. COSE III research area showing PROBE station wind barbs in knots. Heavy dashed line represents the westward extent of decoupled flow determined by the computer program. This example is for 10 km of decoupled flow from winds recorded January 12, 1982 at 05:00 GMT. Long wind barbs are 5 ms^{-1}.

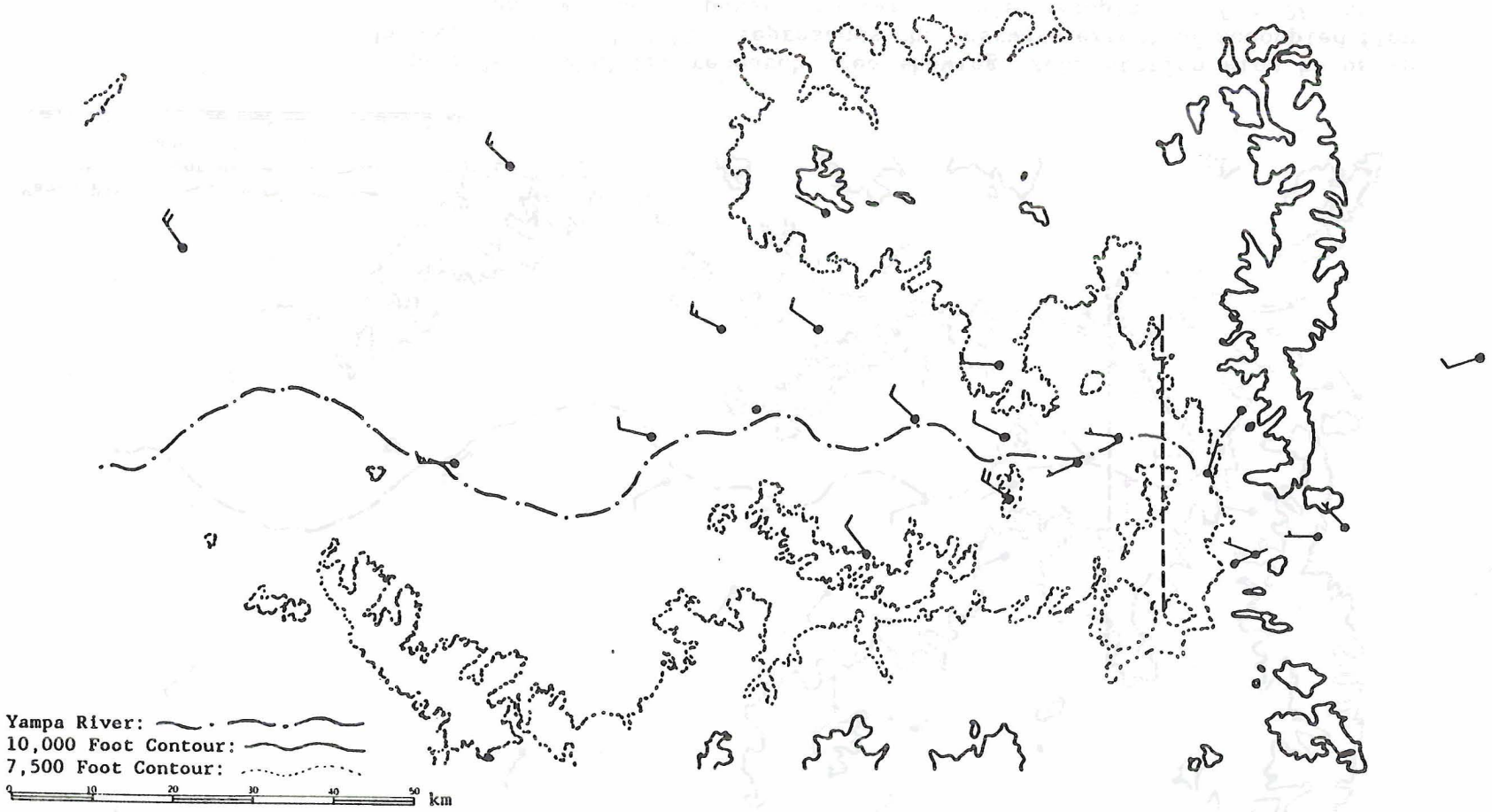

Figure 9. COSE III research area showing PROBE station wind barbs in knots. Heavy dashed line represents the westward extent of decoupled flow determined by the computer program. This example is for 18 km of decoupled flow from winds recorded December 13, 1981 at 20:00 GMT. Long wind barbs are 5 ms^{-1}.

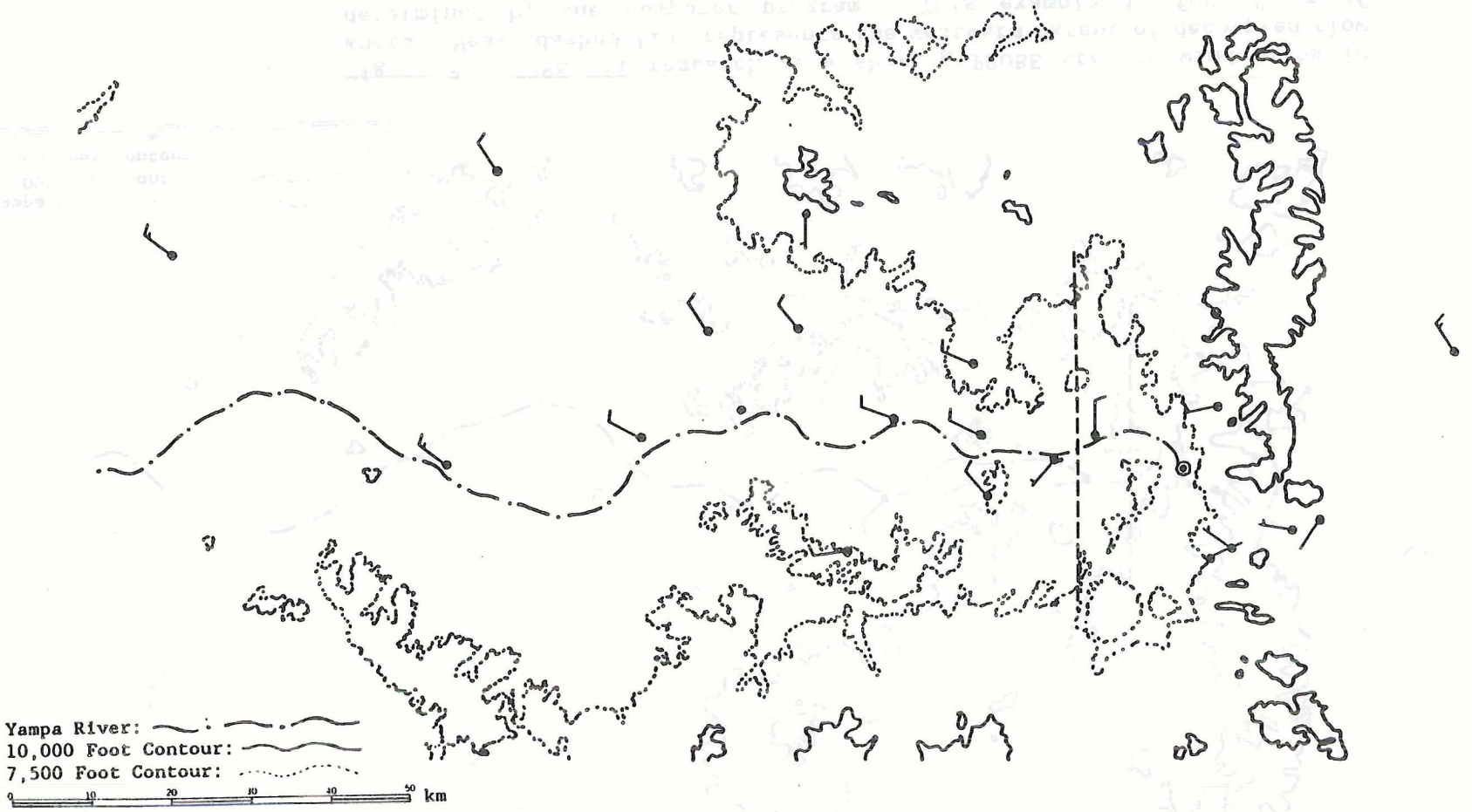

Figure 10. COSE III research area showing PROBE station wind barbs in knots. Heavy dashed line represents the westward extent of decoupled flow determined by the computer program. This example is for 26 km of decoupled flow from winds recorded December 13, 1981 at 22:00 GMT. Long wind barbs are 5 ms^{-1}.

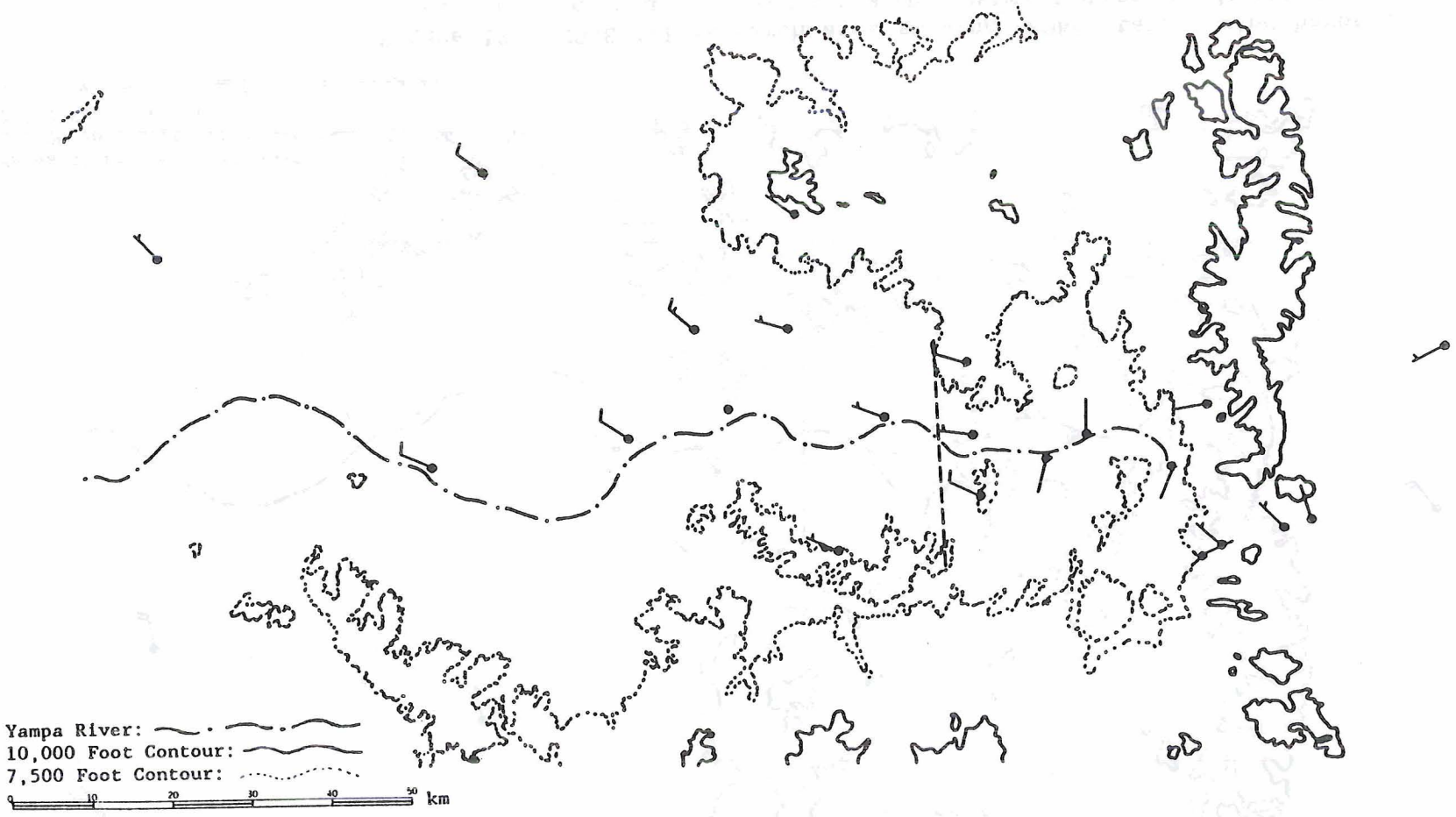

Figure 11. COSE III research area showing PROBE station wind barbs in knots. Heavy dashed line represents the westward extent of decoupled flow determined by the computer program. This example is for 38 km of decoupled flow from winds recorded December 14, 1981 at 00:00 GMT. Long wind barbs are 5 ms^{-1}.

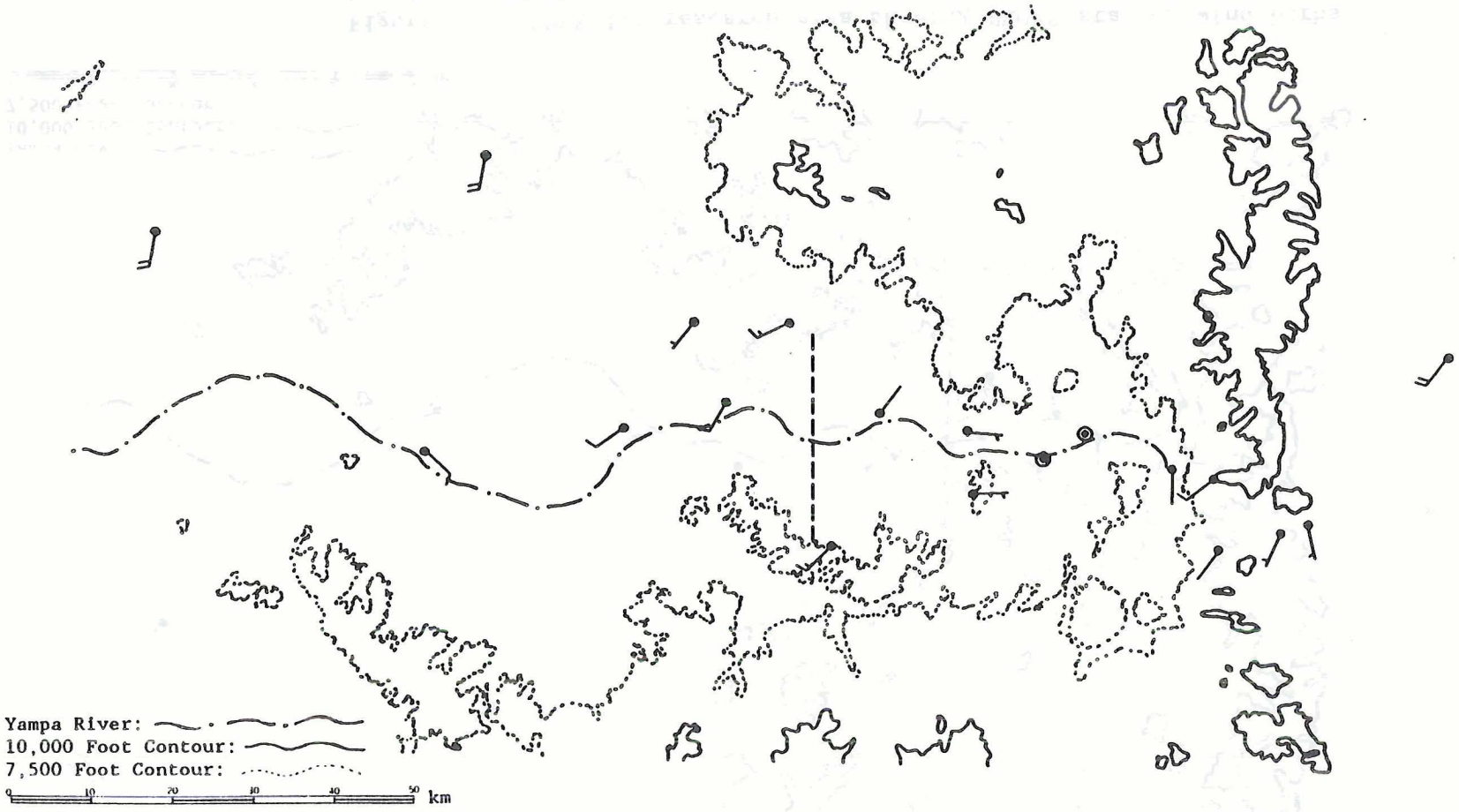

Figure 12. COSE III research area showing PROBE station wind barbs in knots. Heavy dashed line represents the westward extent of decoupled flow determined by the computer program. This example is for 58 km of decoupled flow from winds recorded January 5, 1982 at 10:00 GMT. Long wind barbs are 5 ms^{-1}.

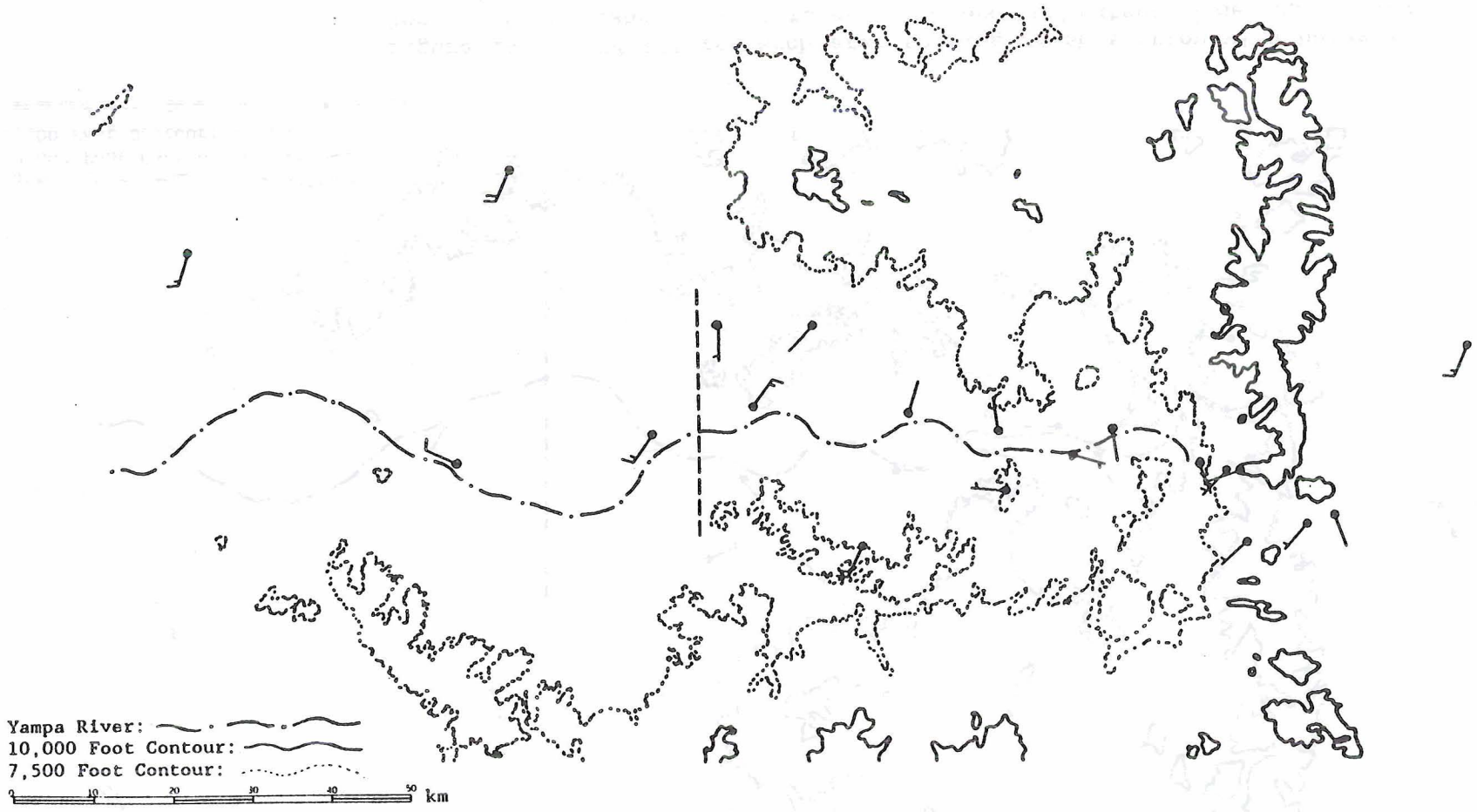

Figure 13. COSE III research area showing PROBE station wind barbs in knots. Heavy dashed line represents the westward extent of decoupled flow determined by the computer program. This example is for 74 km of decoupled flow from winds recorded January 5, 1982 at 20:00 GMT. Long wind barbs are 5 ms^{-1}.

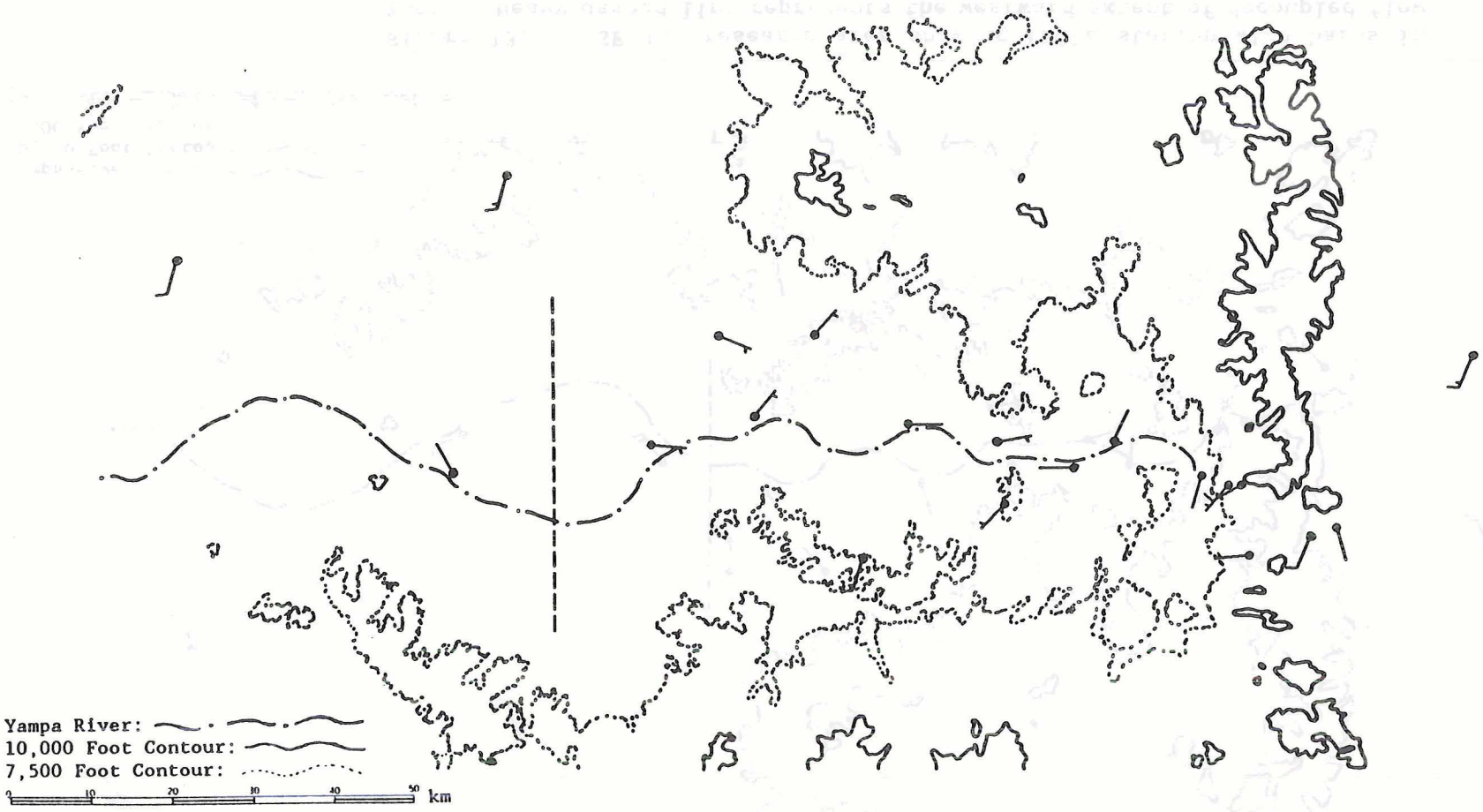

Figure 14. COSE III research area showing PROBE station wind barbs in knots. Heavy dashed line represents the westward extent of decoupled flow determined by the computer program. This example is for 92 km of decoupled flow from winds recorded January 5, 1982 at 19:00 GMT. Long wind barbs are 5 ms^{-1}.

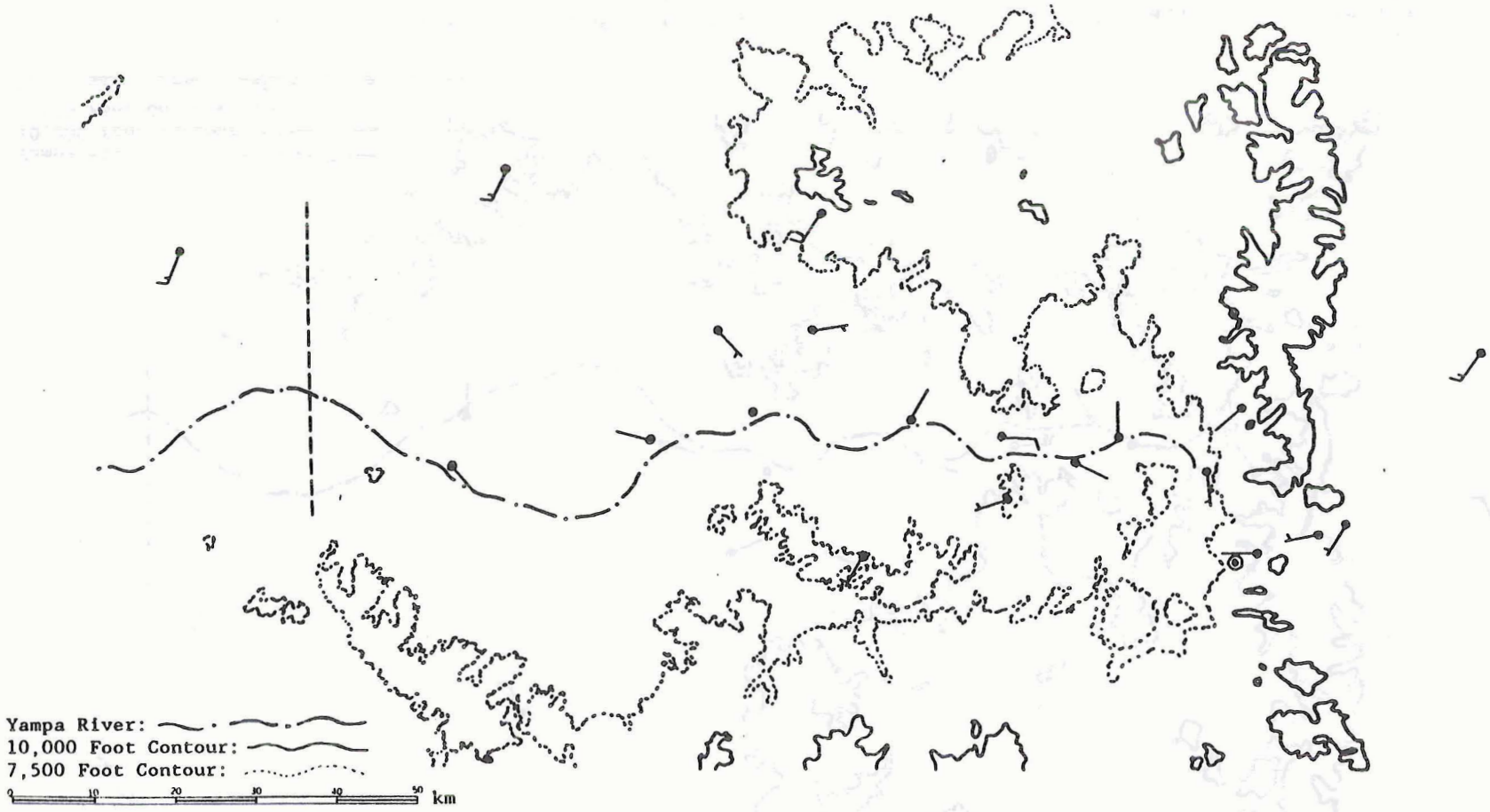

Figure 15. COSE III research area showing PROBE station wind barbs in knots. Heavy dashed line represents the westward extent of decoupled flow determined by the computer program. This example is for 120 km of decoupled flow from winds recorded December 14, 1981 at 16:00 GMT. Long wind barbs are 5 ms^{-1}.

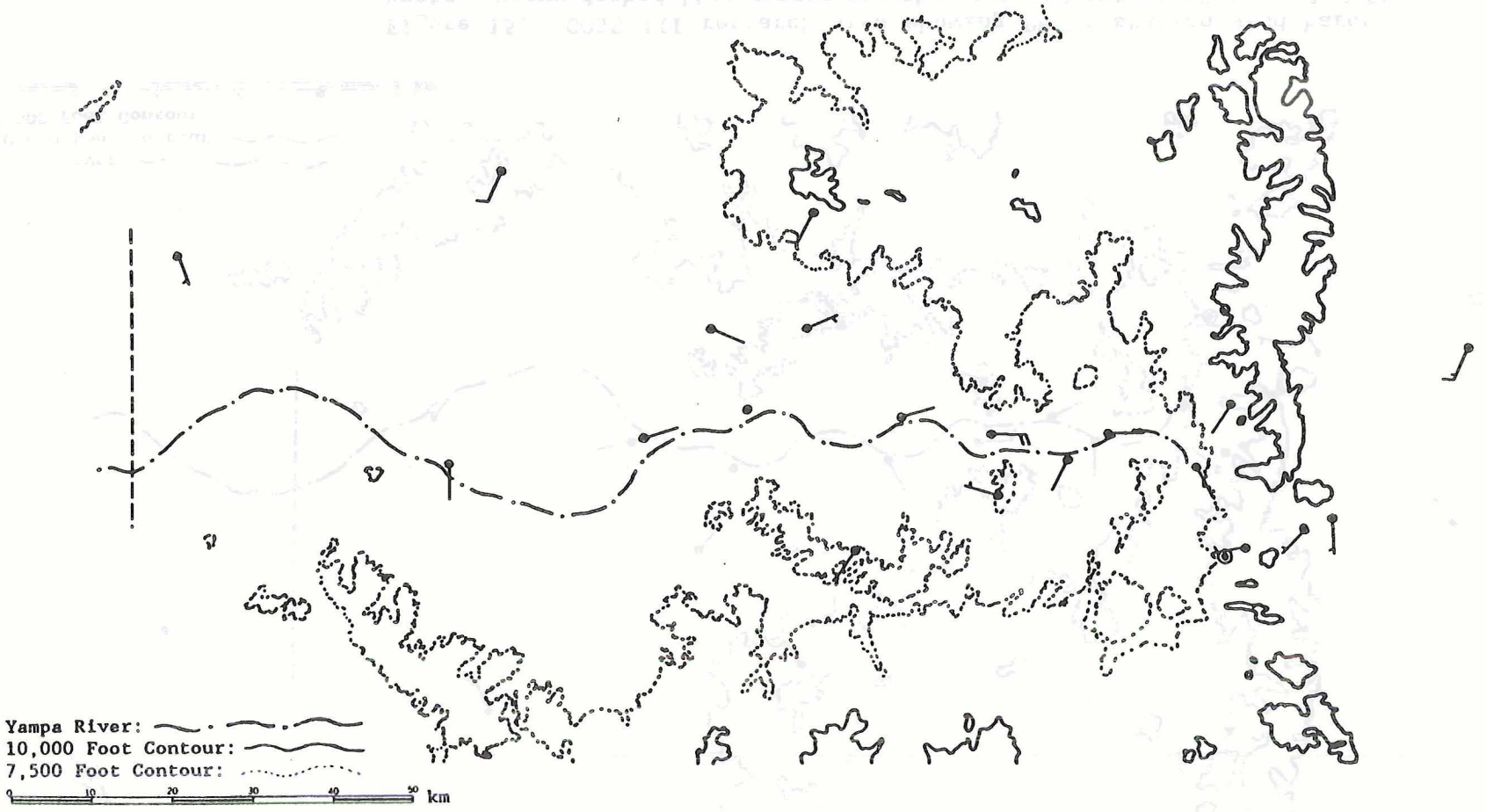

Figure 16. COSE III research area showing PROBE station wind barbs in knots. Heavy dashed line represents the westward extent of decoupled flow determined by the computer program. This example is for 140 km of decoupled flow from winds recorded December 14, 1981 at 12:00 GMT. Long wind barbs are 5 ms^{-1}.

valley floor, were examined to determine what percent of the time they registered decoupled flow at their elevations using a simple 2 ms^{-1} threshold value for determining whether the flow was decoupled or not. These values were then plotted, in Figure 17, against the distance west of each of the 3 stations that the upwind edge of low-level decoupled flow was determined to be.

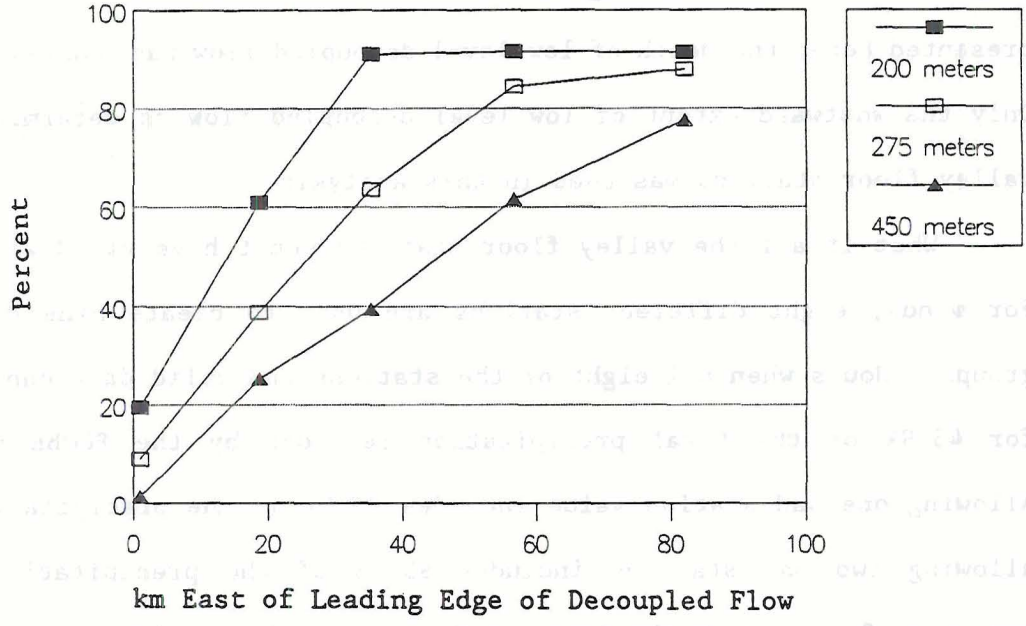

Figure 17. The likelihood, in percent, of decoupled low-level flow as determined by stations 200, 275, and 450 meters above the valley floor using a 2 ms^{-1} threshold value for decoupled flow plotted against the distance west of each station that the westernmost edge of decoupled flow was determined.

Figure 17 shows that in the vicinity of the leading edge of decoupled flow, there was only a 20 percent chance that the decoupled flow was 200 meters deep or deeper. Whereas, 40 km back from the leading edge of decoupled flow, there was a 90 percent chance that the layer of

decoupled flow was at least 200 meters deep and a 40 percent chance that it was at least 450 meters deep. When the extent of decoupled flow was very large, there was nearly an 80 percent chance that 80 km east of the leading edge of low-level decoupled flow, the layer of decoupled flow was 450 meters or more thick.

An analysis involving the depth of low-level decoupled flow will be used in the case study analysis presented in Chapter 6. However, for purposes of the climatological analysis of 1½ months of PROBE data presented here, the depth of low-level decoupled flow was not considered. Only the westward extent of low-level decoupled flow as determined by 8 valley floor stations was used in this analysis.

What if all the valley floor stations don't have valid wind data? For winds, eight different stations are used to create nine different groups. Hours when all eight of the stations had valid data can account for 43.9% of the total precipitation recorded by the PROBE network. Allowing one bad station value includes 83.9% of the precipitation, and allowing two bad stations includes 95.4% of the precipitation. For purposes of this study the data set that allows for one bad wind reportwas used, and the station without good wind data was treated as if it registered continuing decoupled flow, assuming no station to the east had already signaled an end to the westward distance of decoupled flow. Choosing this data set over the "error free" data set decreases the effect of single event anomalies by greatly increasing the total precipitation.

3.2.2.4. Precipitation

Treating bad precipitation data is an altogether different problem. Bob Rilling carefully hand corrected the precipitation from all

twenty-four stations on an hourly basis. Yet the data set is nowhere near complete. Many of the stations report missing data for weeks on end. STP, the station on the top of Storm Peak, is the worst example of this. Rilling also has many stations showing periods of hours to days when the gauge was "stuck", often due to snow bridging over the precipitation gage, with an amount shown that registered when the gauge was no longer stuck. Because the precipitation intensity varied greatly on an hourly basis, it was decided to treat the "stuck" periods as missing data.

Another problem that needed to be addressed was how to compare the precipitation when 24 stations (none missing) reported with the precipitation when only 20 stations (4 stuck or missing) reported. This problem was approached by dividing the stations into five location groups with two stations left over that didn't readily fall into any group. These groups, shown in Figures 18 and 19, are:

Over the Barrier: HYC, COL, and HEB

On the Barrier: STP, FTP, BUR, DLK, and PIC

Upper Valley: MIL, STW, and RAD

Middle Valley: CGE, HYD, CGN, and CNE

Lower Valley: CSW, LAY, and SUN

Valley Sides: BLK, WLF, CHV, and HGM

The two stations left over and treated individually are DIV and HAR.

The station DIV is in the northwest part of the research area and recorded only 0.7% of the total network precipitation. The station HAR appears to be right in the Yampa Valley between Hayden and Milner, but it is on a ridge 275 meters above the nearby Yampa River. HAR recorded 3.6% of the total precipitation. Another station that should be mentioned is

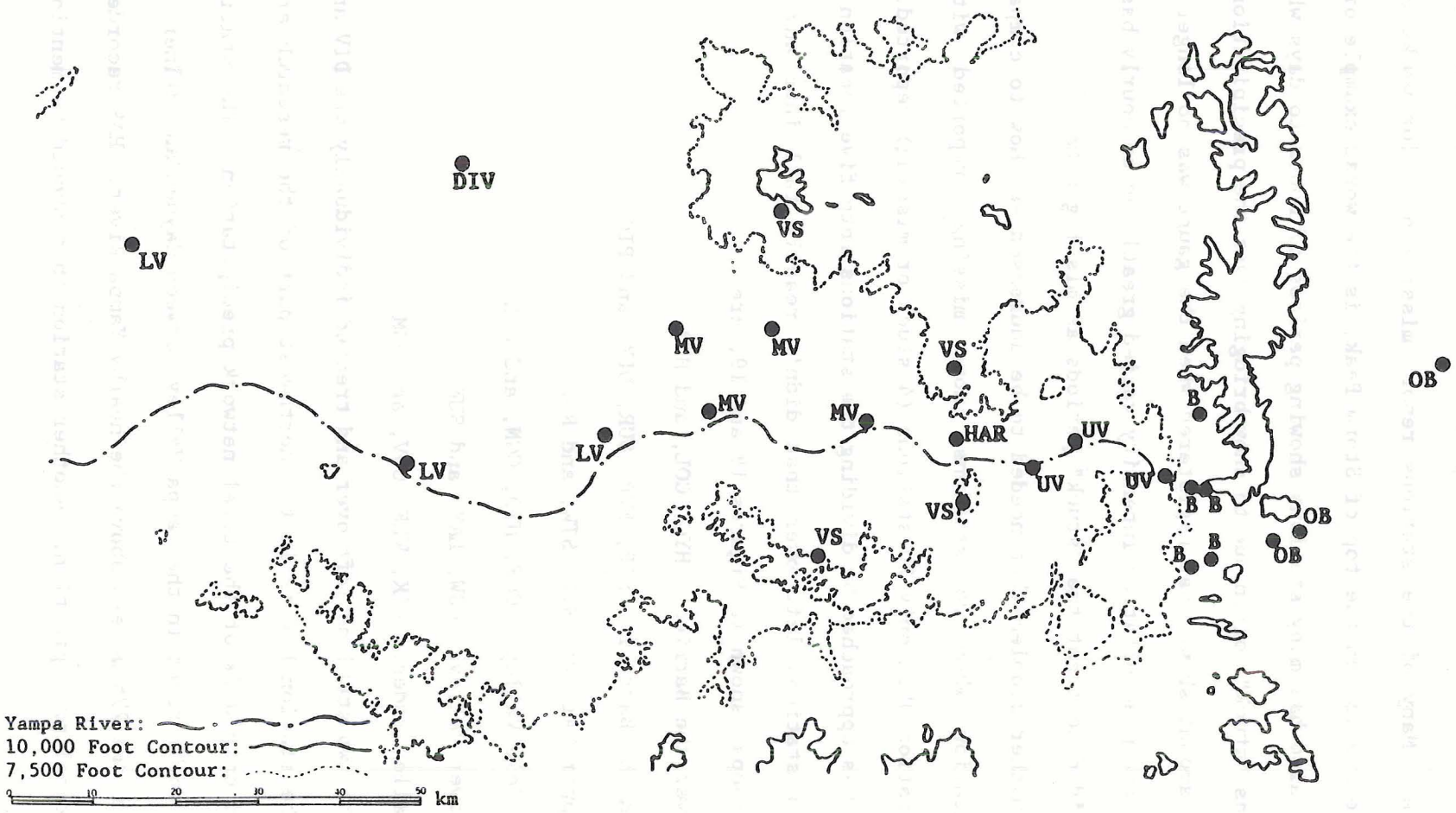

Figure 18. Map of the COSE III research area showing PROBE stations precipitation groups: OB for Over the Barrier, B for Barrier, UV for Upper Valley, MV for Middle Valley, LV for Lower Valley, VS for Valley Sides, and two individual stations HAR and DIV.

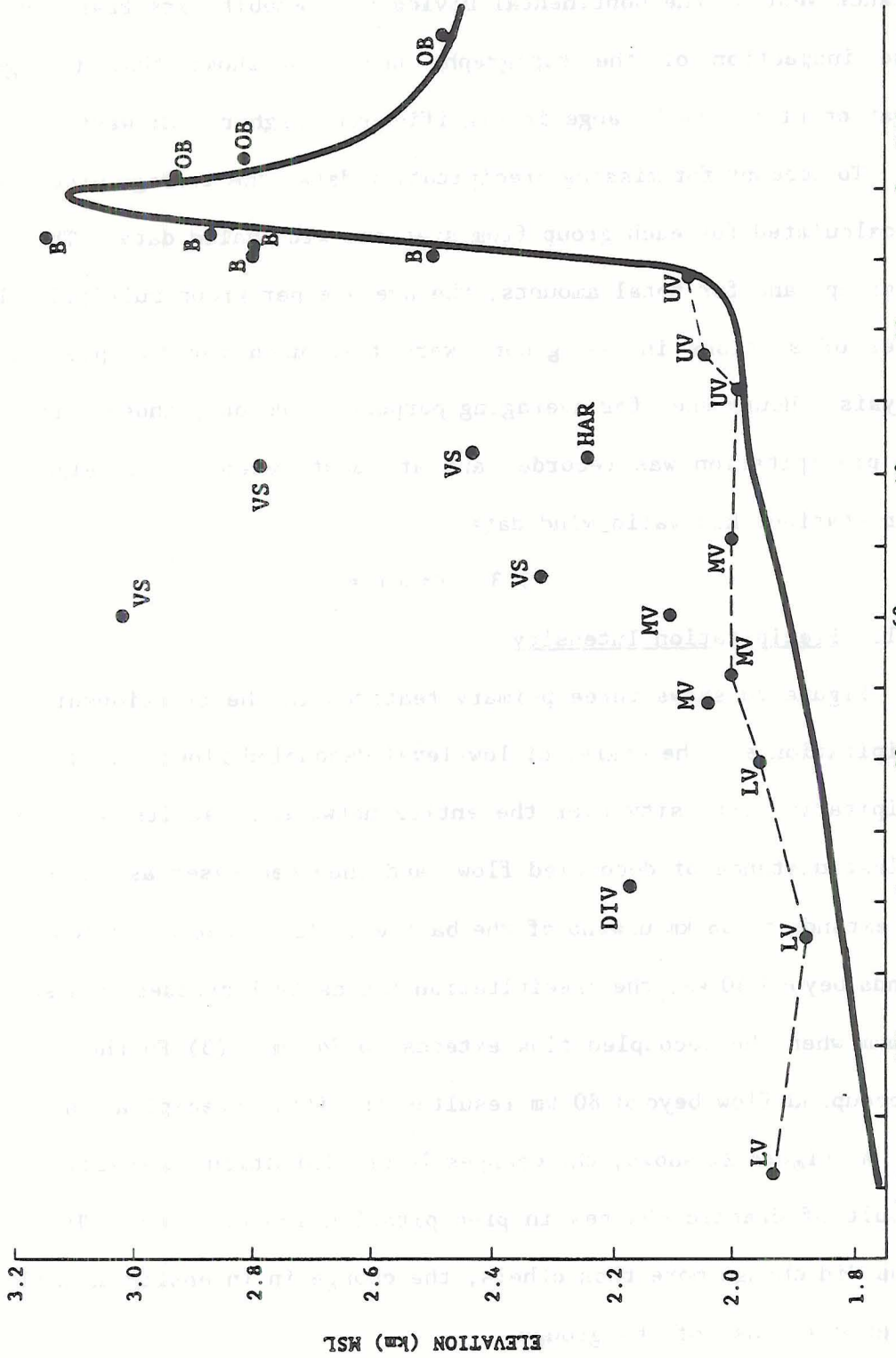

Figure 19. XZ cross section of the COSE III research area showing PROBE station precipitation groups. The dashed line connects the 8 valley floor PROBE stations used to determine the extent of decoupled flow.

HYC. HYC is in the "Over the Barrier" group yet it is actually a short distance west of the Continental Divide near Rabbit Ears Pass. However, close inspection of the topography near HYC shows that the general elevation of the Park Range is significantly higher 8 km west of HYC.

To account for missing precipitation data, the average precipitation was calculated for each group from stations with valid data. The average per group, and for total amounts, the average per group multiplied by the number of stations in the group, were then used for the precipitation analysis. Hours used for averaging purposes were only those during which some precipitation was recorded and at least seven of the eight valley floor stations had valid wind data.

3.3. Results

3.3.1. Precipitation Intensity

Figure 20 shows three primary features in the relationship between precipitation and the degree of low-level decoupled flow: (1) The average precipitation intensity over the entire network is at its peak with the smallest distance of decoupled flow, and then decreases as the decoupled flow extends to 38 km upwind of the barrier. (2) After the decoupled flow extends beyond 40 km, the precipitation intensity increases to a secondary maximum when the decoupled flow extends to 74 km. (3) Further extension of decoupled flow beyond 80 km resulted in little precipitation.

As Figure 21 shows, the changes in precipitation intensity, were not a result of drastic changes in precipitation in one group. Though some groups did change more than others, the change in intensity as a whole is reflected in most of the groups.

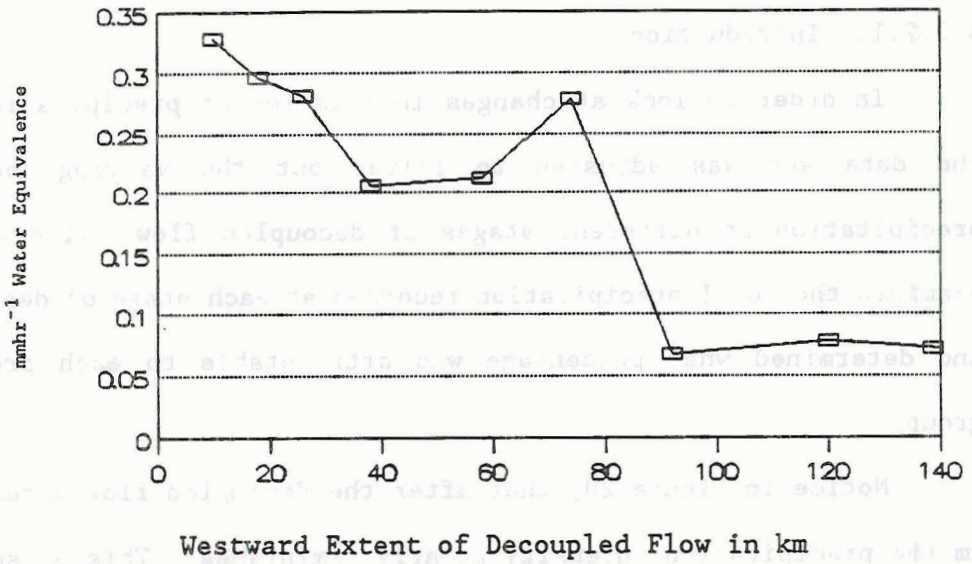

Figure 20. Precipitation intensity over the entire PROBE mesonetwork in mm of water equivalence per station per hour.

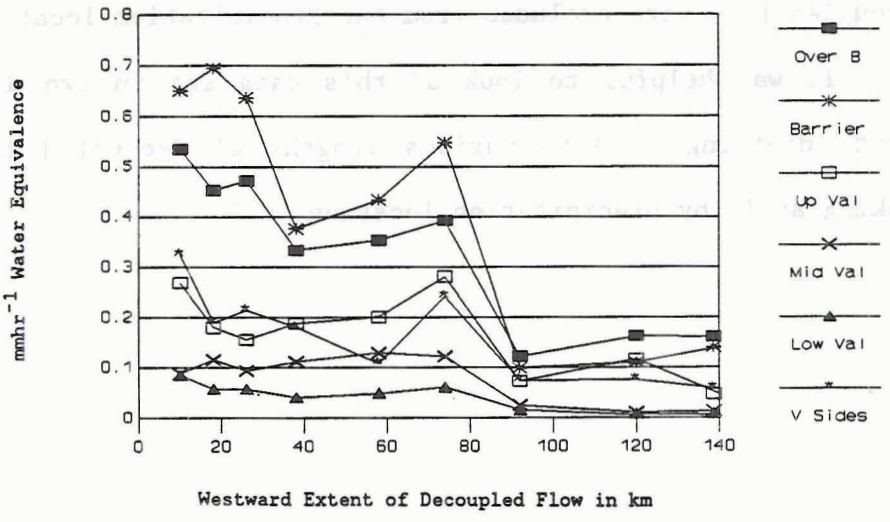

Figure 21. Precipitation intensity versus westward extent of decoupled low-level flow by precipitation group on a per station basis.

3.3.2. Precipitation Location

3.3.2.1. Introduction

In order to look at changes in location of precipitation clearly, the data set was adjusted to filter out the varying intensity of precipitation at different stages of decoupled flow. The method used examined the total precipitation recorded at each stage of decoupled flow and determined what percentage was attributable to each precipitation group.

Notice in Figure 20, that after the decoupled flow extends past 80 km the precipitation intensity greatly diminishes. This presents a data resolution problem. The precipitation records do not show any value less than 3 mm of water equivalence precipitation per hour. When the precipitation was very light, this threshold makes comparing precipitation from one location to another less accurate. Also, when the precipitation is very light, single event anomalies carry more weight. Therefore, the three decoupled flow divisions with the greatest westward magnitude of decoupled flow were excluded from the precipitation location analysis.

It was helpful to look at this data set in two different ways: First, dividing it into various lengths of decoupled flow; second, looking at it by precipitation location.

3.3.2.2. By Westward Extent of Decoupled Flow

3.3.2.2.1. Decoupled Flow Equals 10 km

As Figure 22 shows, the precipitation in the Yampa Valley clearly has a strong orographic component with the barrier stations getting the most precipitation, followed by the over the barrier stations. Upwind of the barrier, the average precipitation shows a clear upper valley to lower valley decrease. Though the trend is not as clear for the precipitation occurring during 10 km of decoupled flow.

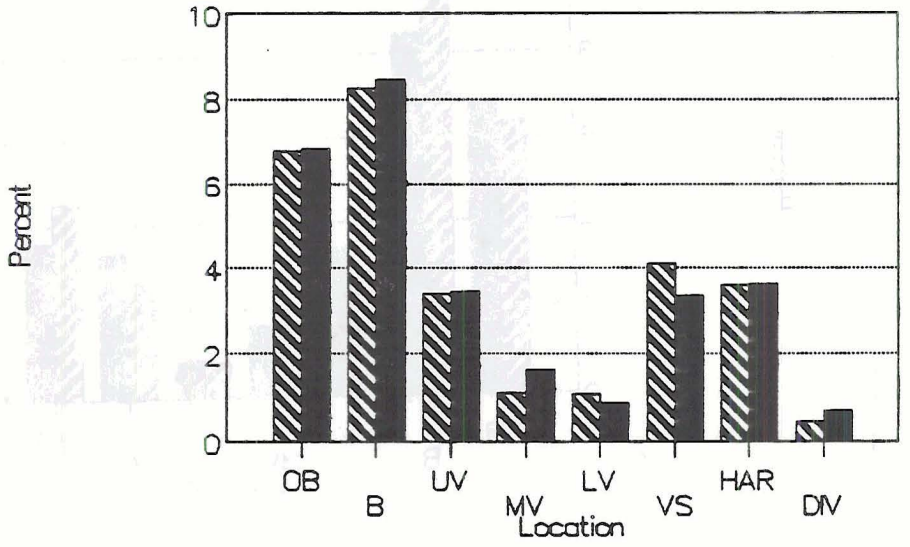

Figure 22. Percent of precipitation on a per station basis by location. Black represents average for entire data set. Striped represents precipitation percentage when decoupled flow was 10 km in length.

When the magnitude of low-level decoupled flow is at its smallest, the precipitation amounts are very close to average at almost all stations. The middle valley with less than average and valley sides with more than average are the most deviant of the precipitation locations.

3.3.2.2.2. Decoupled Flow Equals 18 km

Figure 23 shows that when the decoupled flow is just into the upper valley, the precipitation on the barrier is greater than average. Nearby over the barrier is less than average and the upper valley is quite a bit less than average.

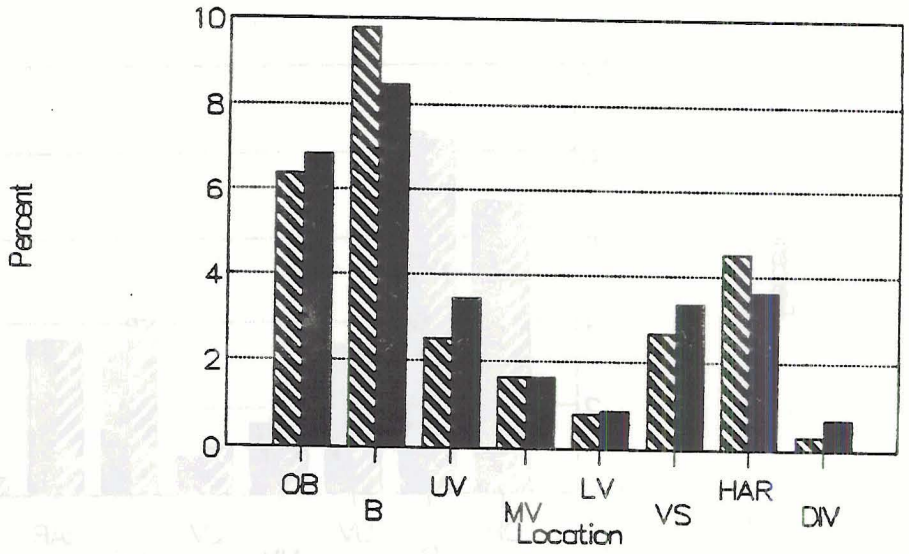

Figure 23. Percent of precipitation on a per station basis by location. Black represents average for entire data set. Striped represents precipitation percentage when decoupled flow was 18 km in length.

3.3.2.2.3. Decoupled Flow Equals 26 km

As shown in Figure 24, with the westward distance of decoupled flow still in the upper valley, the barrier still experiences greater than average precipitation. The upper valley receives considerably less than average precipitation and now the middle valley also shows less than average. The over the barrier group, however, is now reporting a little more than average.

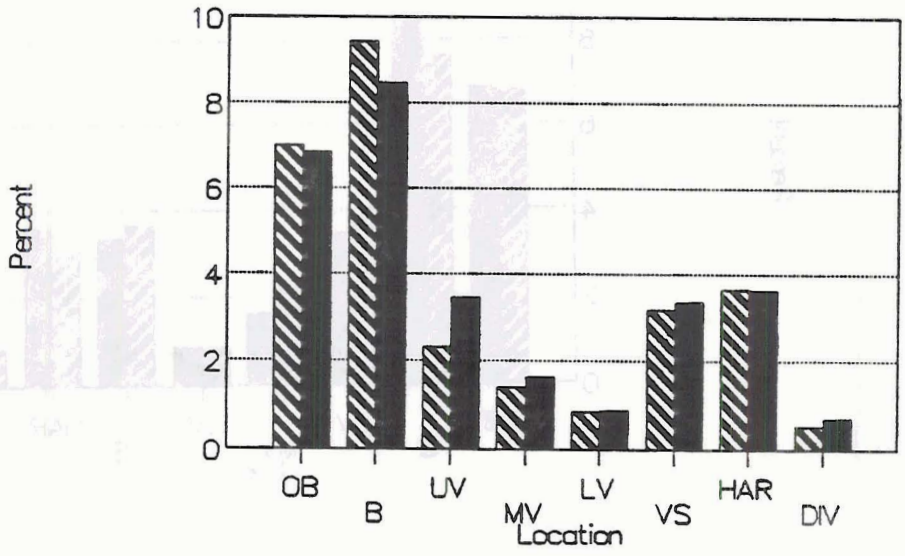

Figure 24. Percent of precipitation on a per station basis by location. Black represents average for entire data set. Striped represents precipitation percentage when decoupled flow was 26 km in length.

3.3.2.2.4. Decoupled Flow Equals 38 km

Figure 25 indicates that with the mountain-cum-decoupled flow cross section covering all of the upper valley and approaching the middle valley, both the upper valley and the middle valley for the first time report above average precipitation. Precipitation on the barrier, however, is now below average.

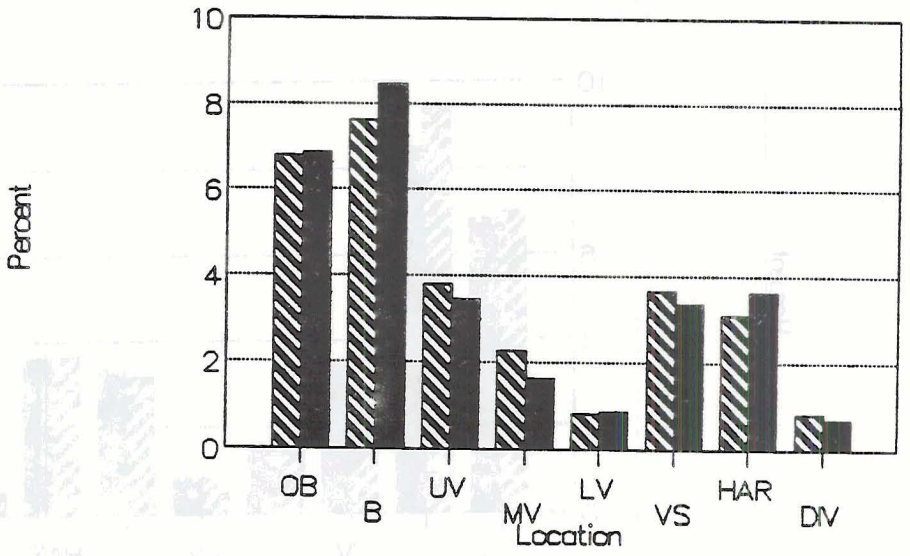

Figure 25. Percent of precipitation on a per station basis by location. Black represents average for entire data set. Striped represents precipitation percentage when decoupled flow was 38 km in length.

3.3.2.2.5. Decoupled Flow Equals 58 km

With the decoupled flow stretching 58 km down the valley, all valley groups are reporting above average precipitation, as shown in Figure 26. The barrier and over the barrier groups are also both reporting slightly above average, so therefore, the two with less than average at this stage of decoupled flow are the valley sides and station HAR.

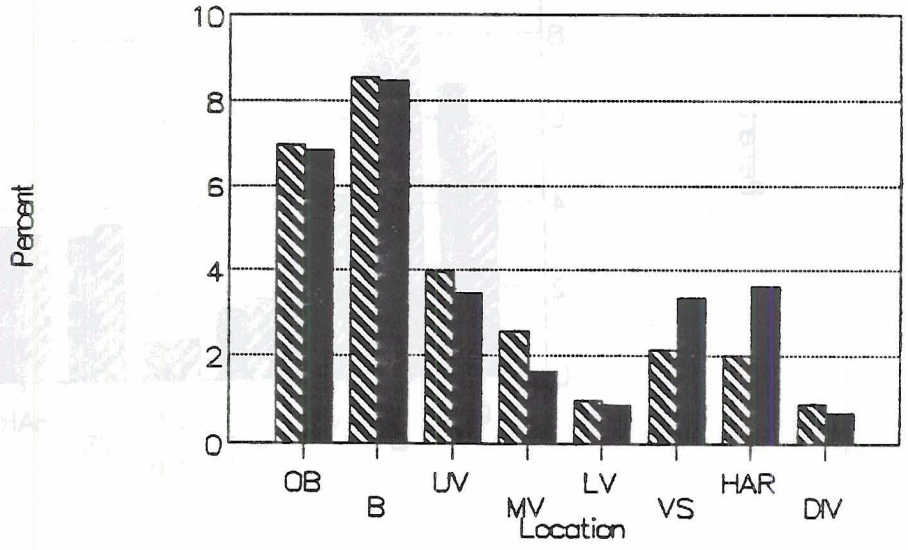

Figure 26. Percent of precipitation on a per station basis by location. Black represents average for entire data set. Striped represents precipitation percentage when decoupled flow was 58 km in length.

3.3.2.2.6. Decoupled Flow Equals 74 km

With the decoupled flow now stretching 74 km down the valley, shown in Figure 27, all valley floor groups are reporting above average, as is the far western station of DIV. The barrier and over the barrier groups are reporting below average.

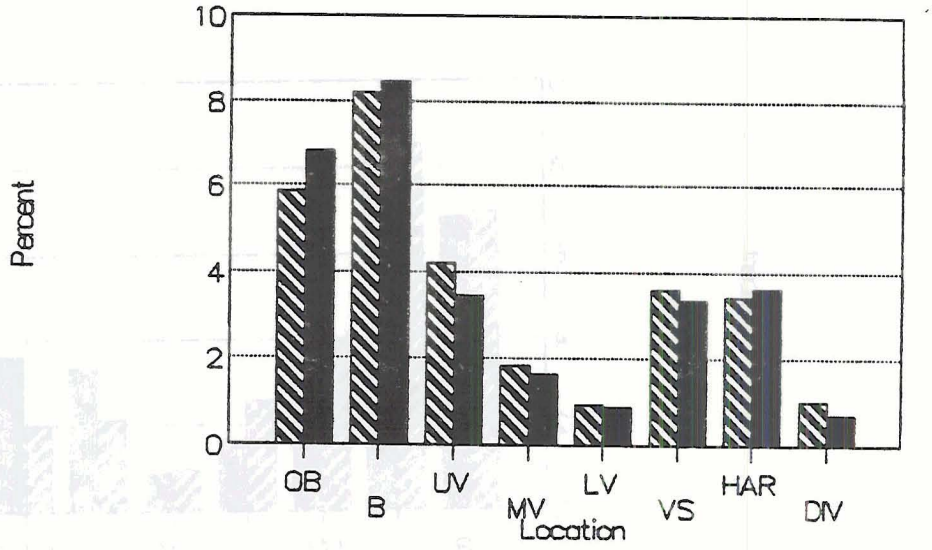

Figure 27. Percent of precipitation on a per station basis by location. Black represents average for entire data set. Striped represents precipitation percentage when decoupled flow was 74 km in length.

3.3.2.3. By Location

3.3.2.3.1. Over the Barrier

The percent of precipitation over the barrier, shown in Figure 28, has a secondary minimum at 18 km and then holds fairly steady until it decreases at 72 km of decoupled flow.

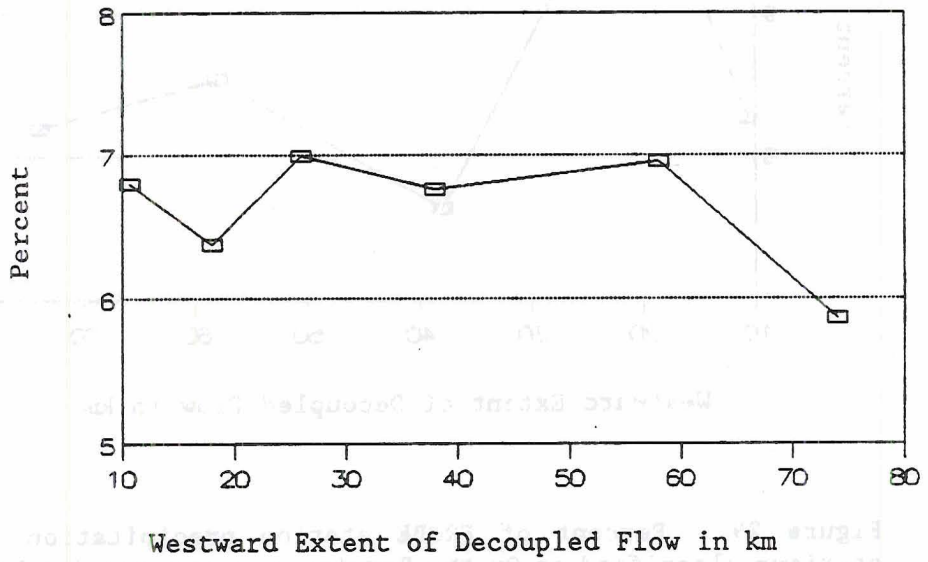

Figure 28. Percent of PROBE station precipitation recorded by stations classified as Over the Barrier on a per station basis plotted against the length of decoupled flow.

3.3.2.3.2. On the Barrier

Precipitation on the barrier has a distinct maximum at 18 km of decoupled flow and a distinct minimum at 38 km of decoupled flow, as shown in Figure 29.

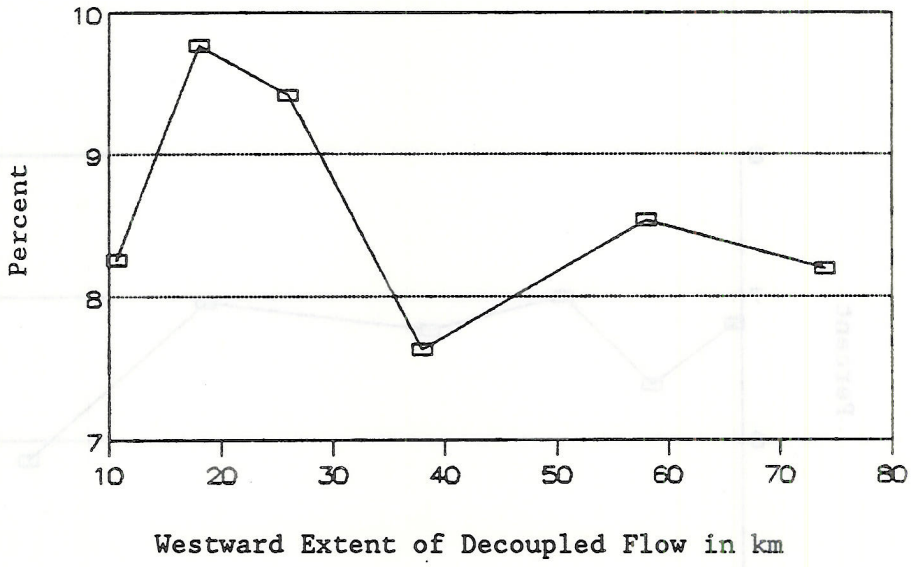

Figure 29. Percent of PROBE station precipitation recorded by stations classified as On the Barrier on a per station basis plotted against the length of decoupled flow.

3.3.2.3.3. Upper Valley

Precipitation in the upper valley, shown in Figure 30, has a distinct minimum at 26 km of decoupled flow with a maximum reached at the farthest length of decoupled flow.

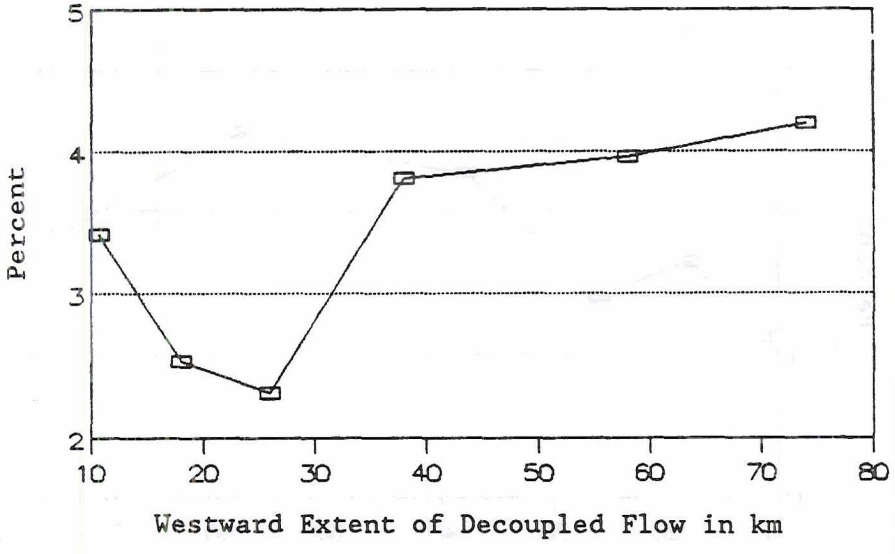

Figure 30. Percent of PROBE station precipitation recorded by stations classified as Upper Valley on a per station basis plotted against the length of decoupled flow.

3.3.2.3.4. Middle Valley

The "middle valley" ranges from 40 to 75 km west of the Continental Divide. The prime feature of the precipitation percentage in the middle valley, shown in Figure 31, is the distinct maximum when the decoupled flow is in the middle valley.

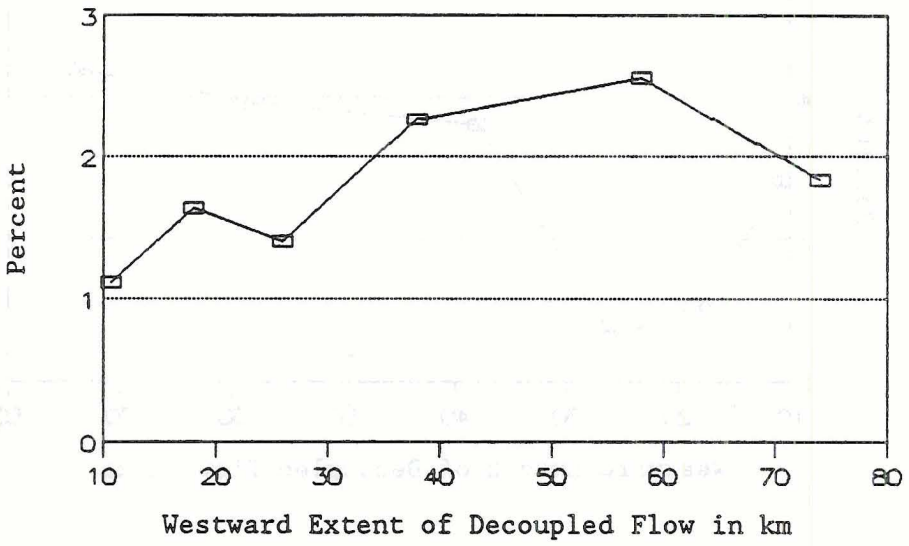

Figure 31. Percent of PROBE station precipitation recorded by stations classified as Middle Valley on a per station basis plotted against the length of decoupled flow.

3.3.2.3.5. Lower Valley

Figure 32 shows the precipitation percentage for the lower valley. Though the change is small, the lower valley precipitation percentage has a peak when the decoupled flow is at its shortest and overall precipitation intensity is at its highest, and a minimum when decoupled flow is 18 km. Also, there is a secondary peak when the westward distance of decoupled flow is 58 km.

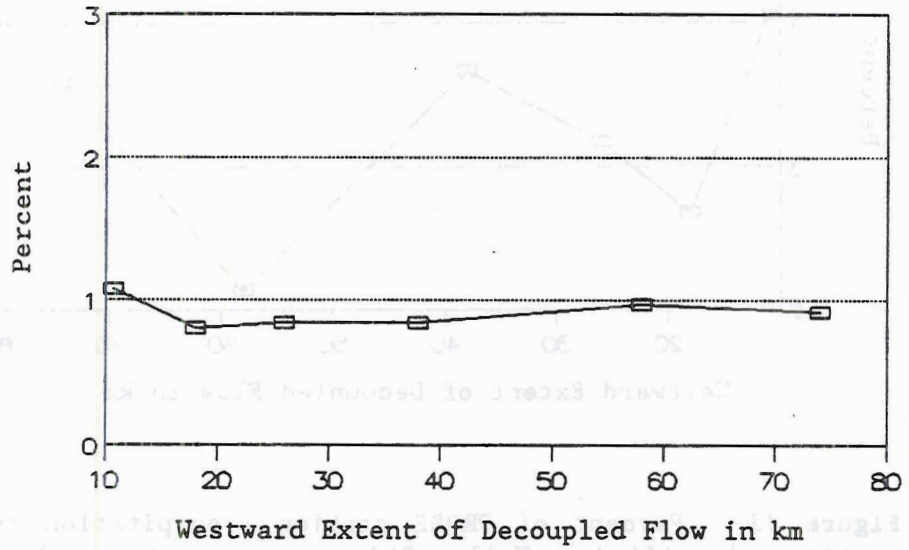

Figure 32. Percent of PROBE station precipitation recorded by stations classified as Lower Valley on a per station basis plotted against the length of decoupled flow.

3.3.2.3.6. Valley Sides

Rather than stating that the precipitation on the valley sides has two distinct minima and three maxima as shown in Figure 33, it is perhaps more accurate to simply say that the precipitation on the valley sides is highly variable.

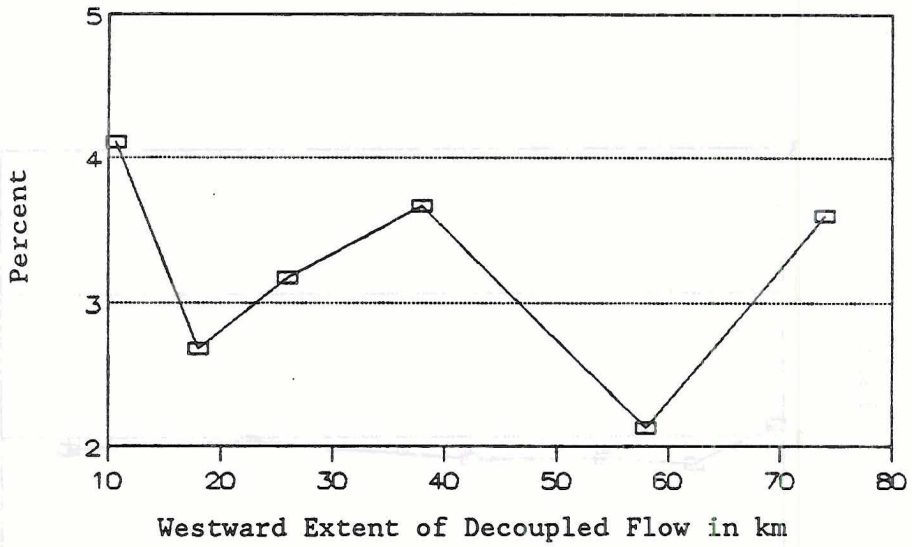

Figure 33. Percent of PROBE station precipitation recorded by stations classified as Valley Sides on a per station basis plotted against the length of decoupled flow.

3.3.2.3.7. Station HAR

Station HAR has a distinct maximum at 18 km of decoupled flow and a minimum at 58 km of decoupled flow, as shown in Figure 34.

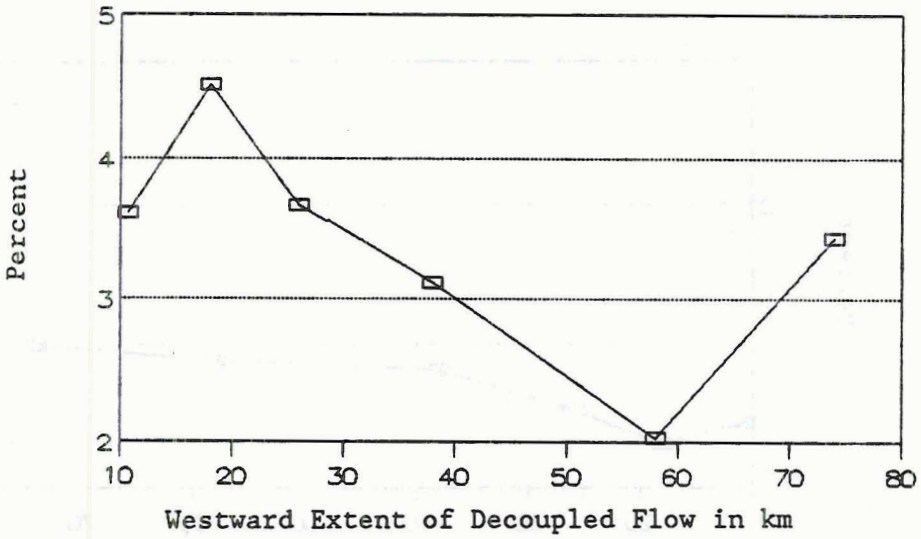

Figure 34. Percent of PROBE station precipitation recorded by station HAR plotted against the length of decoupled flow.

3.3.2.3.8. Station DIV

Figure 35 shows the precipitation percentage at station DIV. Station DIV, 98 km west of the barrier, has a maximum precipitation percentage at the farthest length of decoupled flow used in this analysis.

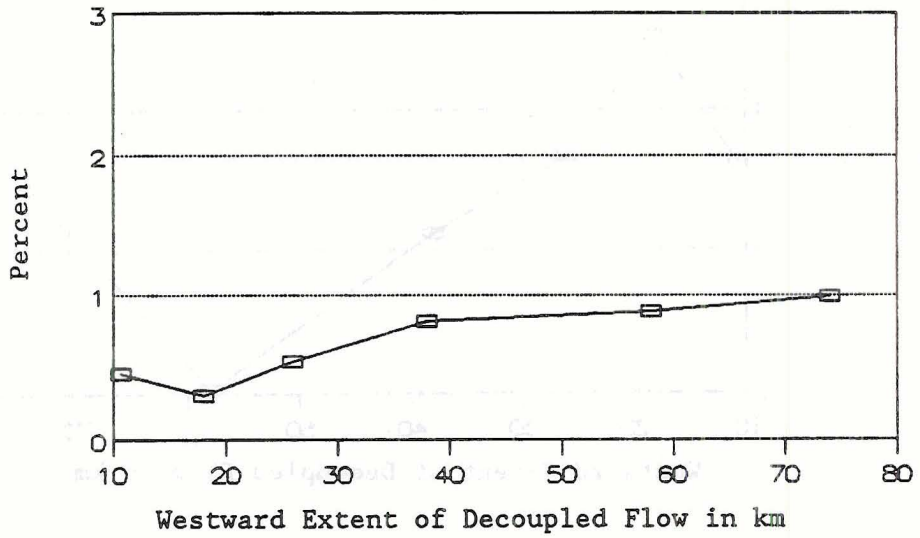

Figure 35. Percent of PROBE station precipitation recorded by station HAR plotted against the length of decoupled flow.

3.4. Discussion

3.4.1. Precipitation Intensity

Decoupled low-level flow can be created by dynamic blocking of oncoming flow or by radiatively inducing drainage flows. While a theoretical framework relating the magnitude of radiatively induced drainage flows with precipitation intensity is not clear, a connection between dynamic blocking and precipitation intensity can be theorized.

Pierrehumbert and Wyman's (1985) modeling work showed that in the nonrotating case (which may be most applicable in the cases of modest degree of blocked flow due to the effect of the valley sides), the Froude number is the "sole parameter" controlling blocking of oncoming flow. The Froude number is Fr=U/Nh, where U is the speed of the oncoming flow, N is the Brunt-Väisälä frequency, $N^2=(g/\theta_r)(d\theta/dz)$, and h the maximum mountain height. The Froude number therefore is essentially the square root of the ratio of the kinetic energy in the horizontal flow over the energy required to lift a parcel of air from the surface to mountain top height through the stably stratified environment. Therefore, for a given atmospheric stability, the degree of blocked flow tends to be small when cross-barrier winds are strong, and large when cross-barrier winds are weak. It is hypothesized that this link is generally applicable for the storm events studied.

Orographic clouds have been likened to cumulus clouds turned on their sides with the cross-barrier flow feeding in moisture much the way the updraft does in cumulus clouds. Therefore, for a given atmospheric humidity, strong cross-barrier winds will produce more condensate per hour in an orographic cloud than weak cross-barrier winds. This is a prime

factor in increased precipitation, although just having more condensate form per hour doesn't guarantee that more precipitation will reach the ground since the number of crystals blowing over the barrier and out the other side of the cloud never to reach the ground also increases with increasing cross-barrier winds. Also, when cross-barrier winds are weak and less condensate forms, precipitation can be expected to be light.

Therefore, two of the three prime features of the precipitation intensity versus decoupled flow chart can be explained: both the precipitation maximum for the smallest degrees of decoupled flow and the precipitation minimum for longest of decoupled flows appear to have the same root cause - the intensity of cross-barrier winds.

The other major feature - the secondary maximum when decoupled flow extends to 74 km - will be found in Chapter 4 to be related to particular synoptic classifications.

3.4.2. Precipitation Location

3.4.2.1 By Westward Extent of Decoupled Flow

The trend, when viewed from different lengths of decoupled flow, is:

When the westward distance of decoupled flow is at its smallest, and cross-barrier winds are strong, and precipitation intensity is high, precipitation is spread throughout the Yampa Valley in proportions that are very close to average for the season.

When the westward magnitude of low-level decoupled flow is limited to the upper valley, the barrier receives a greater than average proportion of precipitation while the valley stations receive less than average.

When the westward length of decoupled flow is in the middle valley, the valley stations receive greater than average proportion of precipitation while the barrier receives less than average.

To explain these observed changes, it is hypothesized that air flowing up and over the barrier must also rise up and over the low-level decoupled flow. This hypothesis implies that for orographic lift, what matters is not the cross section of the mountain, but rather the cross section of the mountain and its region of low-level decoupled flow. If the low-level decoupled flow extends 60 km upwind of the barrier, then the orographic lift would initially be experienced 60 km farther upwind as the oncoming air rises over the decoupled flow.

The location of precipitation in mountainous regions is directly related to orographic lift. Therefore, starting the mountain's orographic lift farther upstream can alter the precipitation patterns. Ice crystals would have a longer time to grow and fall. And in convectively unstable situations, convection could be initiated farther upstream.

The observed results described in the beginning of this section agree very well with the hypothesis that the magnitude of decoupled flow can alter the location of precipitation by changing the shape of the mountain-cum-decoupled flow cross section, thereby changing the location where a parcel of air experiences forced orographic lifting. When the orographic lift is experienced farther west, the precipitation tends to fall farther west.

3.4.2.2. By Location

3.4.2.2.1. Over the Barrier

The minimum at the farthest distance of decoupled flow makes sense from the two hypothesis noted earlier: (1) Cross-barrier winds are probably lightest blowing a lower percentage of the crystals over the barrier. And, (2) orographic lift experienced farthest upstream allowed a greater percentage of the crystals to fall out before they blow over the barrier.

3.4.2.2.2. On the Barrier

The maximum occurs when the degree of decoupled flow is in the upper valley, this is when the mountain-cum-decoupled flow cross section is only a little larger than the mountain itself and therefore the largest portion of the orographic lift is near the barrier. Also, cross-barrier winds are, probably, a little lighter on these occasions than when the length of decoupled flow is at a minimum and therefore blow less snow over the barrier.

The general decrease in precipitation as the degree of decoupled flow increases makes sense when viewed through the framework of the hypothesis that decoupled flow can change the location of precipitation by causing the lift to be experience farther west. However, the minimum at 38 km cannot readily be explained.

3.4.2.2.3. Upper Valley

The minimum when the westward distance of decoupled flow is in the upper valley is not readily explained with the mountain-cum-decoupled flow hypothesis as previously discussed. But the problem may well lie in the unique topography of the upper valley: the upper valley is fairly wide,

but between the upper valley and the middle valley there is a marked constriction, as illustrated by station HAR which is very close to the Yampa River but 275 meters higher. This means that much of the air moving over the upper valley when the decoupled flow is small and shallow is descending from the ridge that HAR is on. This in turn may account for the minimum when the westward extent of decoupled flow is in the upper valley.

3.4.2.2.4. Middle Valley

Basing predicted precipitation intensity on the hypothesis that what matters in orographic precipitation is not the cross section of the mountain, but rather the cross section of the mountain-cum-decoupled flow, one might predict a precipitation versus decoupled flow graph for the middle valley to have the same shape as Figure 31: The middle valley ranges from 40 km to 75 km. When the orographic lift hypothesized from the leading edge of mountain-cum-decoupled flow is in this region, the precipitation reaches a maximum.

3.4.2.2.5. The Lower Valley

The minimum when decoupled flow is short followed by generally increasing precipitation when decoupled flow extends farther west is in keeping with what one would expect as the start of mountain-cum-decoupled flow lift moves farther west. However, the amount of change is very minor.

3.4.2.2.6. The Valley Sides

The precipitation on the valley sides shows no consistent pattern.

3.4.2.2.7. Station HAR

HAR is located 275 meters above the valley floor on the constricting ridge between the upper valley and the lower valley. Therefore, to properly understand why the intensity of precipitation changes as it does at HAR, one should analyze it in a study that takes the depth of the decoupled flow into account.

3.4.2.2.8. Station DIV

This far western station shows an increase in precipitation percentage as the westward length of decoupled flow increases which is in keeping with the hypothesis that what matters in the distribution of winter precipitation in mountainous regions is not the cross section of the mountain, but the cross section of the mountain-cum-decoupled flow.

3.4.3. Summary

The magnitude of low-level decoupled flow upstream of the Park Range can be correlated with changes in the location and intensity of winter precipitation in the Yampa Valley but the relationship between decoupled flow and precipitation is complex. The changes in location - westward shift in precipitation corresponding to a westward increase in decoupled flow - could be interpreted as supporting Grossman and Durran's, 1984, conclusion that low-level blocking causes lift upstream of the barrier. This aspect of the relationship seems to be causal, with the magnitude of decoupled flow altering the location of precipitation by altering the location of orographic lift as air is forced to rise over the layer of decoupled air as well as the mountain. A good example to support this conclusion is the middle valley stations experiencing their maximum

percentage of precipitation when the westward length of low-level decoupled flow is in the middle valley.

The change in precipitation intensity - decreased intensity with increased decoupled flow - could be interpreted as supporting Marwitz's, 1980 and Lee's, 1981, conclusion that blocked flow decreases the effective height of the barrier. However, Grossman and Durran's conclusion is in conflict with Marwitz's and Lee's conclusions because the lift Grossman and Durran see low-level blocked flow causing is the very same lift that Marwitz and Lee see blocked flow making unavailable. An alternate explanation for the observed change in precipitation intensity with different lengths of decoupled flow has been hypothesized. Using this explanation one can view the relationship between decoupled flow and precipitation intensity to be a result of the two phenomena sometimes having the same root cause. For example, both high precipitation intensity and small westward distance of low-level blocked flow can be caused by strong cross-barrier winds.

4. Variations with Synoptic Classifications

4.1. Introduction

In Chapter 3 the question of how precipitation intensity changed for different magnitudes of low-level decoupled flow was examined. One of the findings was that there was a secondary maximum in precipitation when decoupled flow extended 74 km west of the Continental Divide. This secondary maximum could not be explained through the hypotheses presented in Chapter 3. Different synoptic classifications, their precipitation intensities, and their distributions in the decoupled flow categories will now be examined to see if the secondary maximum in precipitation for 74 km length of decoupled flow is the result of particular synoptic conditions.

4.2. Methods

The first step in this analysis is developing a synoptic classification scheme appropriate for northern Colorado. Many different classifications systems exist. For instance, Yu and Pielke (1986) used Lindsey's classification scheme in their study of air quality under stagnant synoptic cold season conditions in the Lake Powell area of Southern Utah and Northern Arizona. This scheme is based on the classical cyclone model and works quite well in many regions of the country. However, it does not adequately divide the synoptic conditions of northwestern Colorado. For example, Lindsey's scheme has one classification for times when a polar anticyclone is in the research area, and would not differentiate whether or not there was also a trough on the

lee side of the Front Range, which can play a role in orographic precipitation.

Expanding on Lindsey's classification scheme, a classification system more appropriate for northwestern Colorado in December 1981 and January 1982 was developed based on surface observations. This system has the following divisions:

PREFRONTAL-WARM SECTOR and PREFRONTAL-COLD SECTOR: Both of these classifications are in a region of cyclonic curvature of the surface isobars and are ahead of an oncoming cold front and correspond loosely with Yu and Pielke's categories 1 and 2 in Figure 36. Unlike Yu and Pielke's categories 1 and 2, prefrontal-warm sector and prefrontal-cold sector do not rely on the location of a warm front to define them. If warm fronts do pass through northwestern Colorado in December and January,

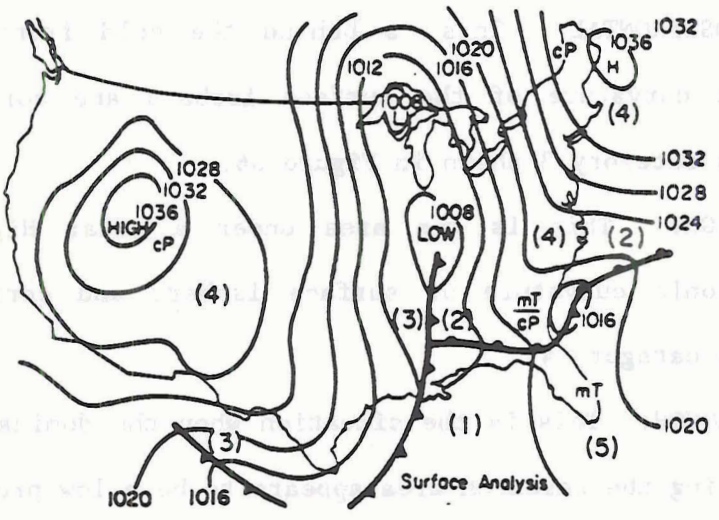

Figure 36. Example of Yu and Pielke's synoptic classification scheme. From Yu and Pielke (1986).

they are difficult to identify in this mountainous area because they may ride over cold air in the valleys rather than displace it. Instead, prefrontal-warm sector and prefrontal-cold sector were primarily differentiated by the temperature gradient across the cold front. All cold frontal passages except 1 had a strong temperature gradient. The synoptic condition ahead of the front that did not have a strong temperature gradient is labeled prefrontal-cold sector.

FRONTAL: If the research area was a small area in the plains, synoptic classifications could jump directly from prefrontal to postfrontal. However, the COSE III research area is 50 by 160 km, large enough that fronts do not pass through instantly. Also, cold fronts can override cold air in valleys and lose their continuity with respect to surface observations, thereby making accurate analysis from surface maps difficult. In order to help differentiate prefrontal conditions from postfrontal, the time between clearly prefrontal conditions and clearly postfrontal conditions is labeled frontal.

POSTFRONTAL: This is behind the cold front in the region of cyclonic curvature of the surface isobars and corresponds to Yu and Pielke's category 3 shown in Figure 36.

HIGH: This is the area under a polar High in a region of anticyclonic curvature of surface isobars and corresponds to Yu and Pielke's category 4.

TROUGH: This is the situation when the dominant synoptic feature influencing the research area appears to be a low pressure trough in the lee of the Front Range. This category also includes other times not

associated with frontal weather when there were strong cross-barrier pressure gradients with higher pressures to the west.

STATIONARY FRONT: There are times when cold fronts can move through the plains but become "stuck" on the Rocky Mountains. These stationary fronts can increase greatly in north/south extent until they stretch all the way from Alberta to New Mexico, but do not penetrate very far west into the Rocky Mountains. This category includes the times when a stationary front, while not necessarily being over the research area, was the major synoptic scale feature in the vicinity of the research area.

LOW: These are situations of relatively low pressure when no other major synoptic feature appears to be affecting the region. There are no fronts nearby. There are no strong pressure gradients. The region is not under a High. Instead, the region is showing relatively low pressure.

UNCERTAIN: These are the times that did not fit into any of the 9 other categories. Only two periods of a few hours each had to be classified as uncertain. During these times it was clear that precipitation was falling, but it was unclear what other synoptic classification could be appropriately applied.

There are two advantages to having a synoptic classification scheme that has as many different classifications as this one. The first advantage is that a phenomenon that occurs only under precise synoptic conditions is less likely to be hidden in a broad classification that involves more varied synoptic conditions. The second advantage is that the uncertain category can be smaller. In this case, only nine of the 708 hours of data had to be classified as uncertain.

Table 3 shows the number of times each synoptic classification occurred in the December 1981 to January 1982 data set being used, as well

Table III

Category	Number of events	Average hours per event	Percent of Hours with Precipitation and Valid Wind Data
Prefrontal-Warm Sector	11	11.8	78
Prefrontal-Cold Sector	1	10.0	100
Frontal	10	3.8	82
Postfrontal	11	10.4	82
High	12	25.3	40
Trough	11	29.5	52
Stationary Front	4	52.5	68
Low	3	14.3	67
Uncertain	2	4.5	100

as the average number of hours per event, and what percent of those hours had precipitation and valid wind data. It is only those hours with precipitation and valid valley floor wind data, shown in Figure 37, that are analyzed in this chapter. The procedure for analyzing this data is the same as that described in Chapter 3 except this time the computer program examines each synoptic classification separately.

4.3. Results

4.3.1. Relationship between Synoptic Classification and Decoupled Flow

One might expect that when a trough was present east of the Rocky Mountains, a strong cross-barrier flow would develop that would diminish the length of low-level decoupled flow. However, as shown in Figure 38, that is not the case for the Yampa Valley. Troughs instead showed a minimum at short distances of decoupled flow. Interestingly, and perhaps

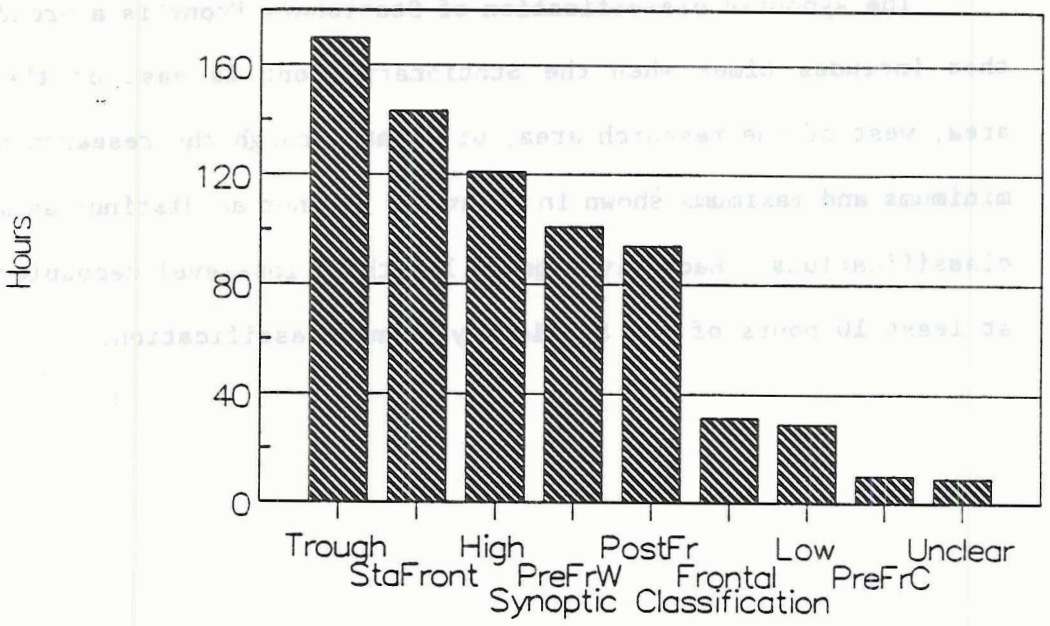

Figure 37. Hours with precipitation and valid valley floor wind data per synoptic classification.

significant to the question of why a secondary precipitation maximum occurred at 74 km of decoupled flow, troughs also showed a secondary minimum at 74 km of decoupled flow.

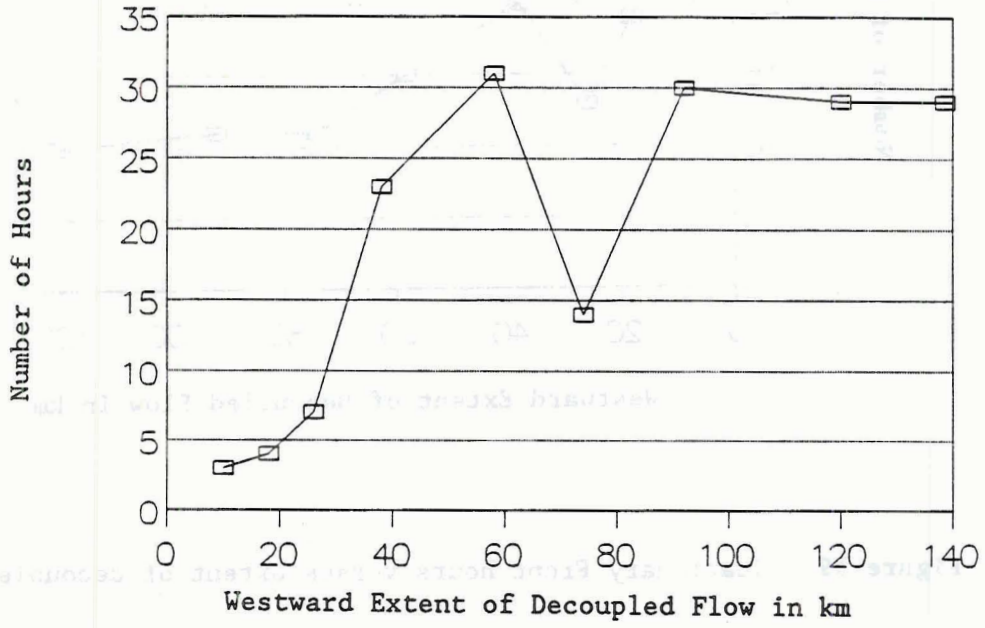

Figure 38. Trough hours versus extent of decoupled flow.

The synoptic classification of Stationary Front is a broad category that includes times when the Stationary Front is east of the research area, west of the research area, or right through the research area. The minimums and maximums shown in Figure 39 are not as distinct as many other classifications. Each division of length of low-level decoupled flow has at least 10 hours of the Stationary Front classification.

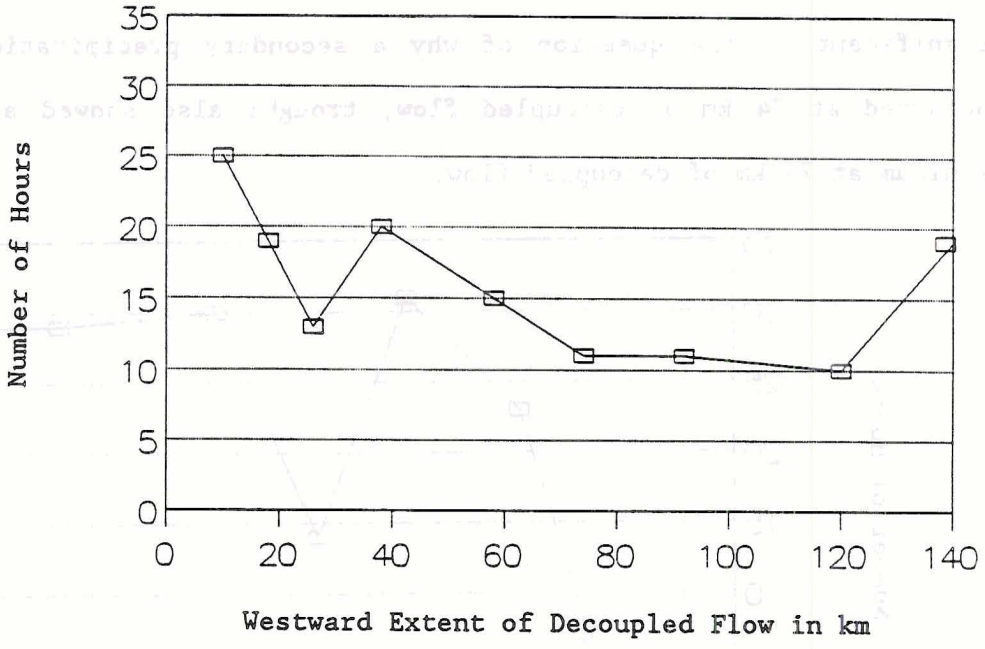

Figure 39. Stationary Front hours versus extent of decoupled flow.

As shown in Figure 40, highs do show a distinct minimum and maximums. There is a marked minimum at 38 km and, interestingly, there are maximums at both very short decoupled flows and very long decoupled flows.

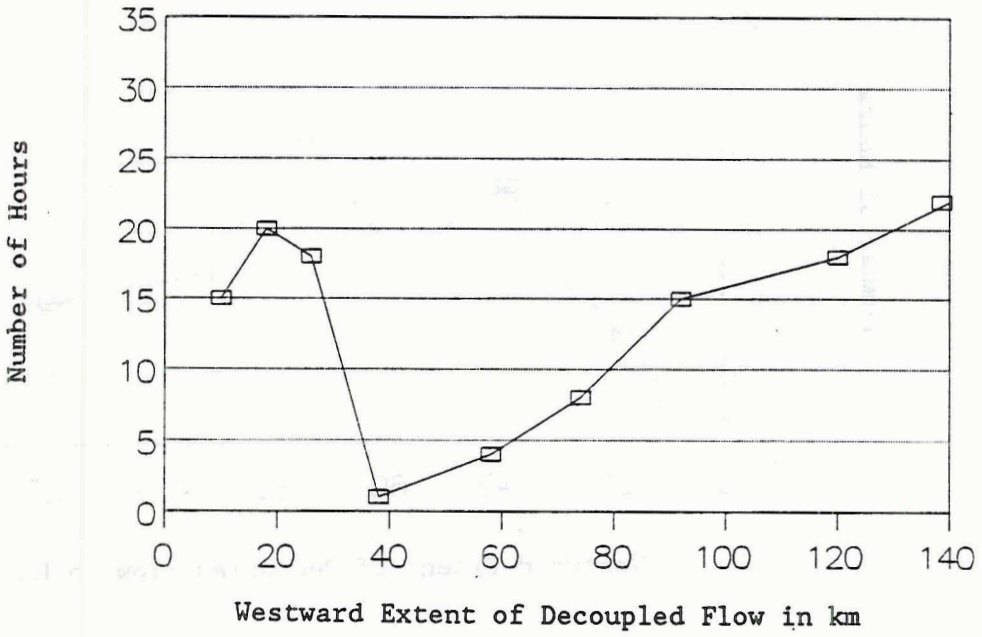

Figure 40. High hours versus extent of decoupled flow.

Figure 41 indicates that stability and wind conditions typical of the synoptic classification Prefrontal - Warm Sector are associated with low-level decoupled flows in the middle range.

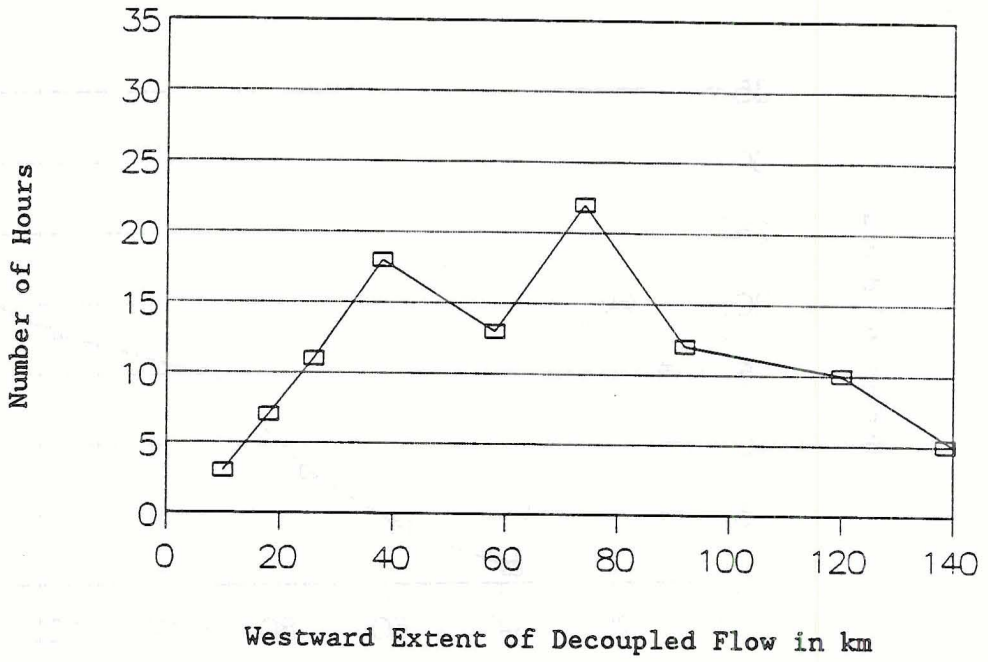

Figure 41. Prefrontal - Warm Sector hours versus extent of decoupled flow.

Figure 42 also shows clearly that certain synoptic conditions favor the creation of particular length of decoupled flow. In this case, Postfrontal conditions create very short low-level decoupled flows.

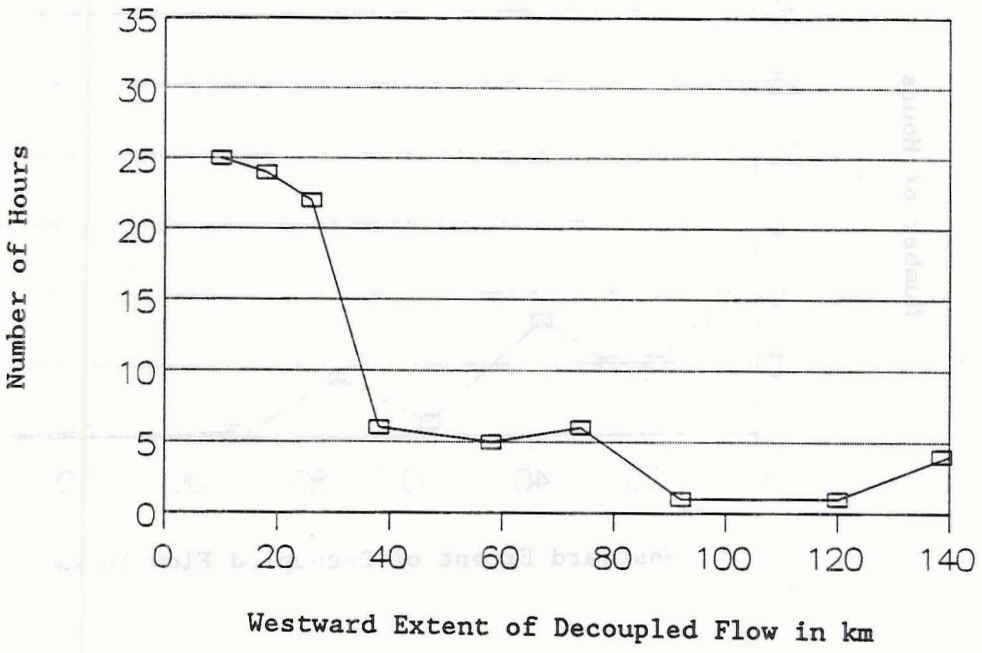

Figure 42. Postfrontal hours versus extent of decoupled flow.

As evident from Figure 43, frontal passage is not conducive to the formation of low-level decoupled flow extending far to the west.

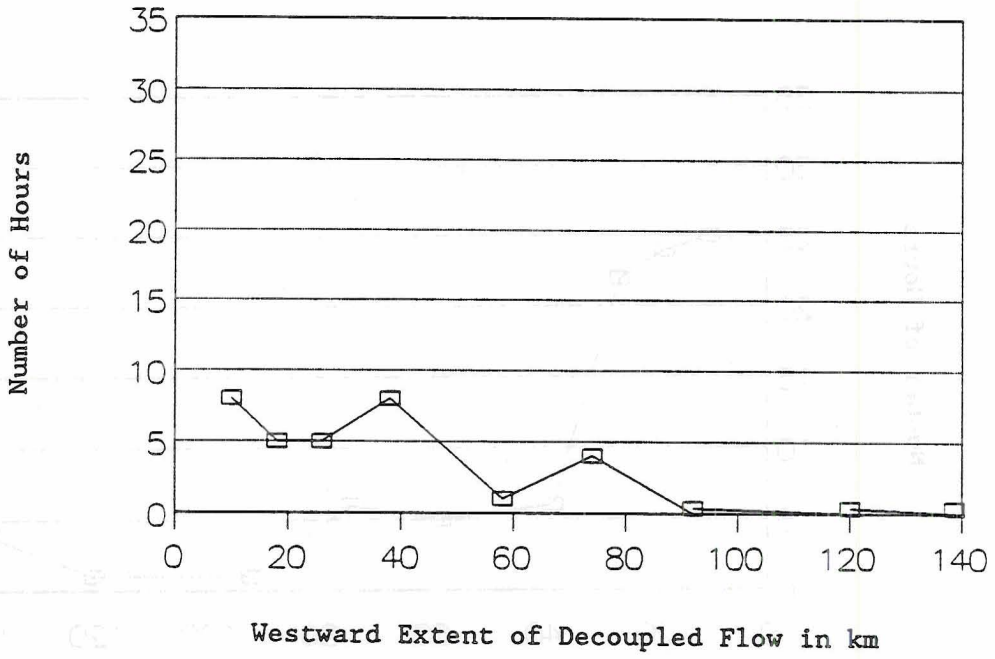

Figure 43. Frontal hours versus extent of decoupled flow.

Lows do favor decoupled flow extending far to the west, as shown in Figure 44.

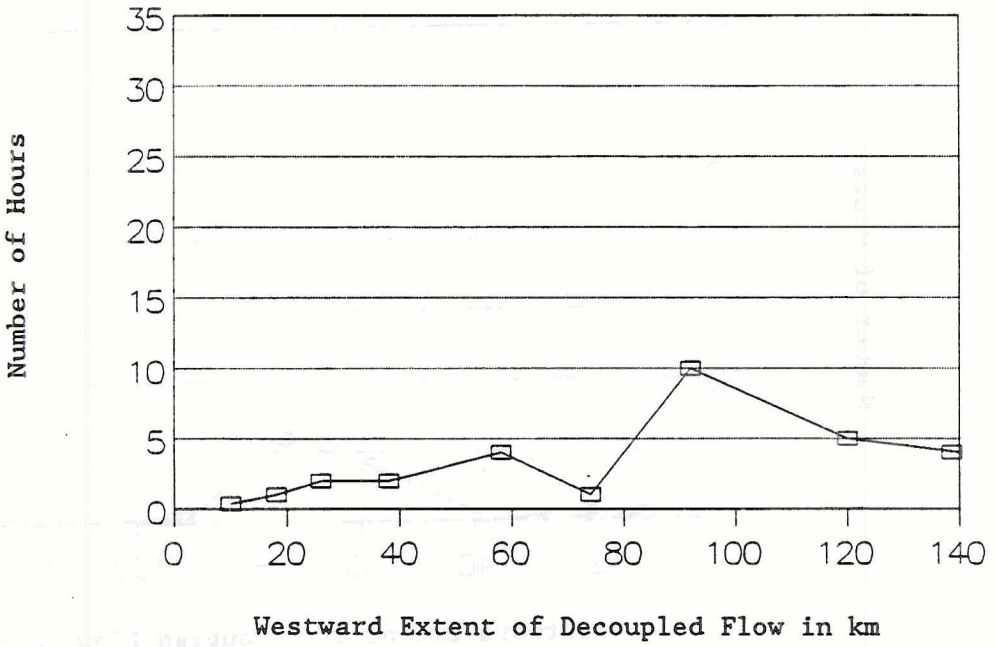

Figure 44. Low hours versus extent of decoupled flow.

The Prefrontal - Cold Sector hours all fell within the 58 to 74 kilometer distance of decoupled flow, as shown in Figure 45.

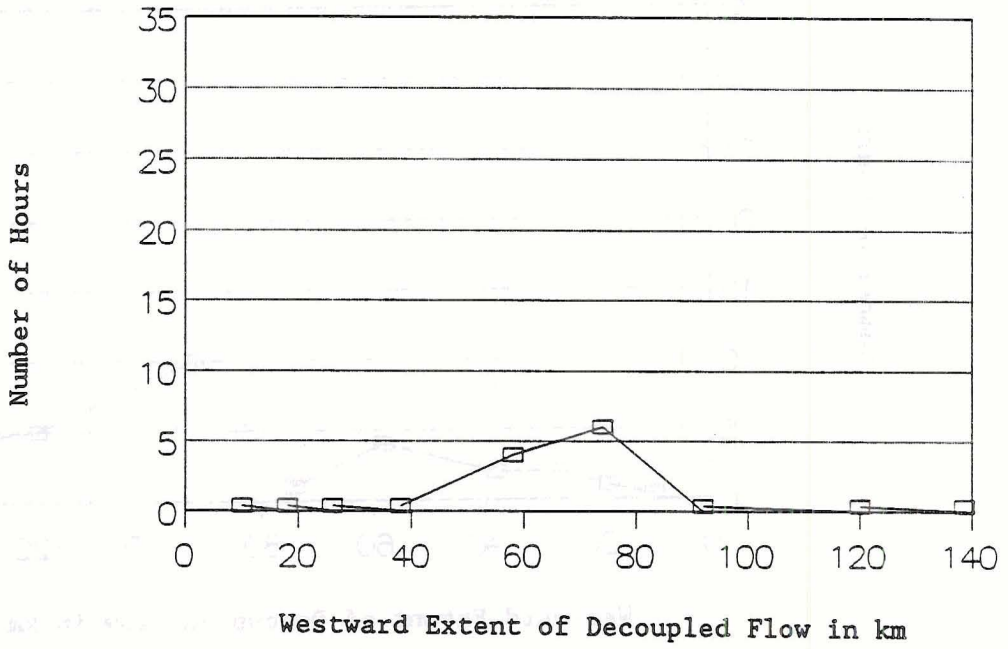

Figure 45. Prefrontal - Cold Sector hours versus extent of decoupled flow.

As Figure 46 indicates, most of the nine hours that had to be classified as Uncertain also fell in the 58 to 74 km length of decoupled flow.

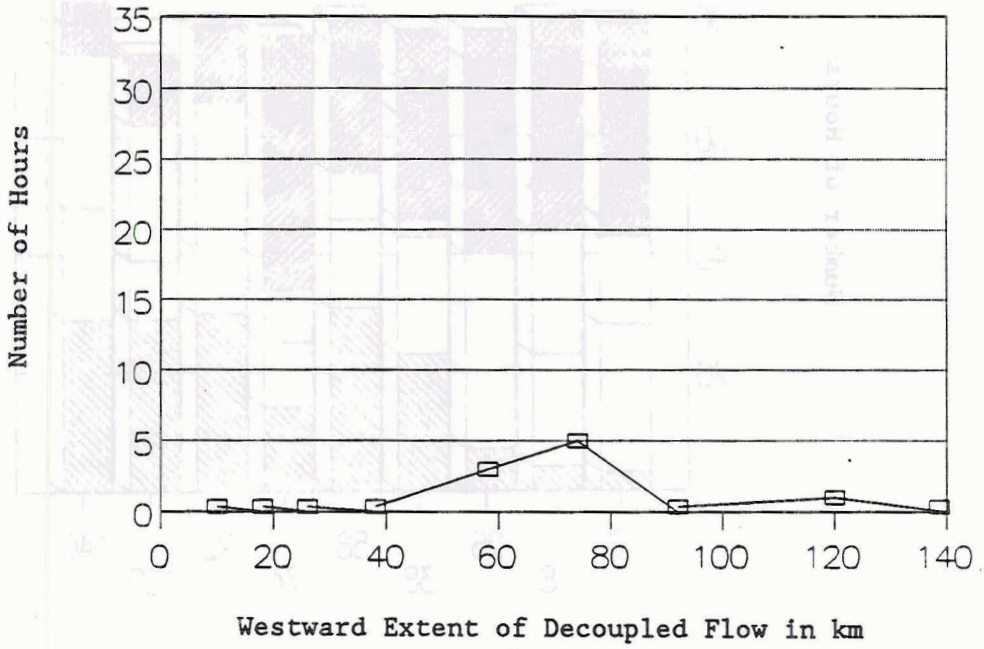

Figure 46. Uncertain hours versus extent of decoupled flow.

The different synoptic classifications and how the mix of them varies with the degree of decoupled flow is shown in Figure 47.

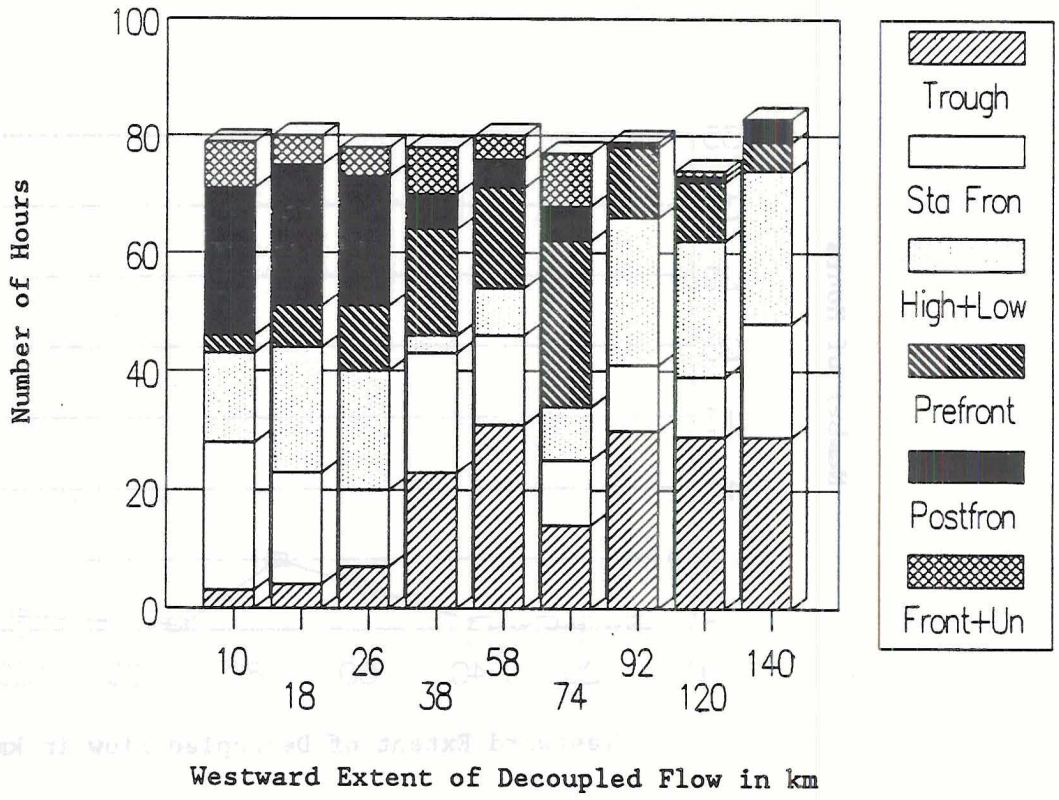

Figure 47. Total synoptic classifications per extent of decoupled flow. To fit on the graph, some classifications had to be combined. So Prefrontal includes both warm and cold sectors.

4.3.2. Relationship between Synoptic Classification and Precipitation

As one would expect, the various synoptic conditions produced highly variable precipitation intensities. As shown in Figure 48, Trough, Stationary Fronts, Highs, and Lows all produced weak precipitation. The Prefrontal - Warm Sector produced a little stronger precipitation. But the really intense precipitation occurred during Postfrontal, Frontal, Prefrontal - Cold Sector, and Uncertain conditions.

The relative importance of each synoptic classification in producing precipitation is shown in Figure 49. More precipitation falls during postfrontal conditions than falls in any other 2 synoptic classifications. Prefrontal - Cold Sector and Uncertain produced intense precipitation but for only a few hours over the course of the study. But as shall be shown

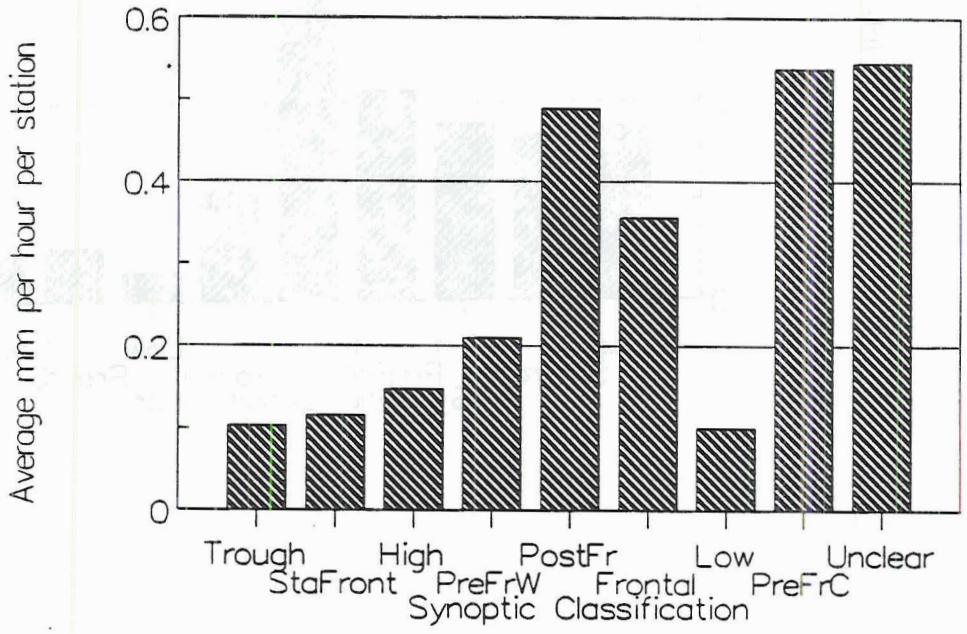

Figure 48. Precipitation intensity per synoptic classification.

in Figure 50, they can have significant impact when stratified by magnitude of decoupled flow.

To create the stacked bar graph in Figure 50, the average precipitation intensity per synoptic classification was multiplied by the number of hours each synoptic classification was present during each

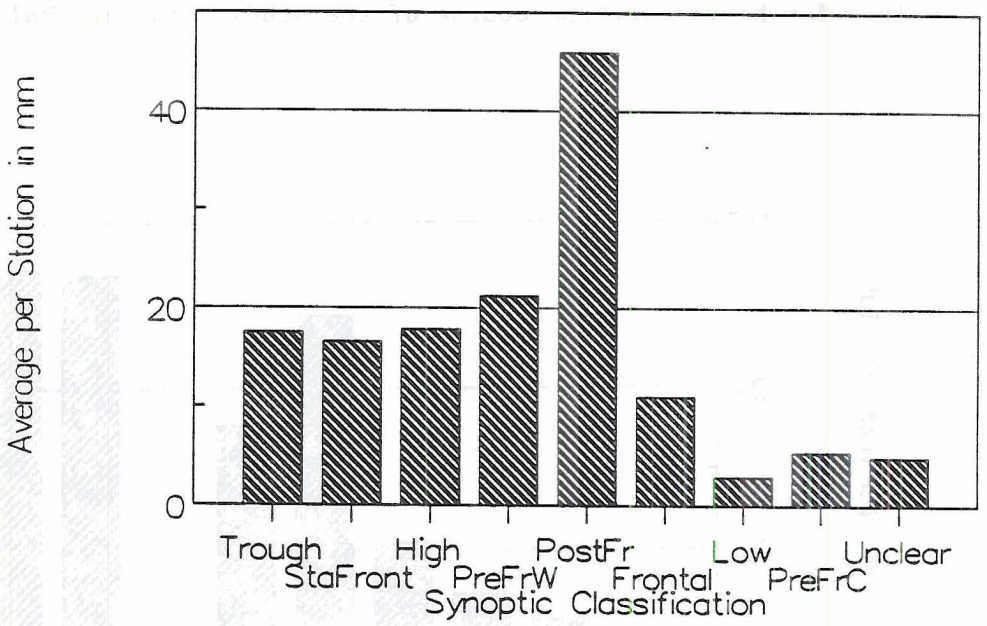

Figure 49. Precipitation produced by synoptic classification. This is precipitation intensity in mm hr^{-1} times the hours for each synoptic classification.

length classification of low-level decoupled flow. When decoupled flow was less than 30 km, precipitation was heavy and came mostly from postfrontal synoptic conditions. When the length of decoupled flow was greater than 90 km, very little precipitation came from the synoptic conditions that produced heavy precipitation. Note that the effects of the few hours of prefrontal-cold sector and uncertain synoptic classifications show up strongly in 2 stages of decoupled flow, 58 and 74

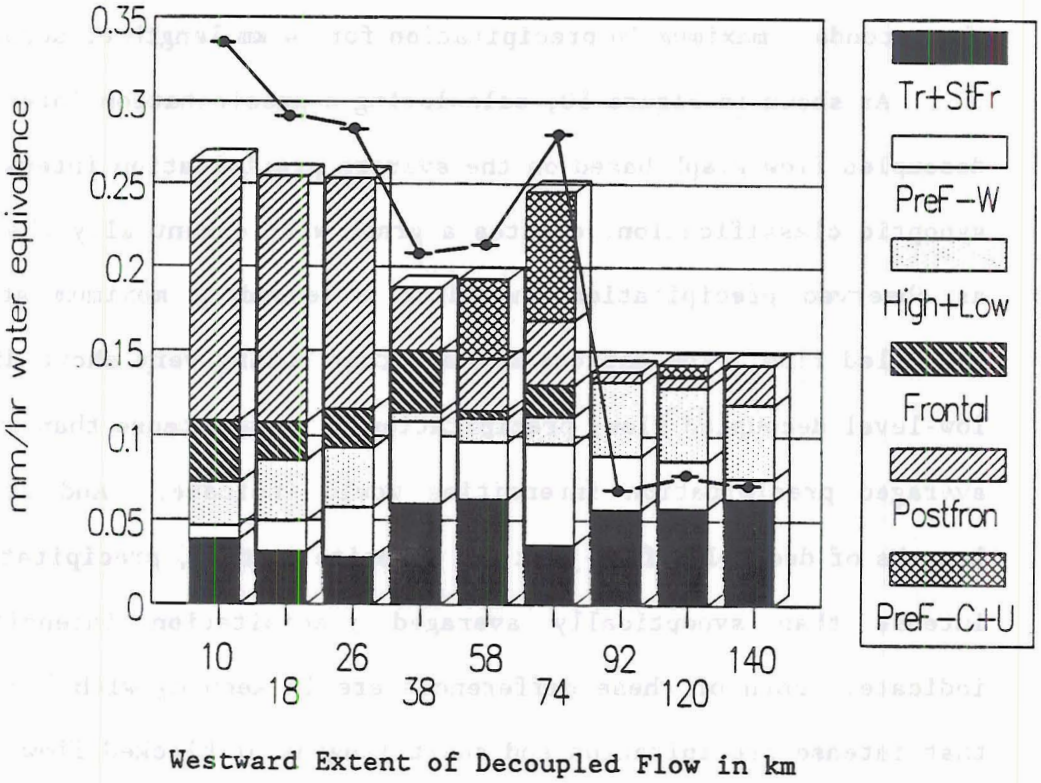

Figure 50. The stacked bar graph represents the calculated contribution to precipitation intensity weighted by the average intensity per synoptic classification. Line and marker graph represents observed precipitation intensity.

km. The line and marker graph superimposed over the stacked bar graph is the actual precipitation intensity calculated in Chapter 3.

4.4. Discussion

One of the prime questions this analysis has sought to answer is: do synoptic conditions play a role in the creation of the precipitation intensity versus decoupled flow curve with particular emphasis on the secondary maximum at 74 km? It was hypothesized in Chapter 3 that one should expect a precipitation maximum at very short degree of low-level decoupled flow and a precipitation minimum at very long distance of low-level decoupled flow. What could not be accounted for in Chapter 3 was the secondary maximum in precipitation for 74 km length of decoupled flow.

As shown in Figure 50, calculating a precipitation intensity versus decoupled flow graph based on the average precipitation intensity of each synoptic classification, creates a graph with essentially the same shape as observed precipitation including a secondary maximum at 74 km of decoupled flow. The differences are that during very short distances of low-level decoupled flow, precipitation is more intense than synoptically averaged precipitation intensities would indicate. And at very long lengths of decoupled flow just the opposite is true, precipitation is less intense than synoptically averaged precipitation intensities would indicate. Both of these differences are in keeping with the hypothesis that intense precipitation and short lengths of blocked flow can both be caused by strong cross-barrier winds and that weak precipitation and long distances of low-level blocked flows can both result from weak cross-barrier winds.

The similarity in the secondary precipitation maximum in both the observed and synoptically averaged precipitation graphs supports the conclusion that the secondary maximum in precipitation at 74 km of decoupled flow is caused by synoptic scale conditions. Specifically, the secondary maximum can be attributed to the intense precipitation associated with Prefrontal-Cold Sector and Uncertain synoptic classifications.

5. Diurnal Variations

5.1. Introduction

When looking at the relationship between the magnitude of low-level decoupled flow upstream of a mountain barrier and winter orographic precipitation, other factors that can influence precipitation should also be examined to isolate the role of low-level decoupled flow. The two other major factors that needed study for this reason are variations with synoptic classifications and diurnal variations. Variations with synoptic classifications were examined in Chapter 4. Diurnal variations in both precipitation and length of low-level decoupled flow will now be examined.

The classic mountain/valley circulation model described by Defant, 1951, depicts diurnal variations in low-level flow in mountains, with upvalley flows during the day time and down valley flows at night. This model predicts low-level winds on sunny summer days very well. However, this research deals with cloudy days in winter. King (1988) has researched low-level flows in several mountain valleys in winter time where he has found low-level drainage flows and cold pooling in high mountain valleys both day and night.

Grant, 1969, has found a significant 3 AM LST maximum in precipitation in some mountain stations such as Climax shown in Figure 51 and in Ouray and Wagon Wheel Gap shown in Figures 52 and 53. Other Colorado stations such as Silverton, Telluride, and Mesa Verde exhibit less diurnal variation with an afternoon maximum as shown in Figure 54.

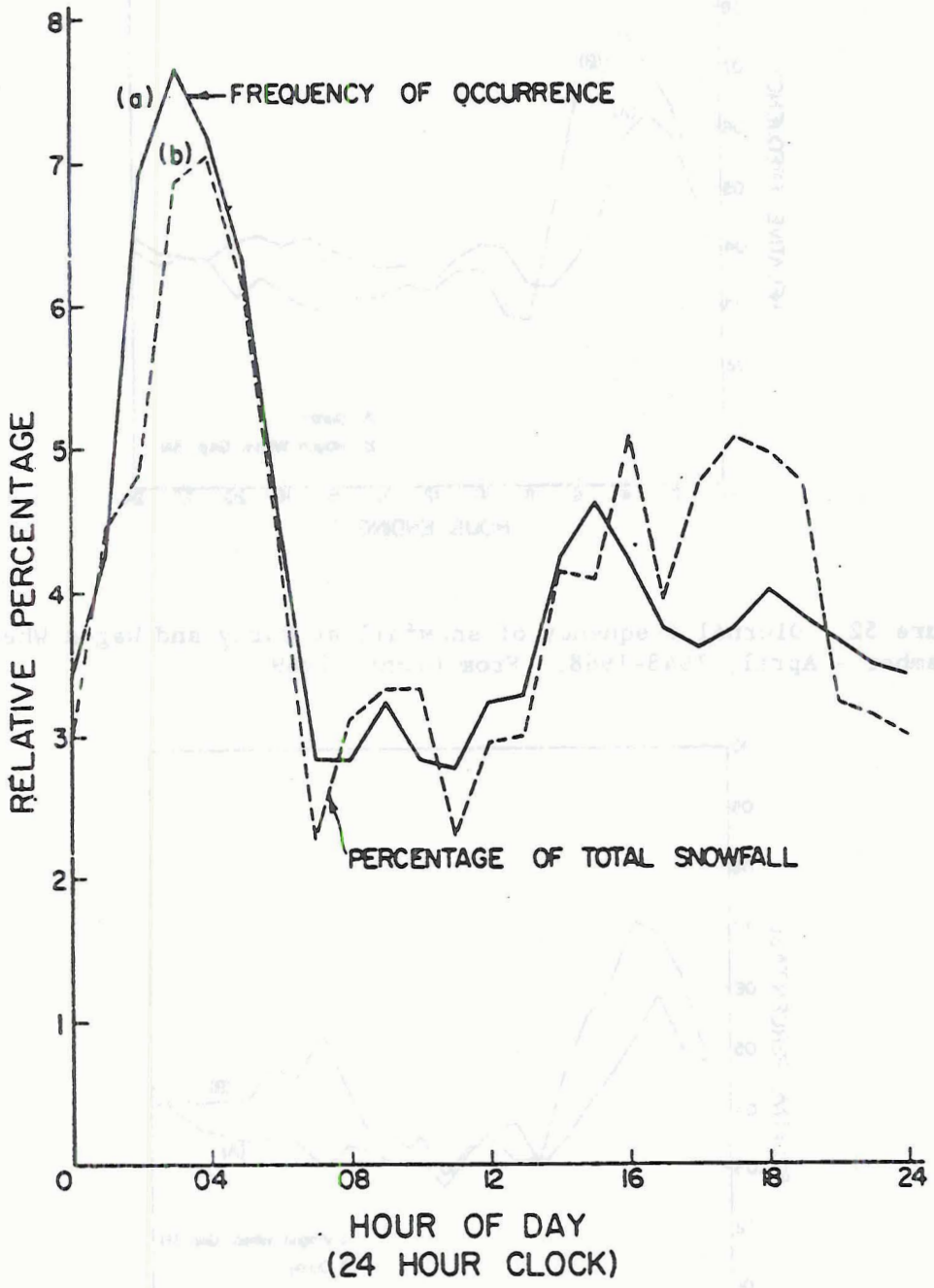

Figure 51. Distribution of snowfall at Climax, Colorado, as a function of the hour of day, November through May, 1964-67. From Grant, 1969.

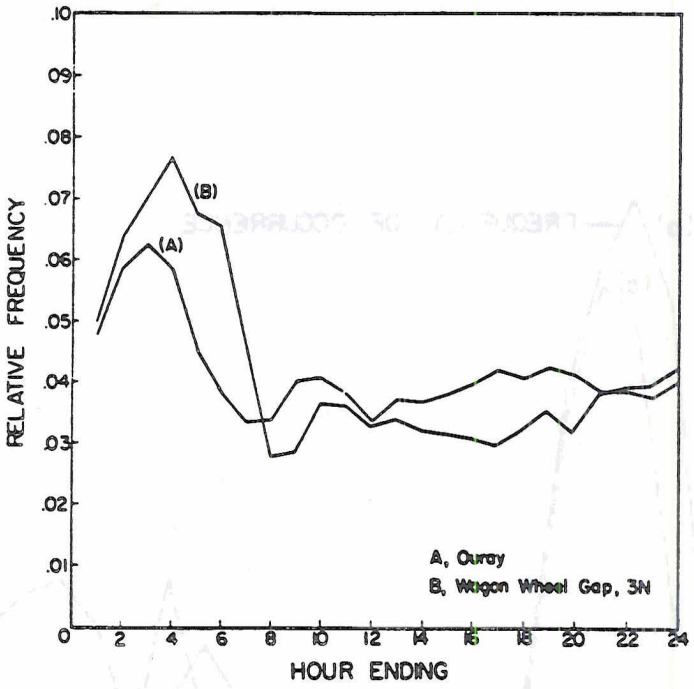

Figure 52. Diurnal frequency of snowfall at Ouray and Wagon Wheel Gap, November - April, 1948-1968. From Grant, 1969.

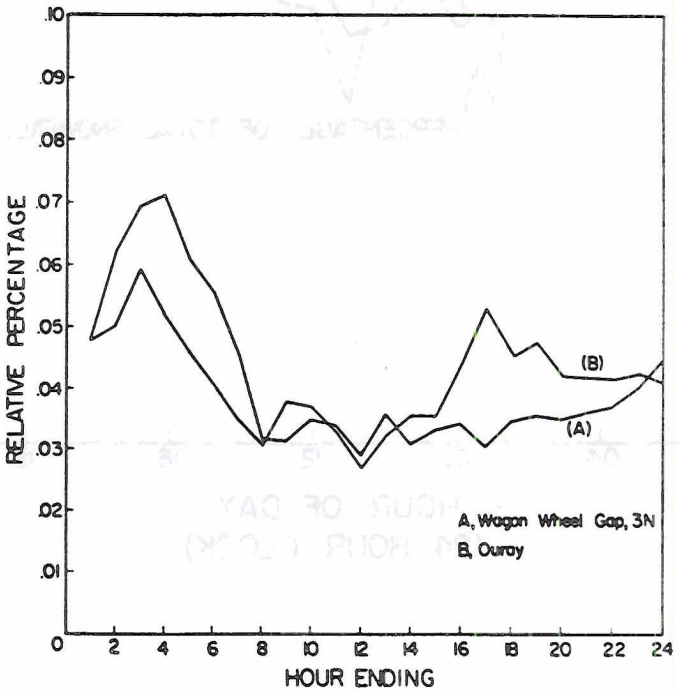

Figure 53. Relative percent of daily snowfall occurring at the respective hours of the day at Wagon Wheel Gap and Ouray, November - April, 1948-1968. From Grant, 1969.

Within the COSE III research area, data from the National Weather Service station at Craig shows a morning maximum in winter and minimum in the afternoon as illustrated Figure 55. Figure 56 shows that for the station located in the Park Range east of Steamboat Springs from 1967 to 1969, the diurnal variation in precipitation was small in December and had a midday maximum and midnight minimum in January.

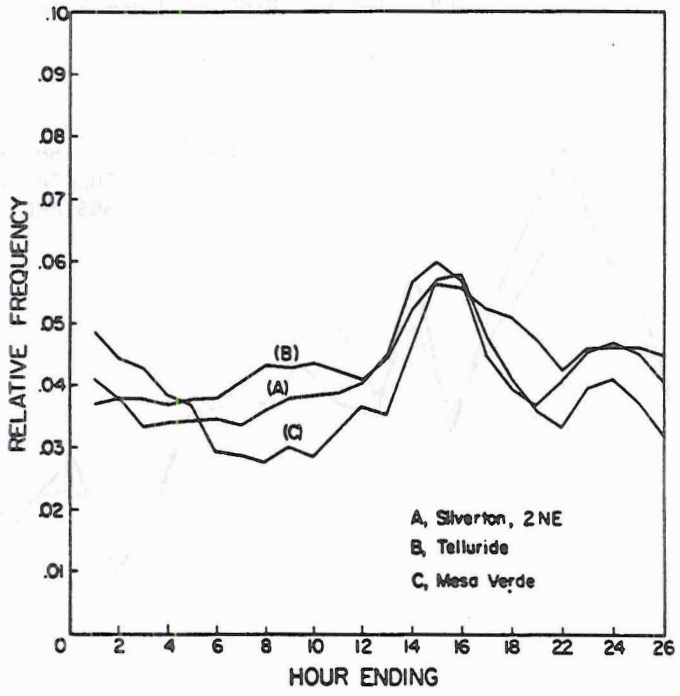

Figure 54. Diurnal frequency of snowfall at Silverton, Telluride, and Mesa Verde, November - April, 1948-1968. From Grant, 1969.

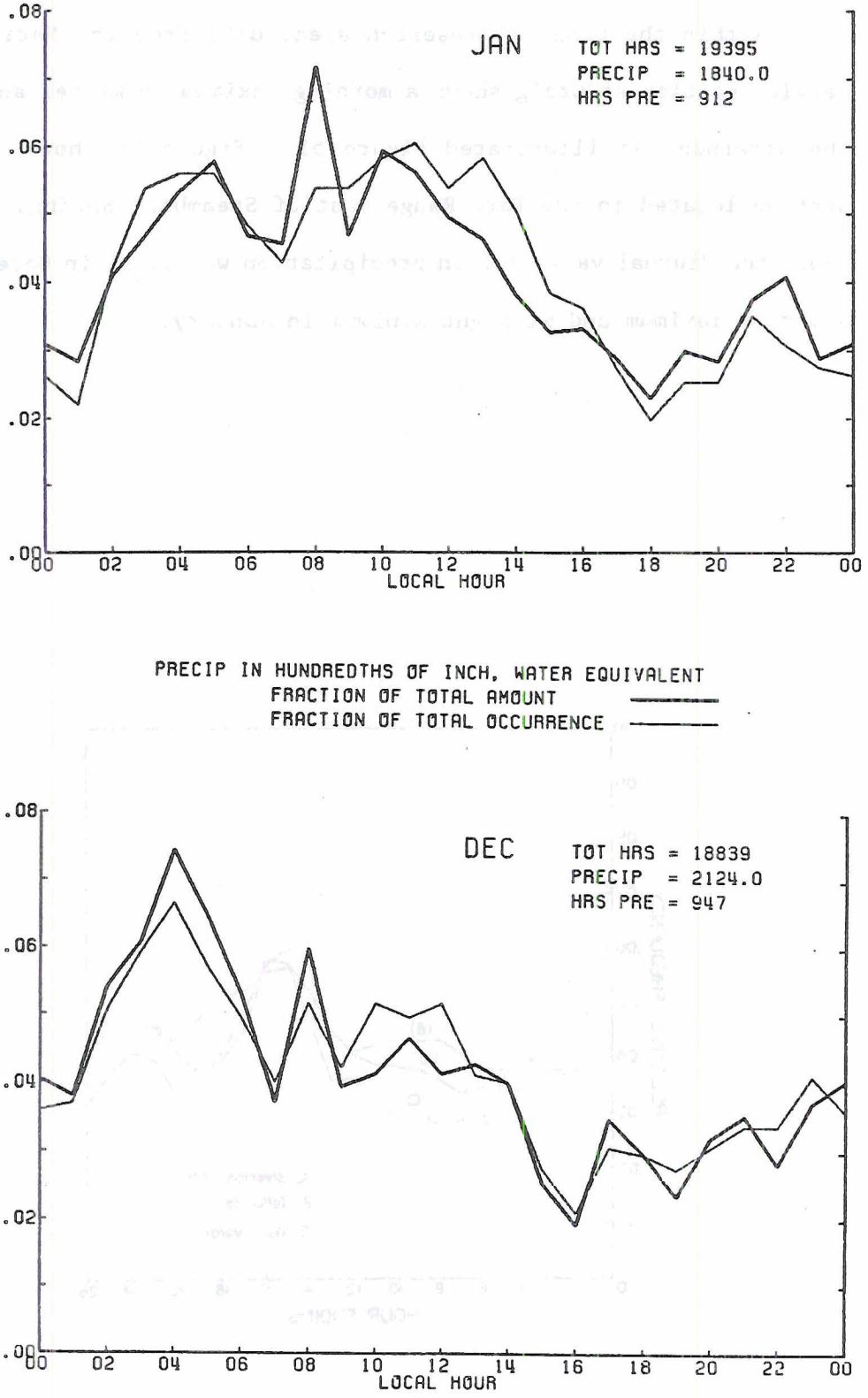

Figure 55. Diurnal variation in precipitation at Craig Colorado for January and December. From Rilling, 1989.

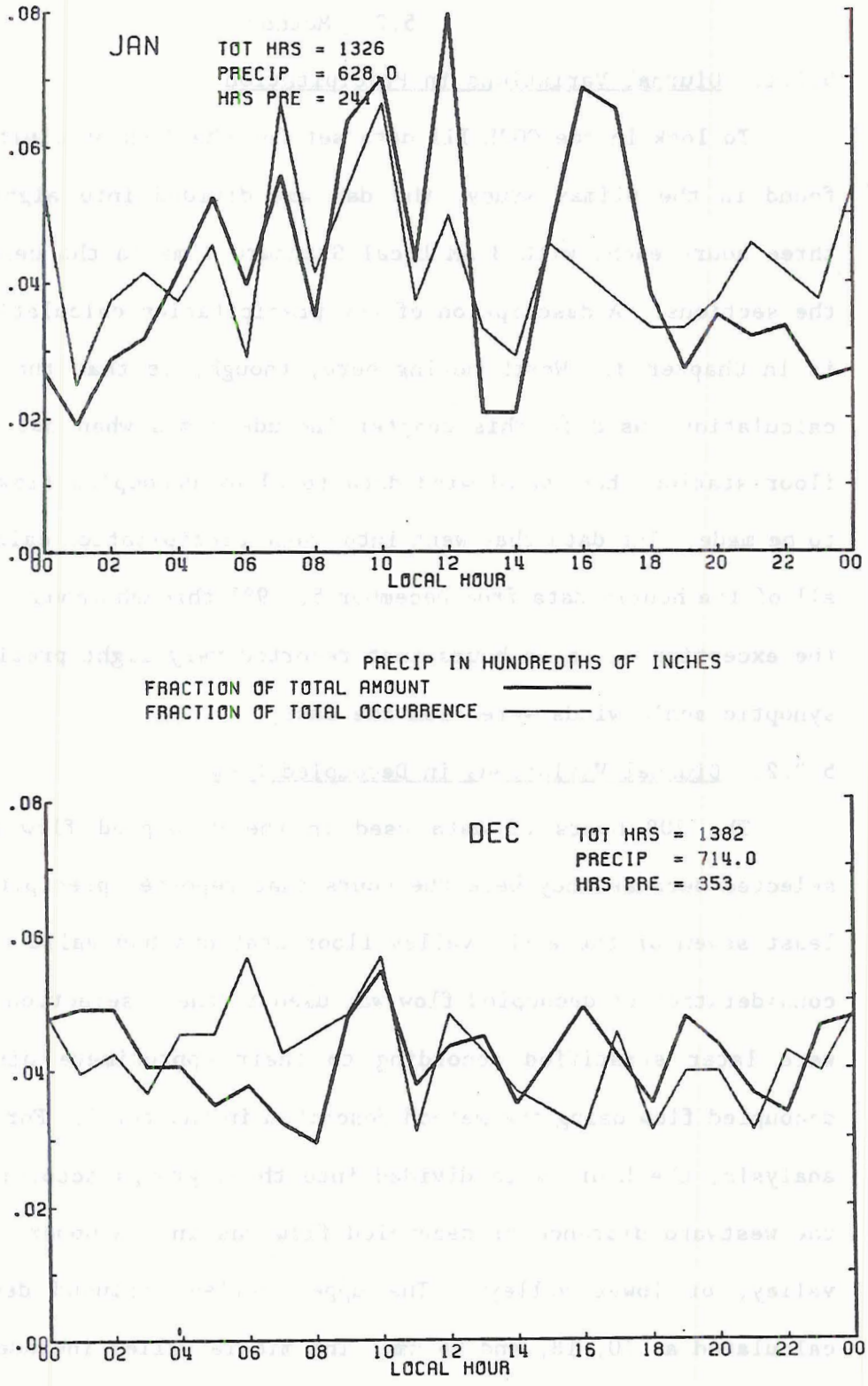

Figure 56. Diurnal variation in precipitation from Rabbit Ears Pass located in the Park Range southeast of Steamboat Springs, CO, for January and December, 1967-1969. From Rilling, 1989.

5.2. Methods

5.2.1. Diurnal Variations in Precipitation

To look in the COSE III data set for the 3 AM precipitation maximum found in the Climax study, the day was divided into eight sections of three hours each, with 3 AM Local Standard Time in the center of one of the sections. A description of how precipitation calculations were made is in Chapter 3. Worth noting here, though, is that the precipitation calculations used in this chapter include times when not enough valley floor stations had valid wind data to allow decoupled flow calculations to be made. The data that went into these precipitation calculations were all of the hourly data from December 5, 1981 through January 31, 1982 with the exception of three hours that reported very light precipitation when synoptic scale winds were from the east.

5.2.2. Diurnal Variations in Decoupled Flow

The 708 hours of data used in the decoupled flow analysis were selected because they were the hours that reported precipitation when at least seven of the eight valley floor stations had valid wind data. No consideration of decoupled flow was used in their selection. These hours were later stratified according to their approximate distance of the decoupled flow using the method described in Chapter 3. For the following analysis, the hours were divided into three groups according to whether the westward distance of decoupled flow was in the upper valley, middle valley, or lower valley. The upper valley included decoupled flows calculated as 10, 18, and 26 km. The middle valley included 38, 58, and 74 km. And the lower valley included decoupled flows stretching 92, 120, and 140 km west of the barrier.

5.3. Results

5.3.1. Diurnal Variations in Precipitation

Total precipitation at all 24 stations in the Yampa Valley and over the barrier did not show a 3 AM maximum during the two month period of the COSE III study. Instead, there are two maxima, one in the morning at 08-10 and the other in the middle of the night at 23-01, shown in Figure 57. The magnitude of diurnal change in total precipitation is about 25%.

To see whether the two precipitation maxima coincided with either intense precipitation or many hours of precipitation, the diurnal variation in the hours reporting precipitation and precipitation intensity

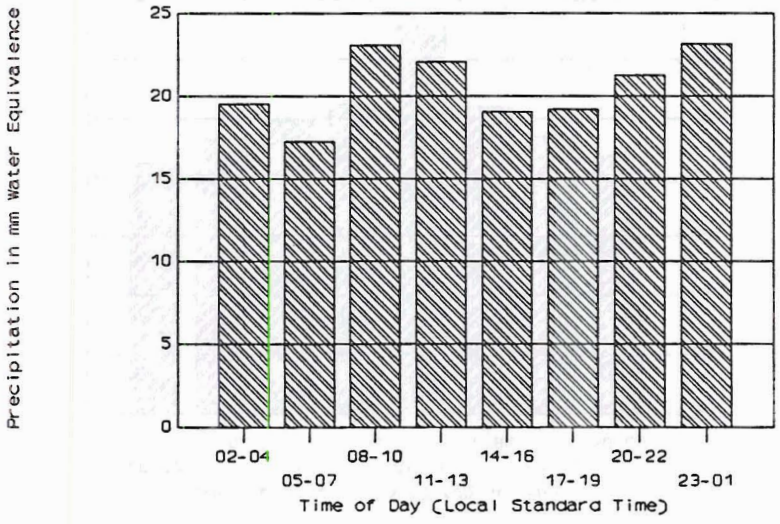

Figure 57. Diurnal variations in total precipitation recorded by PROBE stations in the COSE III study area.

were also plotted. Figure 58 shows that the hours when precipitation was reported at any of the PROBE stations has a significant peak at midday and a minimum at midnight with smooth transitions between the two. The peak in hours does not correspond with a precipitation maximum.

Precipitation intensity shown in Figure 59, does not show such a smooth progression. From a low at midday to a high at midnight, the progression is smooth. But from midnight to midday, the precipitation intensity fluctuates. The peak in precipitation intensity at 23-01 does correspond with a peak in total precipitation. It is also interesting to note that the high for hours corresponds with a low for precipitation intensity and the low for hours corresponds with the high for precipitation intensity.

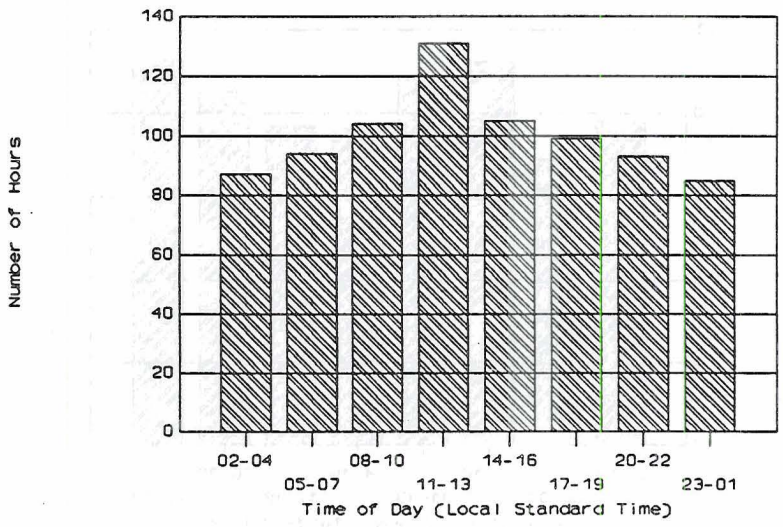

Figure 58. The diurnal variation of hours when precipitation was reported by the PROBE network.

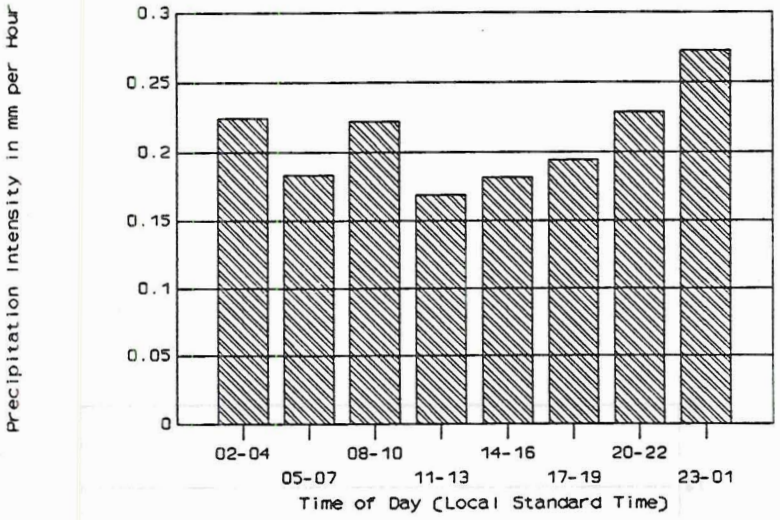

Figure 59. Precipitation intensity on a per station basis averaged for the hours when precipitation was reported at any PROBE station.

To look closer at diurnal variations in precipitation, it can be helpful to look at one precipitation group at a time. This type of analysis would show if there was a 3 AM precipitation maximum that was limited to just the mountain stations. And it would show how the precipitation maxima or minima change with location.

Precipitation Over the Barrier has two maxima and two minima, though, as shown in Figure 60, the magnitude of the diurnal fluctuation is fairly small.

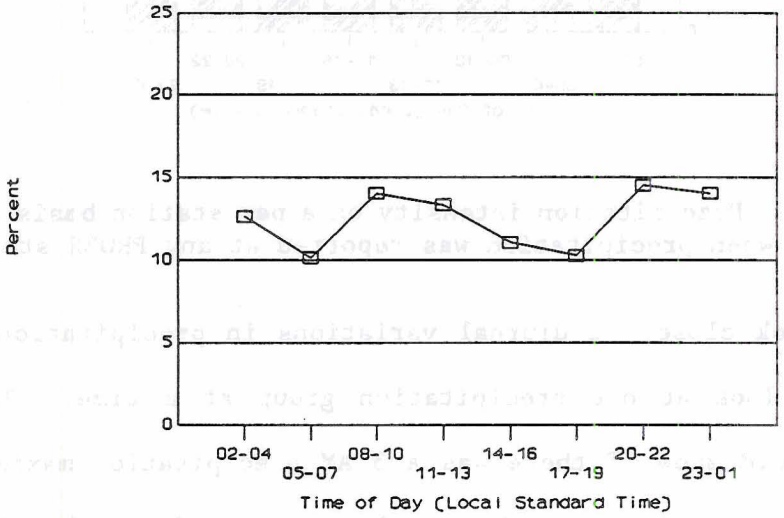

Figure 60. The diurnal variation in precipitation recorded by PROBE stations classified as Over the Barrier.

Precipitation On the Barrier also does not show large diurnal variations. But the variation it does have has a maximum at 20-22 hours and a minimum in the afternoon, 14-16 hours, as shown in Figure 61.

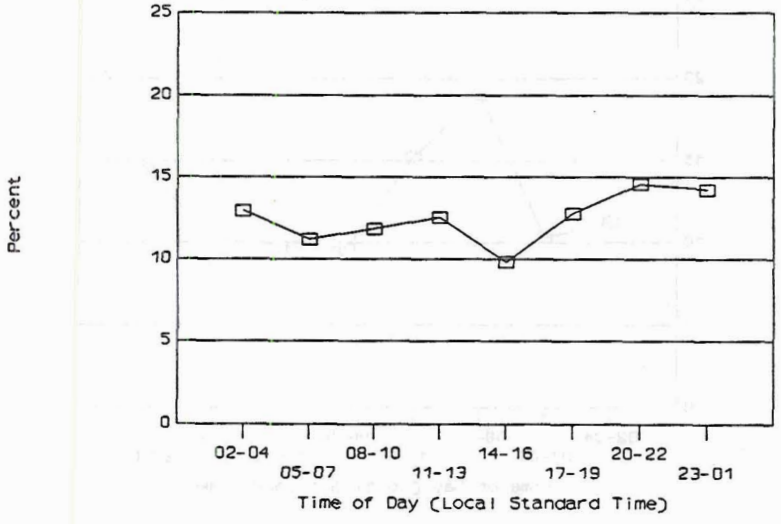

Figure 61. Diurnal variation in precipitation recorded by PROBE stations classified as On the Barrier.

Figure 62 shows that precipitation in the Upper Valley has a distinct maximum in the morning at 08-10, and a secondary maximum at midnight, 23-01.

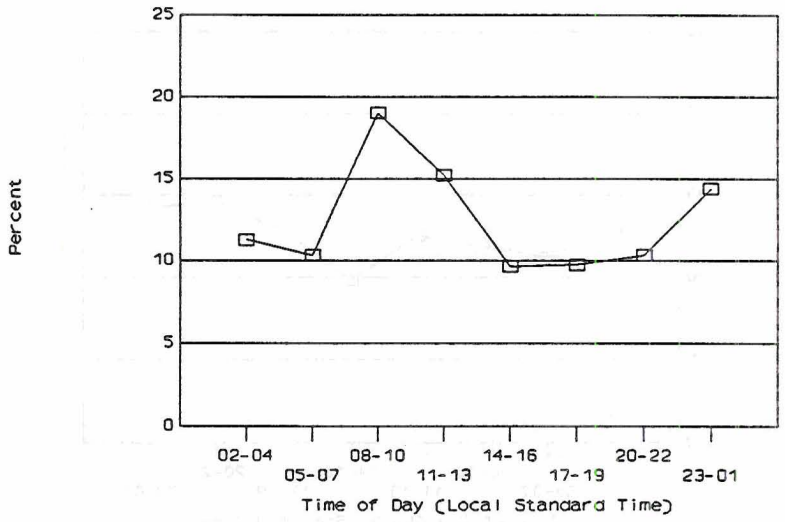

Figure 62. Diurnal variation in precipitation recorded by PROBE stations classified as Upper Valley.

The Middle Valley has a peak in precipitation in the middle of the night, but it also has a strong secondary maximum in the afternoon. The minimum, as shown in Figure 63, is at 05-07 in the morning.

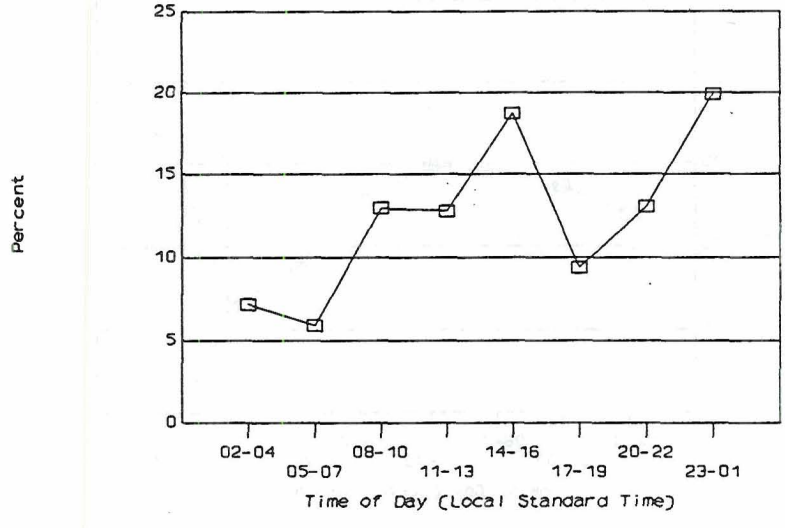

Figure 63. Diurnal variation in precipitation recorded by PROBE stations classified as Middle Valley.

Precipitation in the Lower Valley also has a maximum at midnight. During the rest of the day, the transition is very smooth to and from a secondary maximum at midday, as shown in Figure 64. A distinct minimum is at 20-22 with a secondary minimum at 02-04.

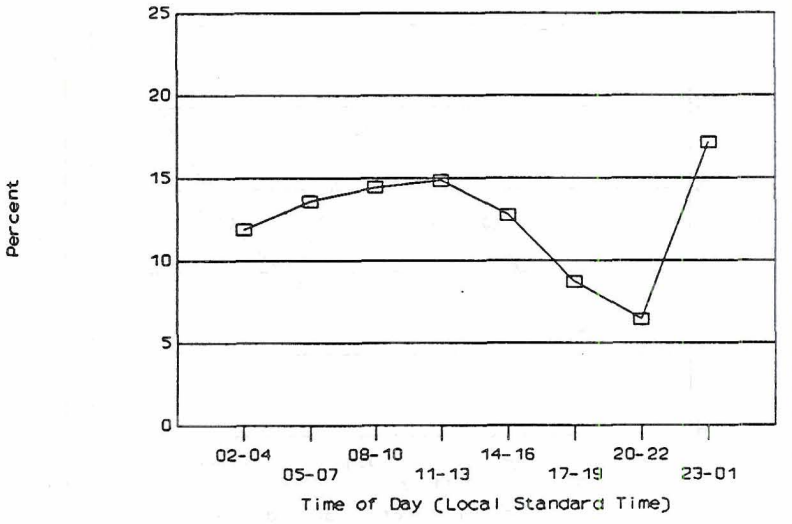

Figure 64. Diurnal variation in precipitation recorded by PROBE stations classified as Lower Valley.

Figure 65 indicates that the Valley Sides show a distinct maximum in the morning from 08-10 LST. The minimum is more diffuse with 20-07 hours showing similar low values.

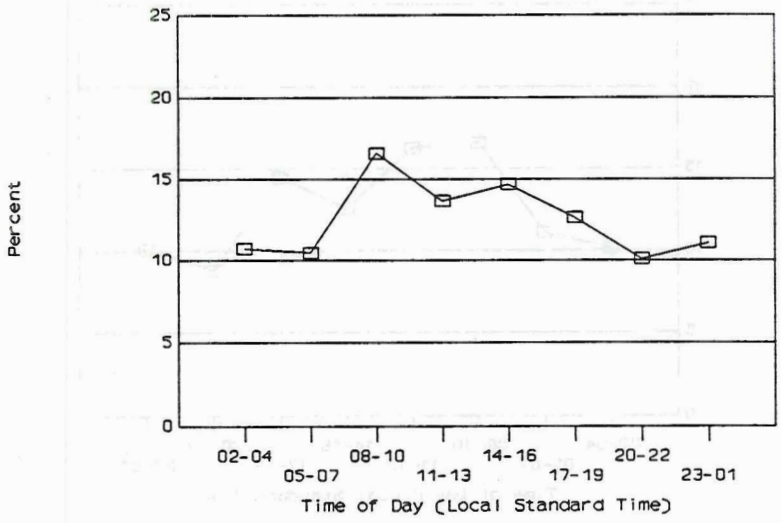

Figure 65. Diurnal variation in precipitation recorded by PROBE stations classified as Valley Sides.

Station HAR shows a maximum during the day, 08-13, and a minimum at night, 20-22. Figure 66 shows that like the Valley Sides, HAR has low values from 20-07 hours.

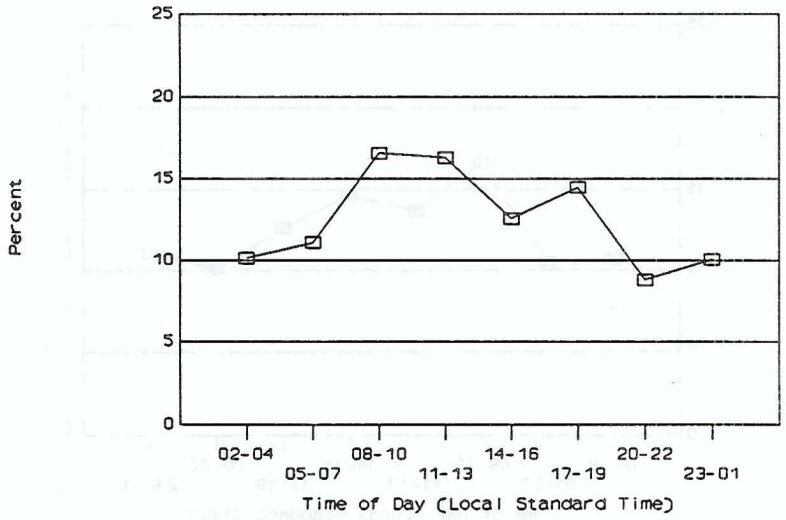

Figure 66. Diurnal variation in precipitation recorded by PROBE station HAR.

Station DIV, located far to the west, has very light precipitation. Consequently, a little fluctuation in precipitation can create a much larger percentage change for DIV than for any of the other groups. DIV showed a maximum during the day, 11-16. Its minimum, all the way down to zero was at 20-22, as shown in Figure 67.

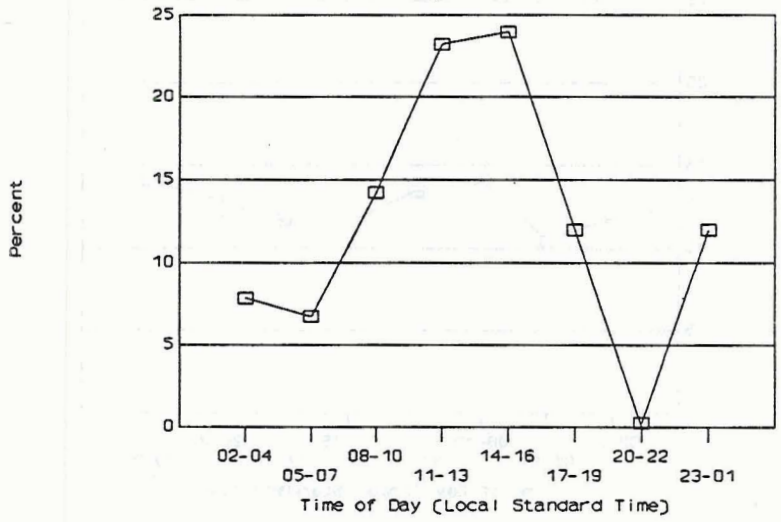

Figure 67. Diurnal variation in precipitation recorded at PROBE station DIV.

For comparison purposes, the total COSE III precipitation is charted in the same percentage manner in Figure 68. This shows slight maxima at 08-10 and 23-01 and minima at 05-07 and 14-19.

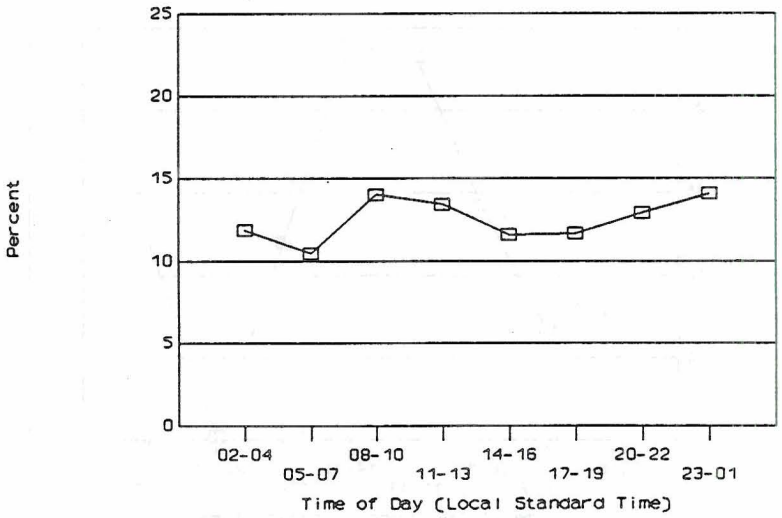

Figure 68. Diurnal variation in precipitation recorded by the entire PROBE mesonetwork.

The data set was analyzed for a phase lag in precipitation between precipitation groups. Figure 69 shows the diurnal precipitation variation in both the Upper Valley and Middle Valley which gives the appearance of a phase lag. The Upper Valley daytime maximum is 08-10 while the Middle Valley's daytime maximum is 14-16. Between 17 and 07 hours, the Upper Valley and Middle Valley's diurnal changes matched exactly in the

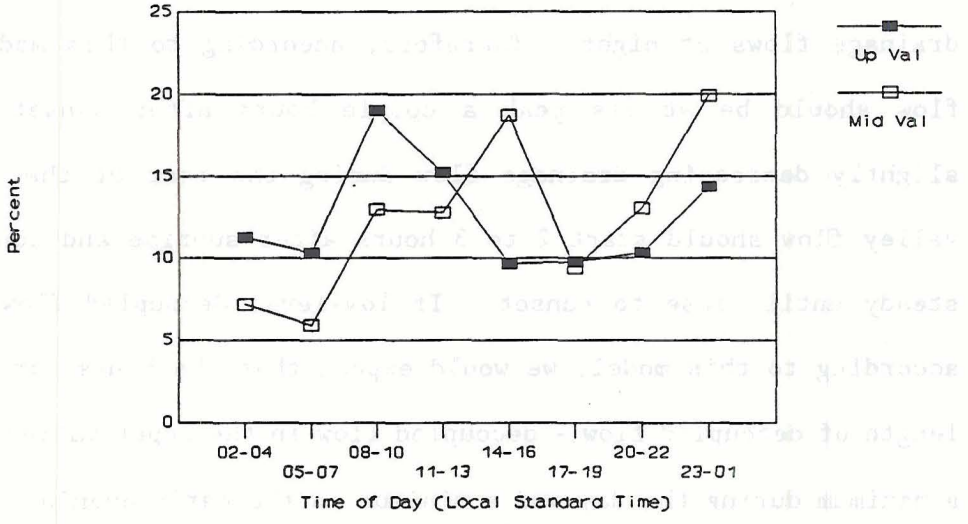

Figure 69. Diurnal variation in precipitation recorded by PROBE stations classified as Upper Valley (solid marker) and Middle Valley (open marker).

direction of change (increasing or decreasing) though not in magnitude.

Another similarity showed up between the Valley Sides and station HAR. Both had fairly steady low values from 20 to 07 hours. And both had maxima at 08-10 and fairly high values from 08 to 19 hours. The physical

similarities between HAR and the Valley Sides - HAR is on a ridge 275 meters above the valley floor but near the center of the valley - might imply that these observed diurnal changes are the result of similar physical processes.

A few other minor similarities can be found, such as the Middle Valley and Lower Valley both having maxima at 23-01, but no major systematic correlations were found.

5.3.2. Diurnal Variations in Decoupled Flow

The essence of the classic mountain/valley circulation model is that solar heating warming the valley will create up slope and up valley flows during the day and radiant cooling at night will create down valley drainage flows at night. Therefore, according to this model, drainage flow should be at its peak a couple hours after sunset followed by slightly decreasing drainage flow during the rest of the night and up valley flow should start 2 to 3 hours after sunrise and continue fairly steady until close to sunset. If low-level decoupled flow is behaving according to this model, we would expect that the hours for the shortest length of decoupled flow - decoupled flow in the upper valley - would show a maximum during the day and a minimum in the early evening. The longest degree of decoupled flow - decoupled flow in the lower valley - should show just the opposite, a maximum at night and minimum during the day. If low-level flow was behaving strictly according to this model, the transition zone of the middle valley should show its peaks during the transition from short decoupled flow maximum to long decoupled flow maximum and vice versa, namely, near sunrise and sunset.

The diurnal variation of the hours when decoupled flow was classified as being in the upper valley are shown in Figure 70. Instead of a minimum in early evening as predicted by the model, decoupled flow in the upper valley has a minimum at 08-10 in the morning. The maximum at 14-16 is close to where the model predicts. But decoupled flow at midnight is still close to the afternoon peak, which does not go along with the model at all.

Decoupled flow in the middle valley, shown in Figure 71, has a peak in the afternoon, 14-16. This behavior is similar to what the model predicts for the upper valley. If this behavior is a result of the forces described in the simple mountain/valley circulation model, it should be

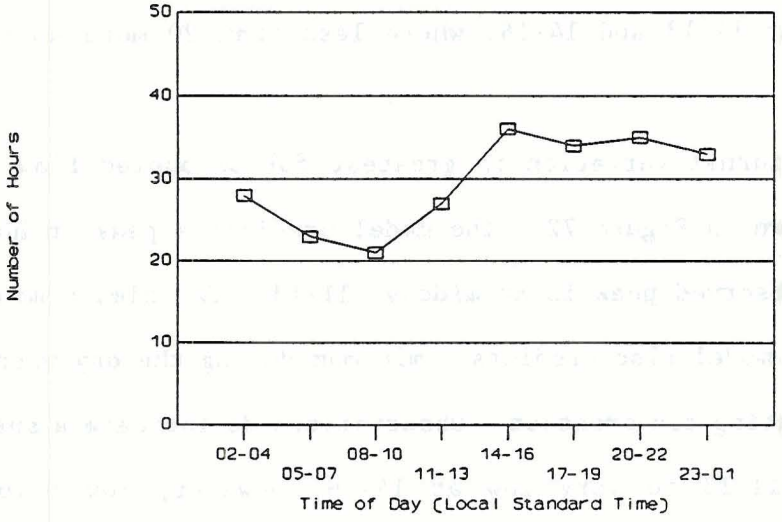

Figure 70. Hours during COSE III when the western extent of decoupled low-level flow was determined to be in the Upper Valley.

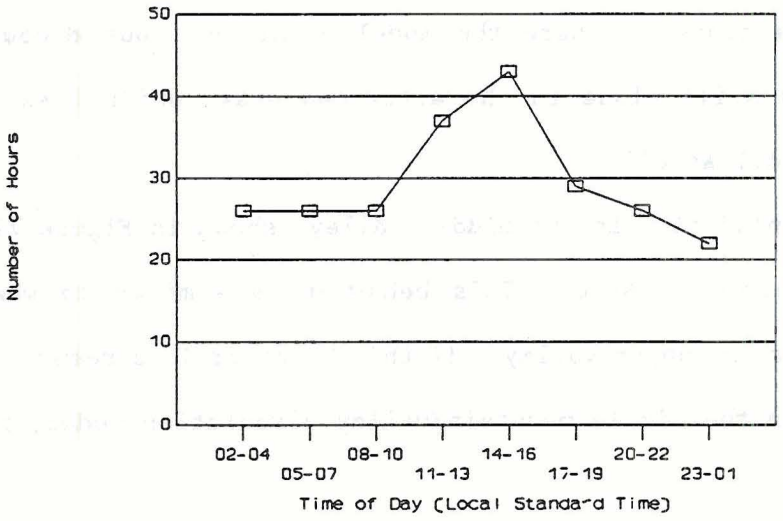

Figure 71. Hours during COSE III when the western edge of decoupled flow was determined to be in the middle valley.

noted that the majority of the hours do not show a diurnal dependence. A baseline reading of approximately 25 hours is significantly deviated from only at 11-13 and 14-16, where less than 20 more hours were added on.

The diurnal variation is greatest for decoupled flow in the lower valley, shown in Figure 72. The model predicts a peak in hours at night while the observed peak is at midday, 11-13. The simple mountain/valley circulation model also predicts a minimum during the day when the effects of solar heating are greatest. Observations do indicate a sharp drop from a high at 11-13 to very low at 14-16, however, low values are also observed late at night.

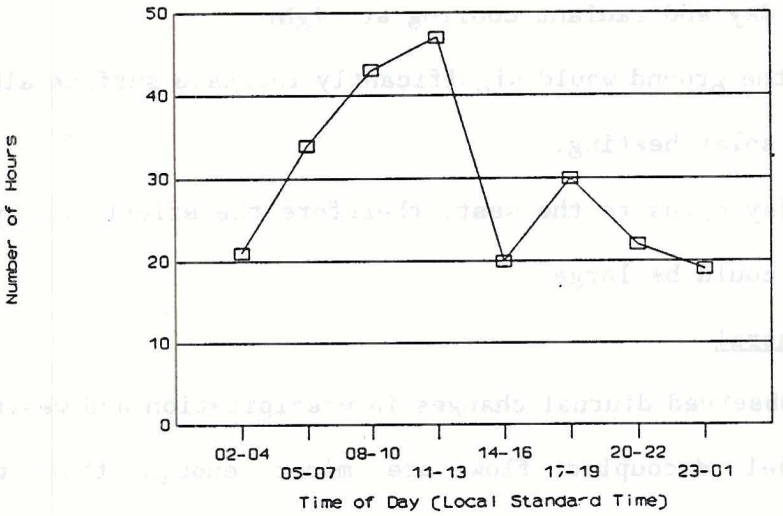

Figure 72. Hours during COSE III when the western edge of decoupled low-level flow was determined to be in the lower valley.

5.4. Discussion

5.4.1. Diurnal Variation in Precipitation

The observed diurnal variation in precipitation during COSE III is small compared to Climax. No clearly discernable phase lag between precipitation in the mountains, upper valley, middle valley, and lower valley can be determined. Though the reason for this may be that the data set is much too small to filter out the noise from individual events.

5.4.2. Diurnal Variation in Decoupled Flow

Though the middle valley shows some diurnal variation in keeping with the classic mountain/valley circulation model, the overall match of

observations with model predictions is poor. There are several reasons why this match should be poor:

- These are only hours when precipitation was reported. Therefore, clouds were covering at least part of the valley, decreasing solar heating during the day and radiant cooling at night.
- Snow on the ground would significantly increase surface albedo, thereby decreasing solar heating.
- The valley opens to the west, therefore the effects of synoptic scale west winds could be large.

5.4.3. General

The observed diurnal changes in precipitation and westward distance of low-level decoupled flow are minor enough that they do not significantly impinge upon the core of the whole research project, namely, examining the relationship between low-level decoupled flow upstream of a mountain barrier and the overlying winter orographic clouds.

6. Case Studies

6.1. Introduction

The previous sections focused on the climatology of the interaction between decoupled flow and winter orographic storms by looking at conditions for the entire month and a half of good PROBE data. This section will now focus on the specifics of two storms. The criteria for selecting the case study storms were: 1) stable conditions when convection was suppressed, 2) basic similarity in synoptic and cloud conditions, and 3) very different low level flow conditions. The storms on January 16, 1982 and January 23, 1982 filled these requirements very well. Both of these storms were shallow orographic cloud systems, a type of storm system that frequently forms in Northern Colorado as a result of a strong cross-barrier flow accompanied by mid-level moisture advected in from the west. A capping inversion is often present during these types of storms which helps keep the clouds shallow.

6.2. Synoptic Conditions

Surface weather maps for both January 16 and January 23 show a stationary front near the research area running in a generally north to south direction. Both of these stationary fronts were depicted stretching from Canada to Texas. The synoptic classification scheme described in Chapter 4 therefore put both of these storms in the classification Stationary Front.

The 700 hPa maps shown in Figures 73 and 74 indicate advection of moisture from the west. Table 4 shows that cloud height winds were

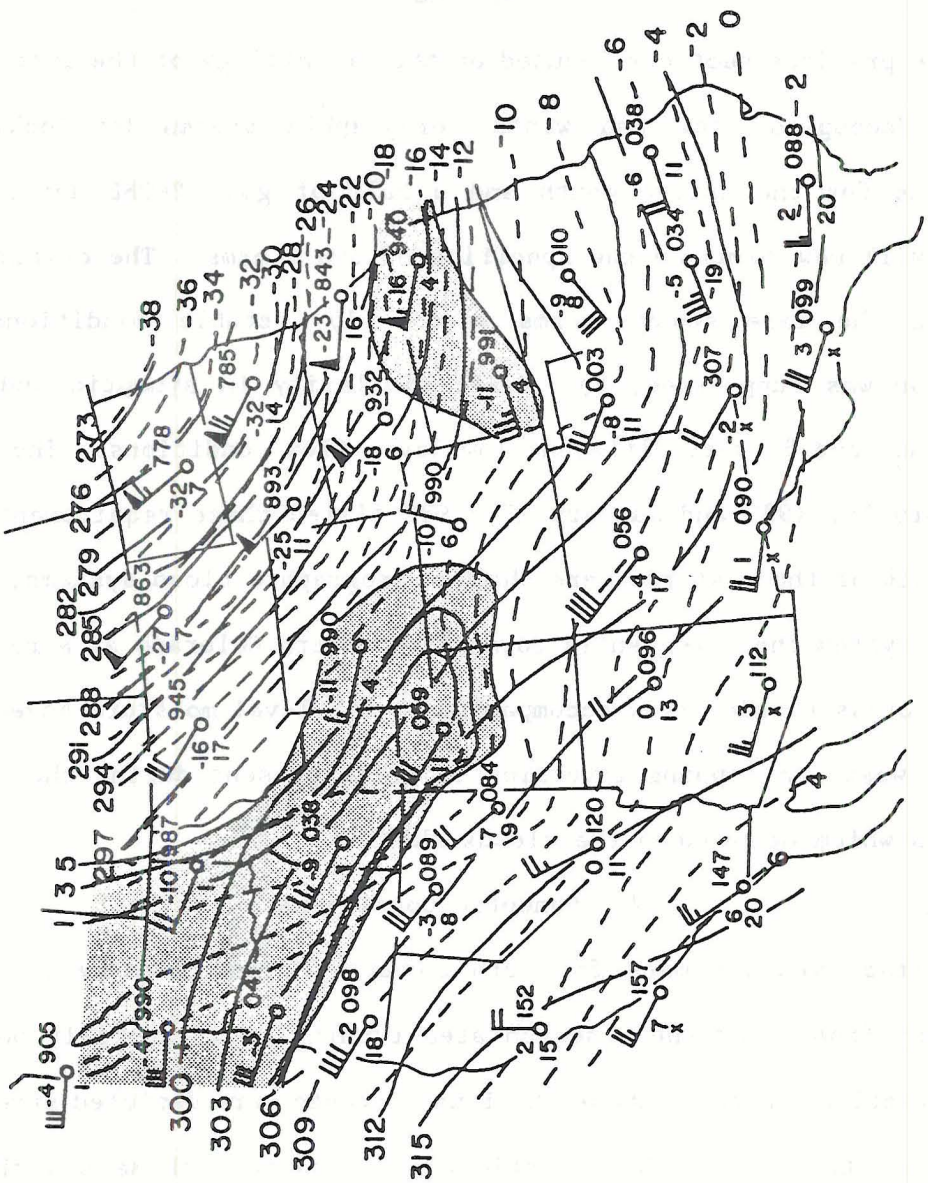

Figure 73. The 700 hPa analysis of height, temperature and dew point depressions ($T-T_d$) fields at 1200 GMT on January 16, 1982. The shaded area denotes region where $T-T_d<5°C$. Long wind barbs are 5 m s^{-1}. Pennant barbs are 25 m s^{-1}. From Rauber, 1987.

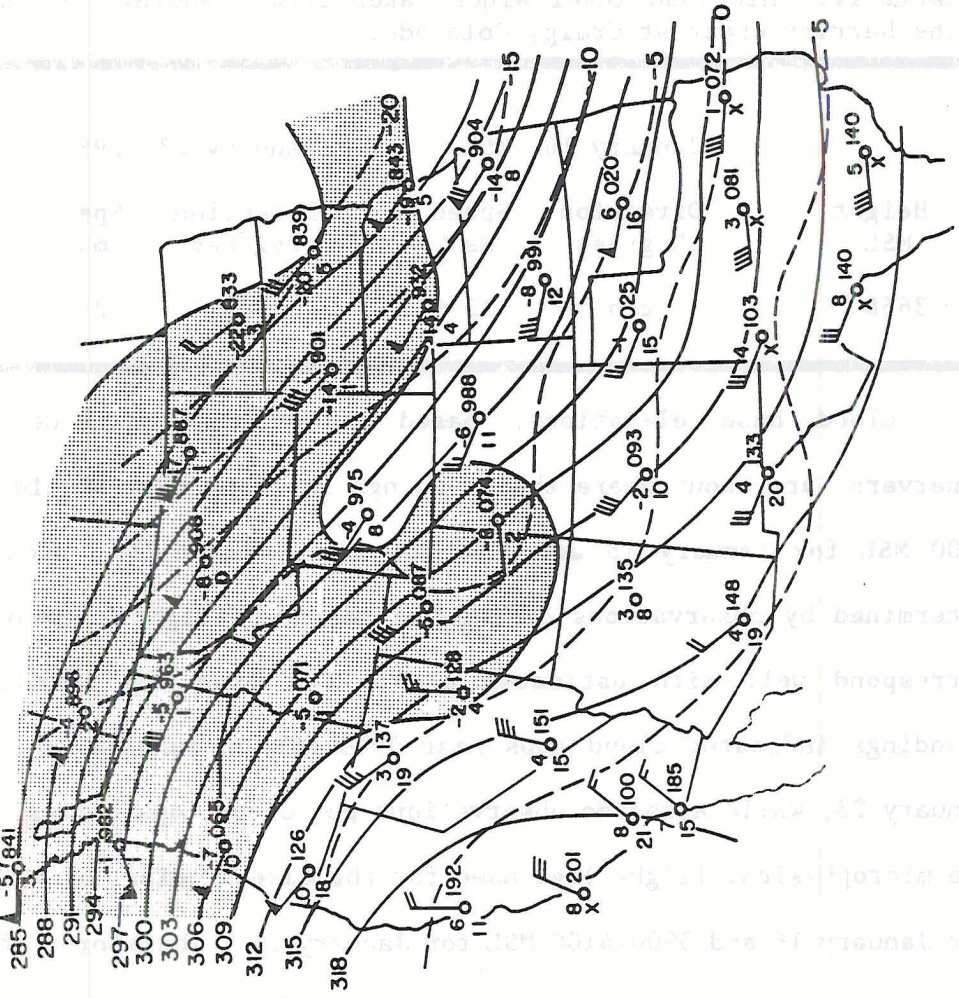

Figure 74. The 700 hPa analysis for 0000 GMT on January 24, 1982. See Figure 73 for data format.

basically perpendicular to the barrier and parallel with the valley with the January 16 winds being weaker than the January 24 winds. Both cases had stable soundings, see Figures 75 and 76, with inversions at the 550 hPa level.

Table IV. Midcloud level winds taken from soundings 70 km upwind of the barrier crest at Craig, Colorado.

	January 16, 1982		January 23, 1982	
Height MSL	Direction Degrees	Speed ms^{-1}	Direction Degrees	Speed ms^{-1}
3658	275	13.9	285	24.7

Cloud base elevations, based on estimations made by ground observers, are about where the soundings indicate they should be: 2800-2900 MSL for January 16 and 3200 MSL for January 23. Cloud tops, as determined by observations during the research flights, however, do not correspond well with estimated cloud tops from the soundings. The soundings indicated cloud tops near 5000 MSL on January 16 and 5700 on January 23, while airborne observations put cloud tops during the time of the microphysical flight legs used for the case studies, at 4100-4300 MSL for January 16 and 3900-4100 MSL for January 23. Therefore, according to airborne observations, both clouds were shallow, approximately 1-1.5 km thick. However, photographs taken from the research aircraft on both days show the presence of some higher clouds above the clouds being studied which probably correspond with the higher cloud tops indicated by the soundings. The upwind edge of the orographic cloud was 70 km upwind of the Continental Divide on January 16, which allowed the aircraft to exit

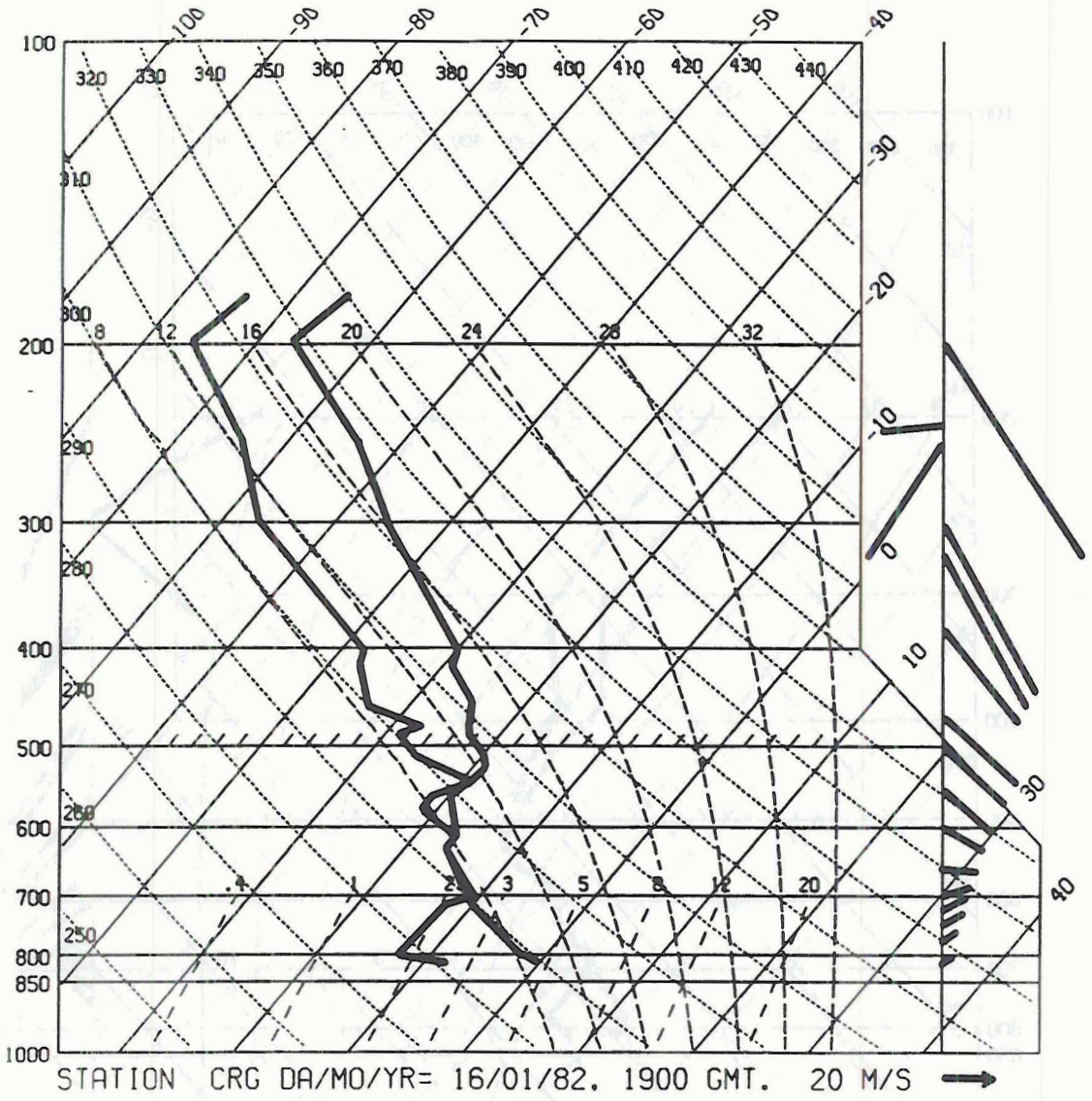

Figure 75. Sounding from rawinsonde taken 70 km upwind of the barrier crest at Craig, Colorado January 16, 1982 at 1900 GMT.

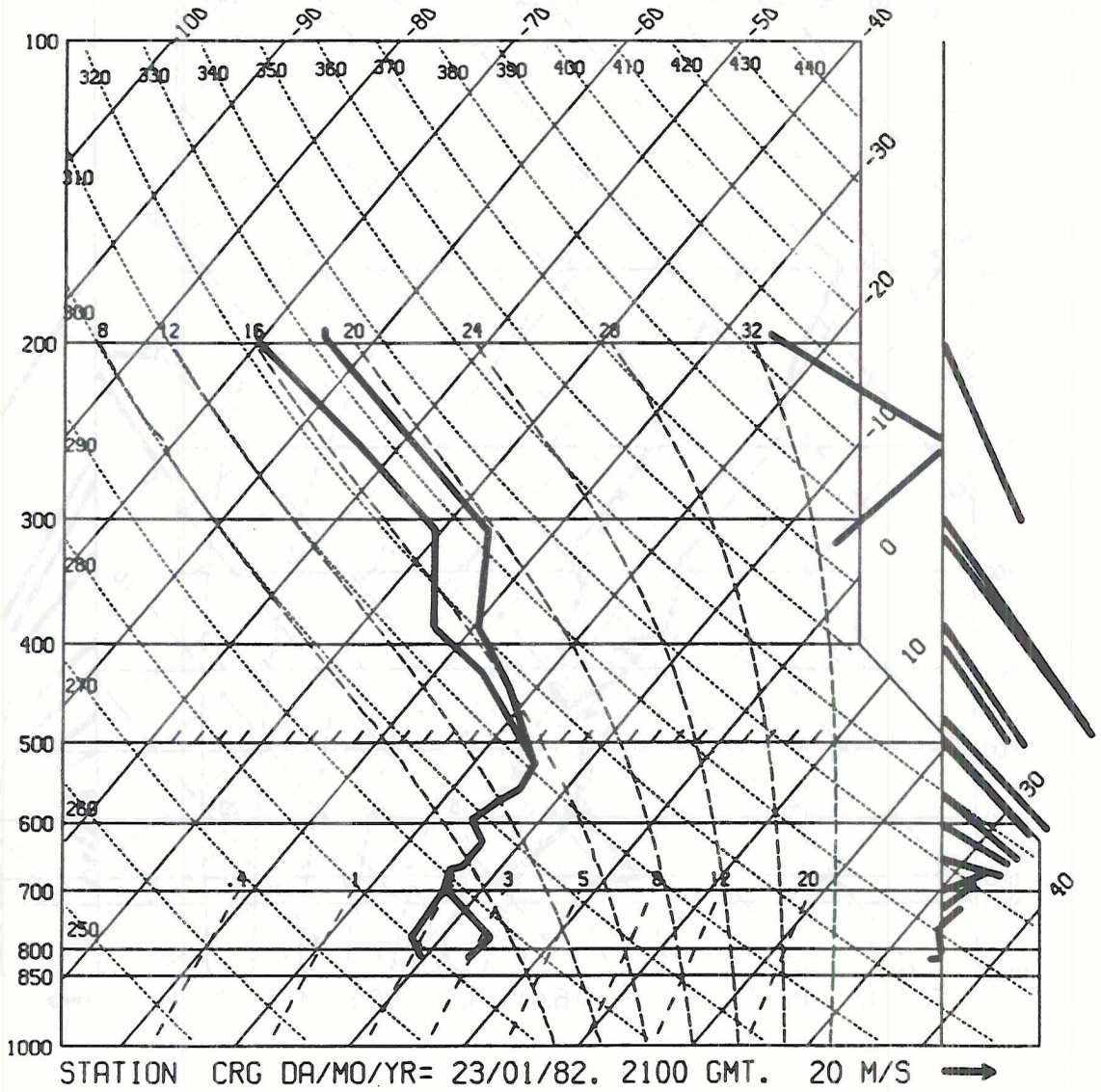

Figure 76. Sounding from rawinsonde taken 70 km upwind of the barrier crest at Craig, Colorado January 23. 1982 at 2100 GMT.

the cloud on the upwind leg. The January 23 cloud stretched farther upwind and the aircraft following its preassigned flight path did not exit the cloud on the upwind side. GOES West hard copy images appear to support the observer in the aircraft's report that "the western side of the COSE area was covered by a fairly uniform, but apparently thin stratus deck."

6.3. Mesoscale Conditions

As mentioned earlier, one of the criteria for selecting these case studies was different low-level flow conditions. Using the same method of the determining magnitude of low-level decoupled flow described in Chapter 3, the 12 hours of the January 16 storm that could be safely grouped together as part of this one storm type had 10 hours with decoupled flow stretching 38 km west of the Continental Divide and two hours at 58 km. In contrast, the 9 hours of the January 23 storm had 6 hours with decoupled flow stretching 74 km, 1 hour at 92 km, and 2 hours at 120 km.

Both radiatively induced drainage flows and mechanical blocking can contribute to the creation of low-level decoupled flow. Since the Froude number ($Fr = u/Nh$, where u is the cross-barrier wind component upstream of the barrier at ridge top height, h is the height of the hill, and N is the Brunt-Väisälä frequency ($N^2 = (g/\theta_r)(d\theta/dz)$)) is essentially the ratio of the kinetic energy in the wind over the potential energy required to lift a parcel of air over the hill through the stably stratified environment, the Froude number may, where appropriate, indicate the degree of blocked flow that could be expected. Calculated from the sounding taken January 16, 1982 at 1900 GMT, Fr = 1.43; January 23, 1982 at 2100

GMT, Fr = 1.09; and still with the January 23 storm, January 24, 1982 at 0000 GMT, Fr = 0.94. So despite January 23 having a greater cross-barrier wind than January 16, the Froude number is lower and the length of decoupled flow is greater on January 23 than January 16.

The winds recorded by the PROBE stations at the time of the analyzed flight through the cloud are shown in Figures 77 and 78. Note the contrast in the middle part of the Yampa valley where the January 16 winds are up valley and the January 23 winds are down valley. This can also be seen clearly on the cross sections of the Yampa Valley in Figures 79 and 80. In the region 50 to 100 km west of the Continental Divide, the January 16 winds are blowing strongly upvalley while the 1.0 ms^{-1} contour on the January 23 cross section is hundreds of meters above the floor of the Yampa Valley.

Two acoustic sounders were operating during COSE III. Unfortunately, snow accumulation on the acoustic sounders prevented data collection from one acoustic sounder on January 16 and both acoustic sounders on January 23. The acoustic sounder located on the valley floor 50 km west of the barrier did provide data on January 16 to a height of 500 meters. These data indicate that during the January 16 storm, there was no significant wind shear or inversion layers present within 500 meters above the surface. This is in keeping with Figure 79 which shows that the region of decoupled flow on January 16 did not stretch that far west of the barrier.

6.4. Precipitation and Cloud Conditions

An analysis of crystal observations for both storms indicated that crystals were primarily planar dendrites and some spacial dendrites. Both

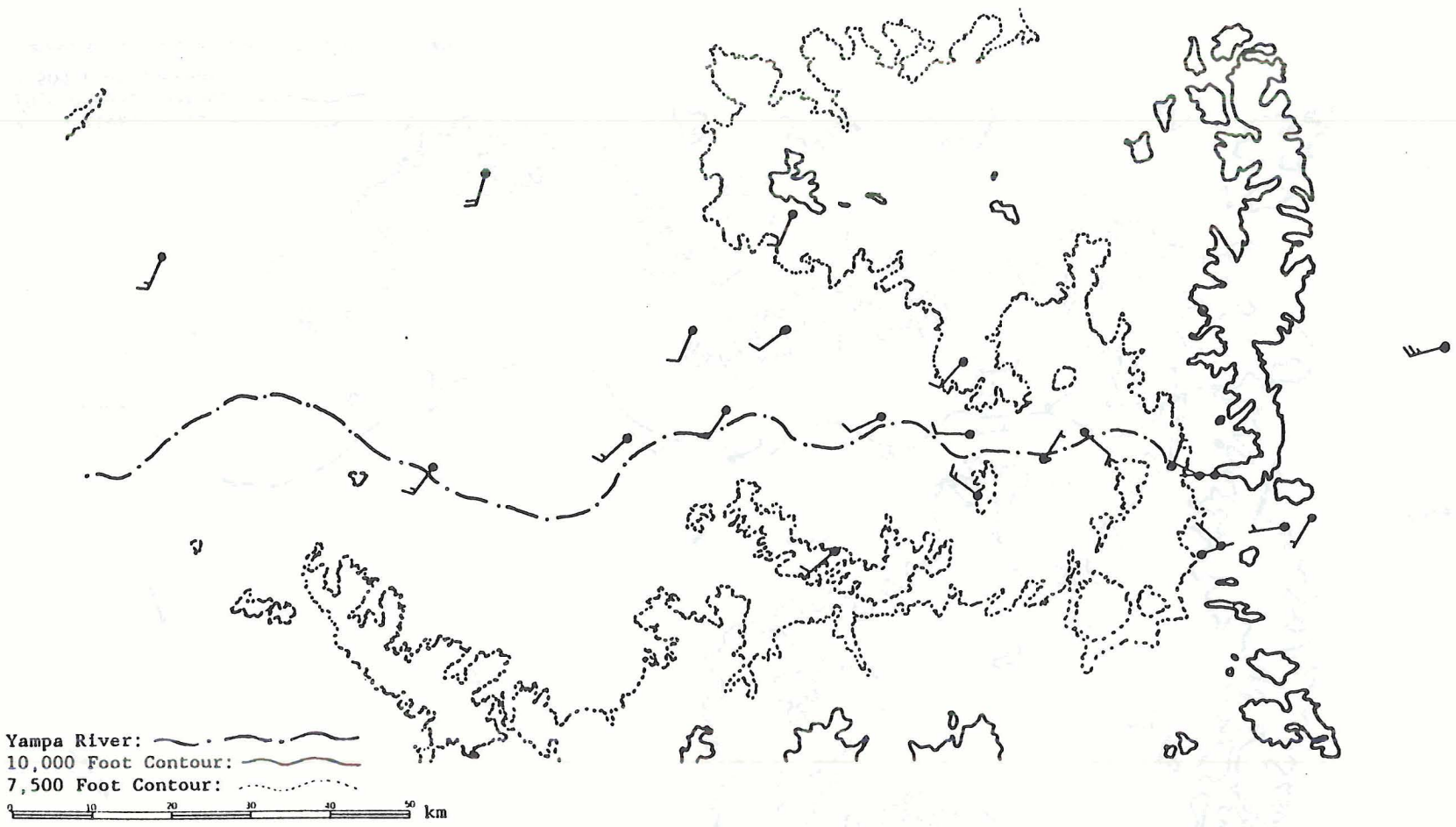

Figure 77. Surface winds from PROBE stations during flight time, January 16, 1982, 1930 GMT. The long barbs are 5 m s^{-1}.

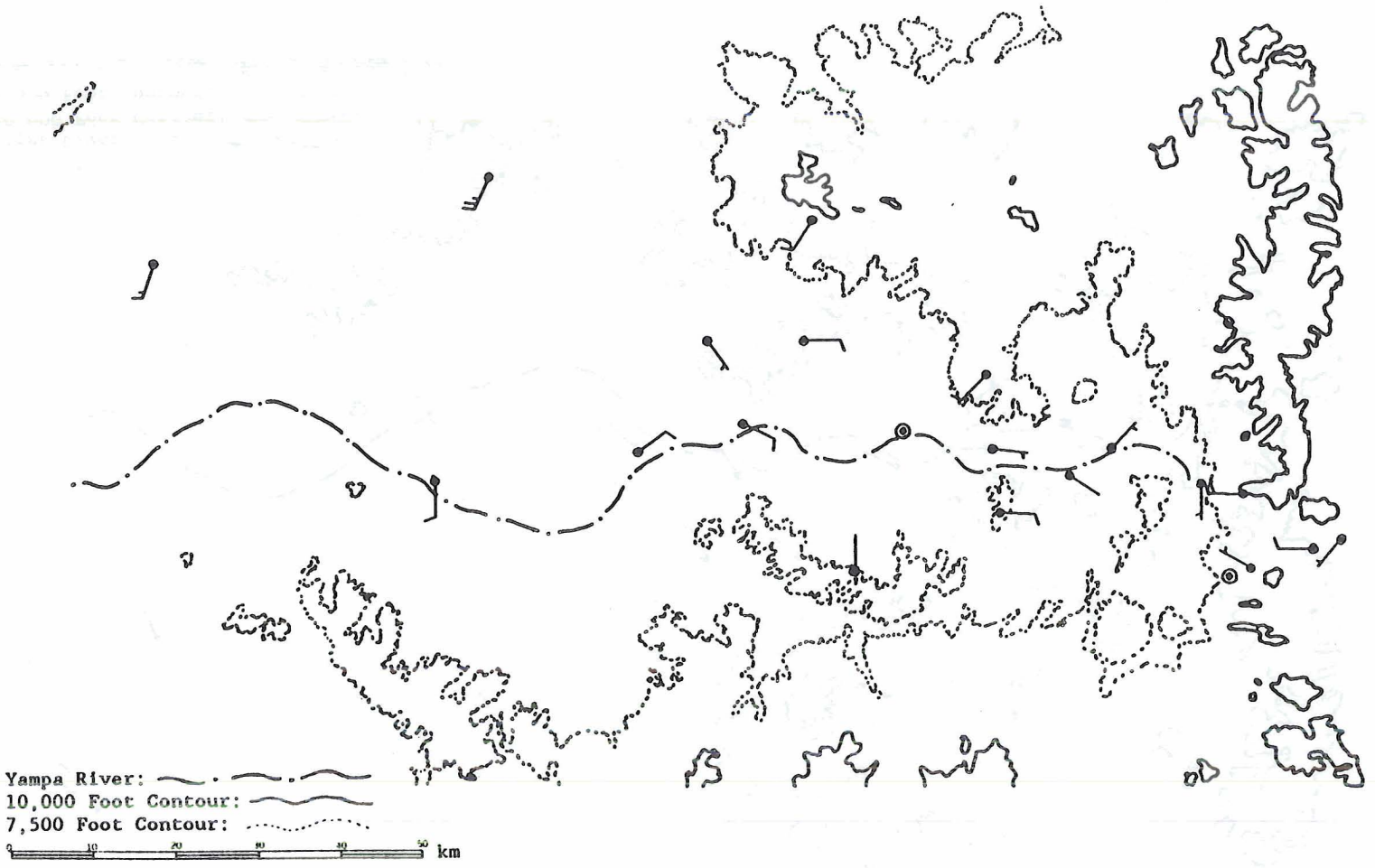

Figure 78. Surface winds from PROBE stations recorded during flight time, January 23, 1982 2245 GMT. Long barbs are 5 m s^{-1}.

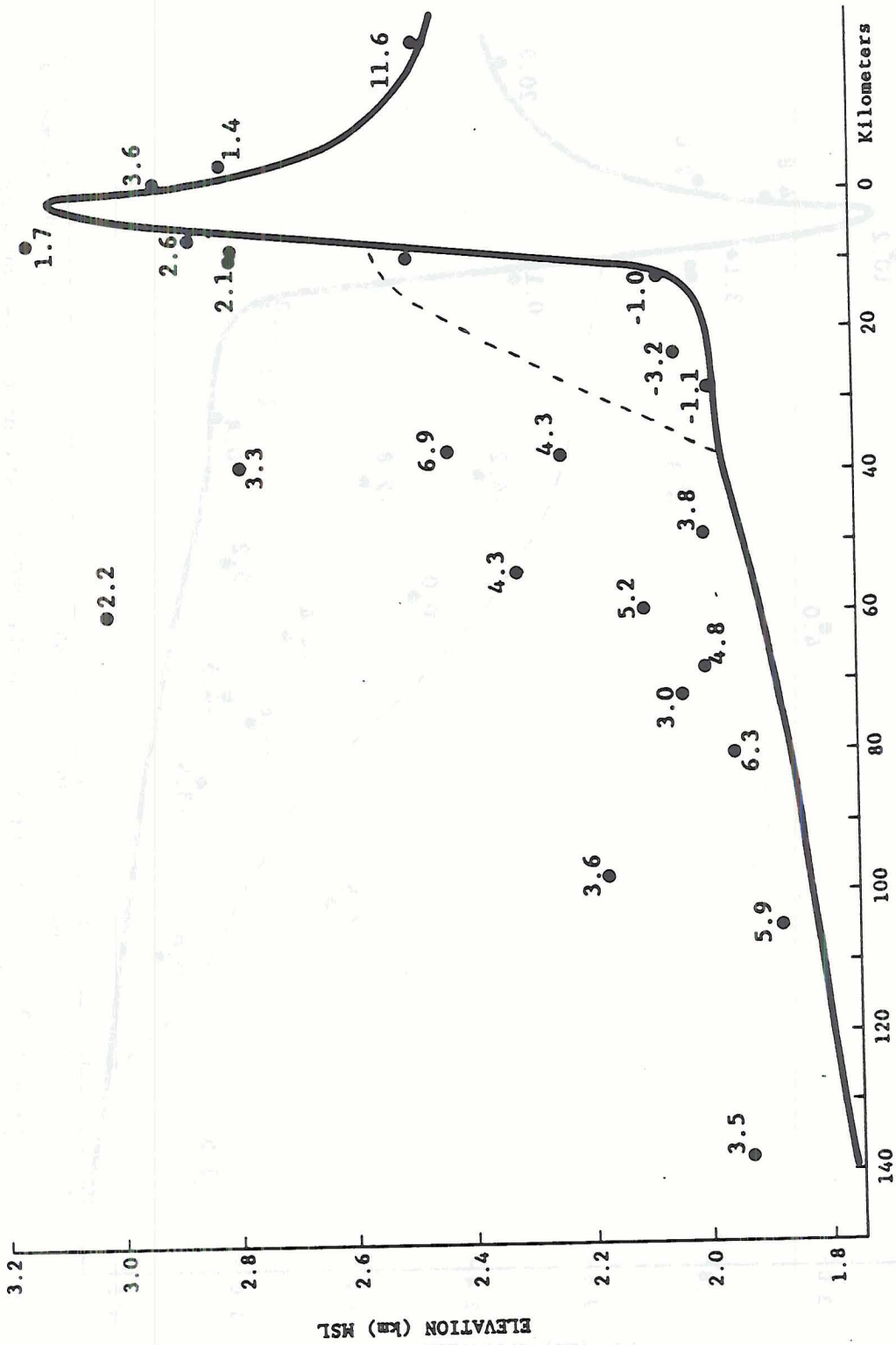

Figure 79. U-wind component from the PROBE stations plotted on a cross section of the research area, January 16, 1982 1930 GMT. The dashed line is the 1.0 ms^{-1} contour.

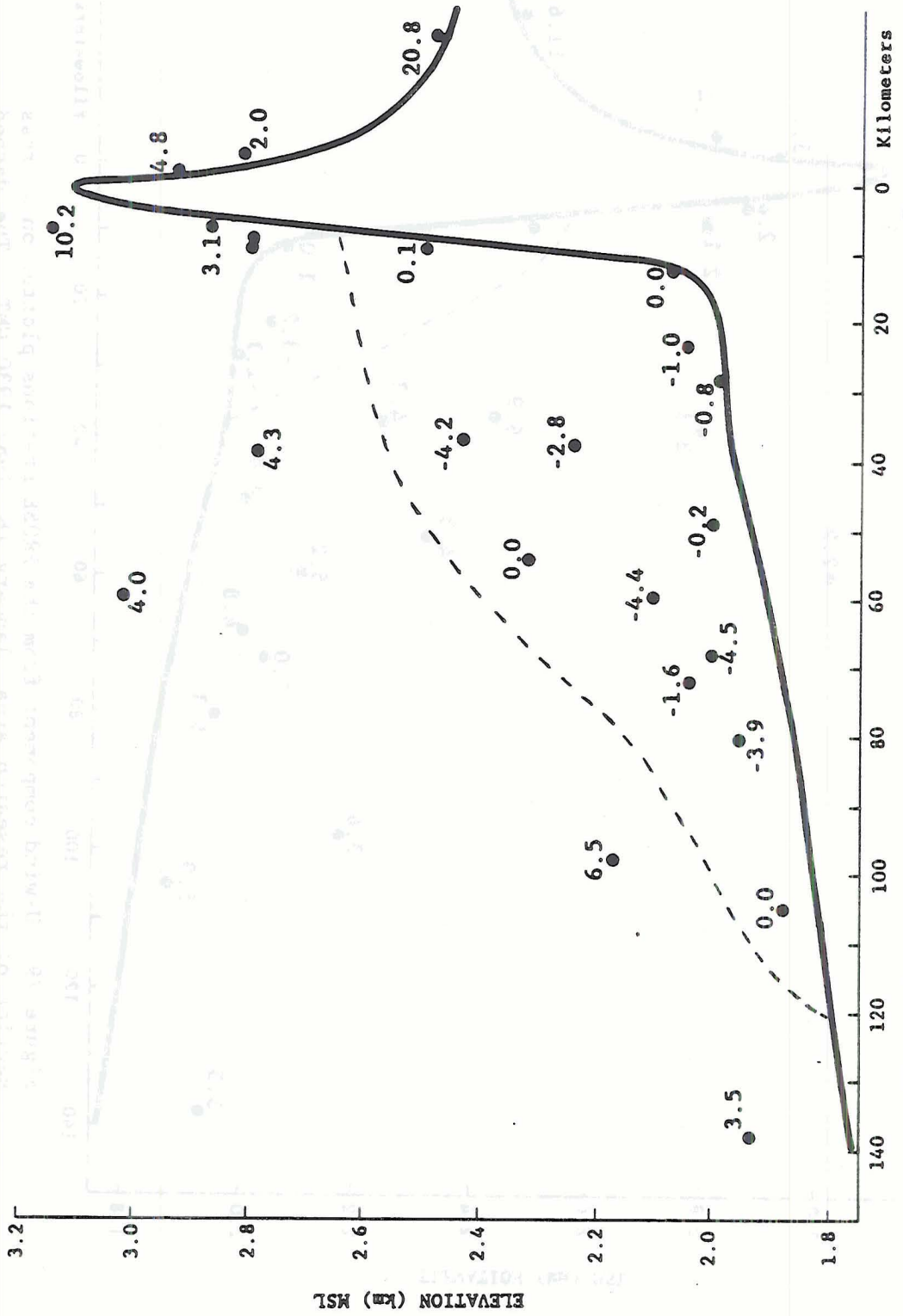

Figure 80. U-wind component from the PROBE stations plotted on a cross section of the Yampa Valley, January 23, 1982 2245 GMT. The dashed line is the 1.0 ms^{-1} contour.

storms had some aggregation with January 24 having more than January 16. And crystal observations from both storms reported light riming, with January 24's observations reporting more riming than January 16.

The January 16 storm produced more precipitation per hour than did the January 23 storm. Table 5 compares the precipitation intensity of both storms at several locations. To more clearly see the differences in precipitation during the two storms, comparing the relative percent of precipitation falling on the various station groups is helpful. Figure 81 does just that, clearly showing that the January 16 storm snowed heaviest on the eastern edge of the research area, decreasing in intensity to the west, with no precipitation falling in the middle or lower valley. January 23, on the other hand, had a precipitation maximum on the barrier,

Table V. Precipitation intensities averaged for 12 hours on January 16 and 9 hours on January 23.

	Precipitation Intensity Average per Station in $mmhr^{-1}$ water equivalence	
	Jan. 16	Jan. 23
Total PROBE Area	0.250	0.198
Over the Barrier	0.739	0.346
On the Barrier	0.536	0.487
Upper Valley	0.333	0.296

had a greater percentage of precipitation falling in the upper valley than January 16, and had some precipitation falling in the middle and lower valley.

Cloud conditions during these storms were measured by an instrumented aircraft. The aircraft flew near cloud top at 625 hPa and 3900 MSL. Figures 82 and 83 show 4 relevant parameters related to one

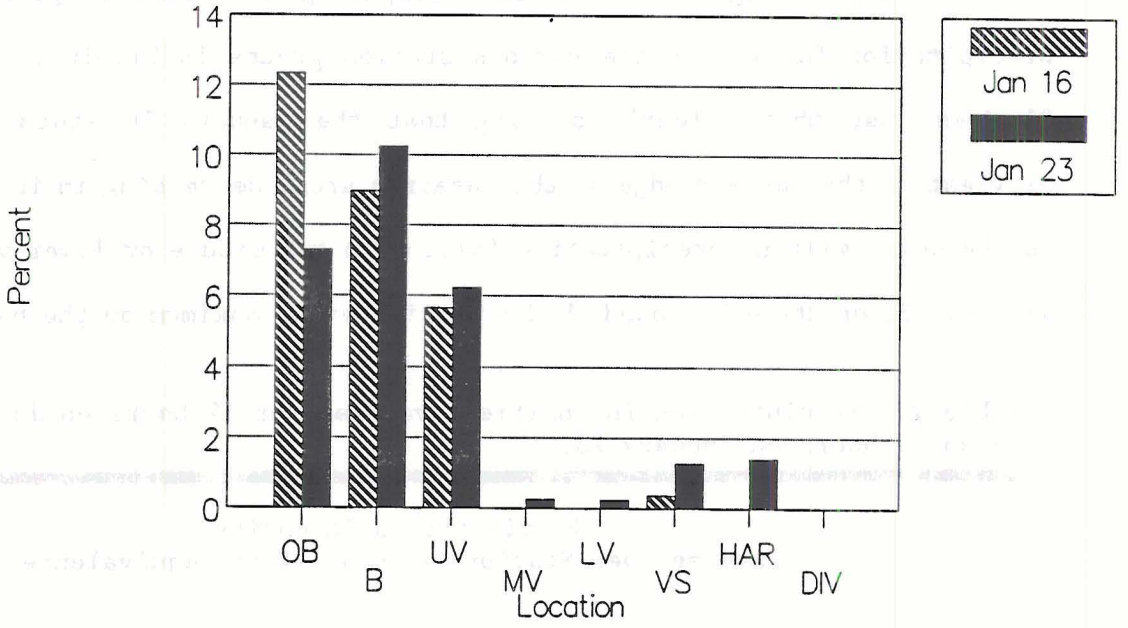

Figure 81. Relative percent of precipitation by location on a per station average. Striped bar represents January 16 and the solid bar represents January 23.

pass through the cloud during each storm. On the bottom of Figures 82 and 83 is the topography over which they flew. Though the aircraft attempted to fly the same path on both days, slight variations off the intended route lead to differences in the underlying topography.

On the top of Figures 82 and 83 is the 2-D ice crystal concentration. Ice crystal concentrations were much higher on January 23 than January 16. Also January 23 ice crystal concentrations remained high over a large region from 30 km upwind of the barrier to 5 km downwind. Ice crystals observed on January 16 on the other hand, had three small regions of moderate ice crystal concentrations, two located over areas where the topography is increasing in height and one in the lee wave cloud.

Second from the top in Figures 82 and 83 is the FSSP liquid water content corrected for airspeed using the technique described in Cerni, 1983. Immediately apparent are the facts that the aircraft did not pass out of the cloud on the upwind side on January 23 and that the liquid water content is much higher on January 23 than January 16. Also, there is a marked decrease in LWC on January 23 at 40-45 km upstream of the Continental Divide.

The third feature on Figures 82 and 83 is the calculated parcel lift. The instrumented aircraft was not able to measure vertical wind velocity accurately enough for the upper region of an orographic cloud, so the parcel lift needed to be calculated in a less direct fashion that required several assumptions.

These assumptions are:

- Steady state conditions exist for the duration of the flight and for the time it takes a parcel to pass through the research area. Ku-Band radar shows little change during these time spans which supports this steady state assumption.

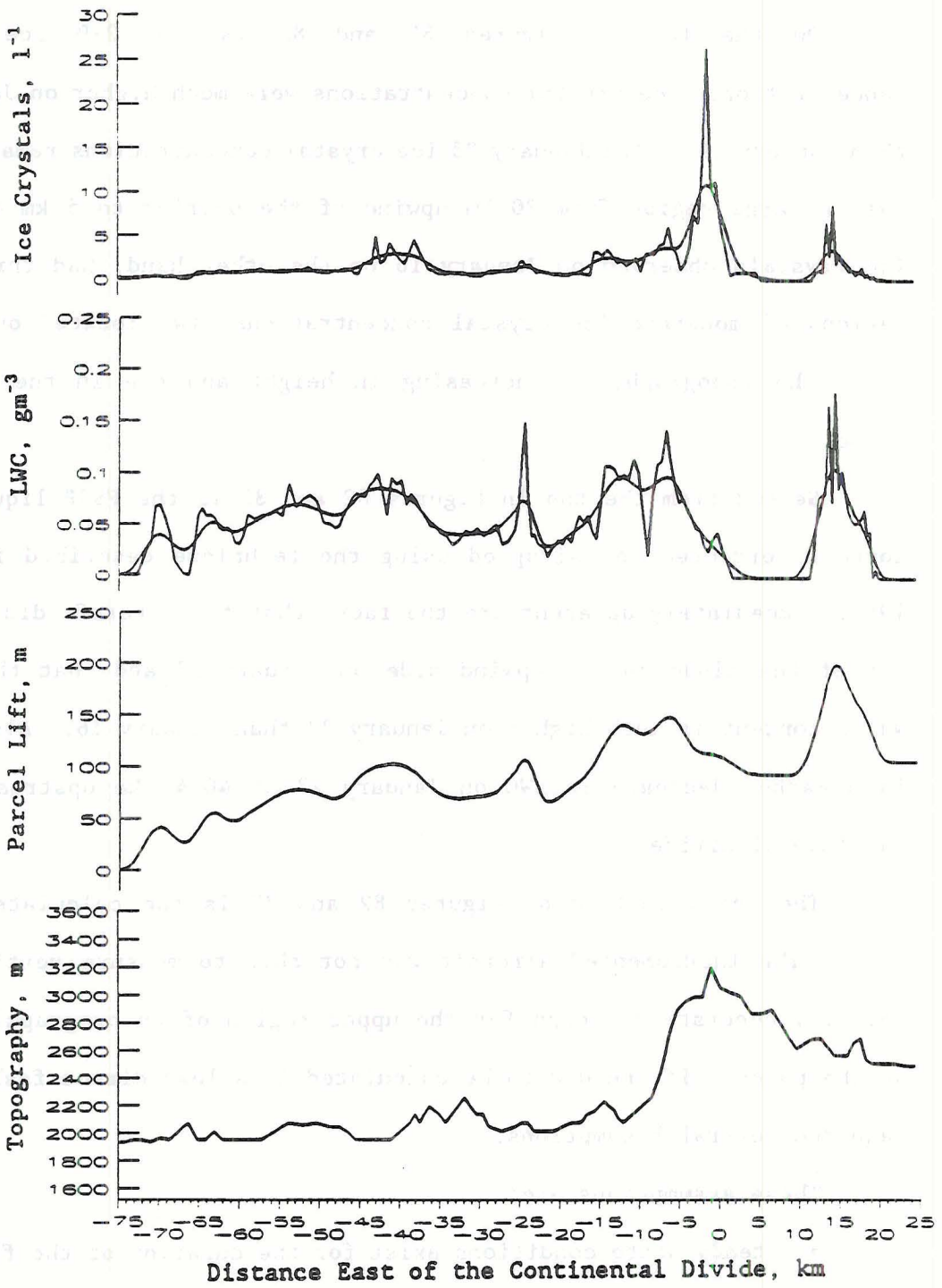

Figure 82. January 16, 1982 data from aircraft flight plotted along west to east coordinate. Top chart is ice crystal concentrations observed and filtered. Second from the top is cloud liquid water content observed and filtered. Third from the top is the calculated parcel lift. Bottom is the topography under flight track.

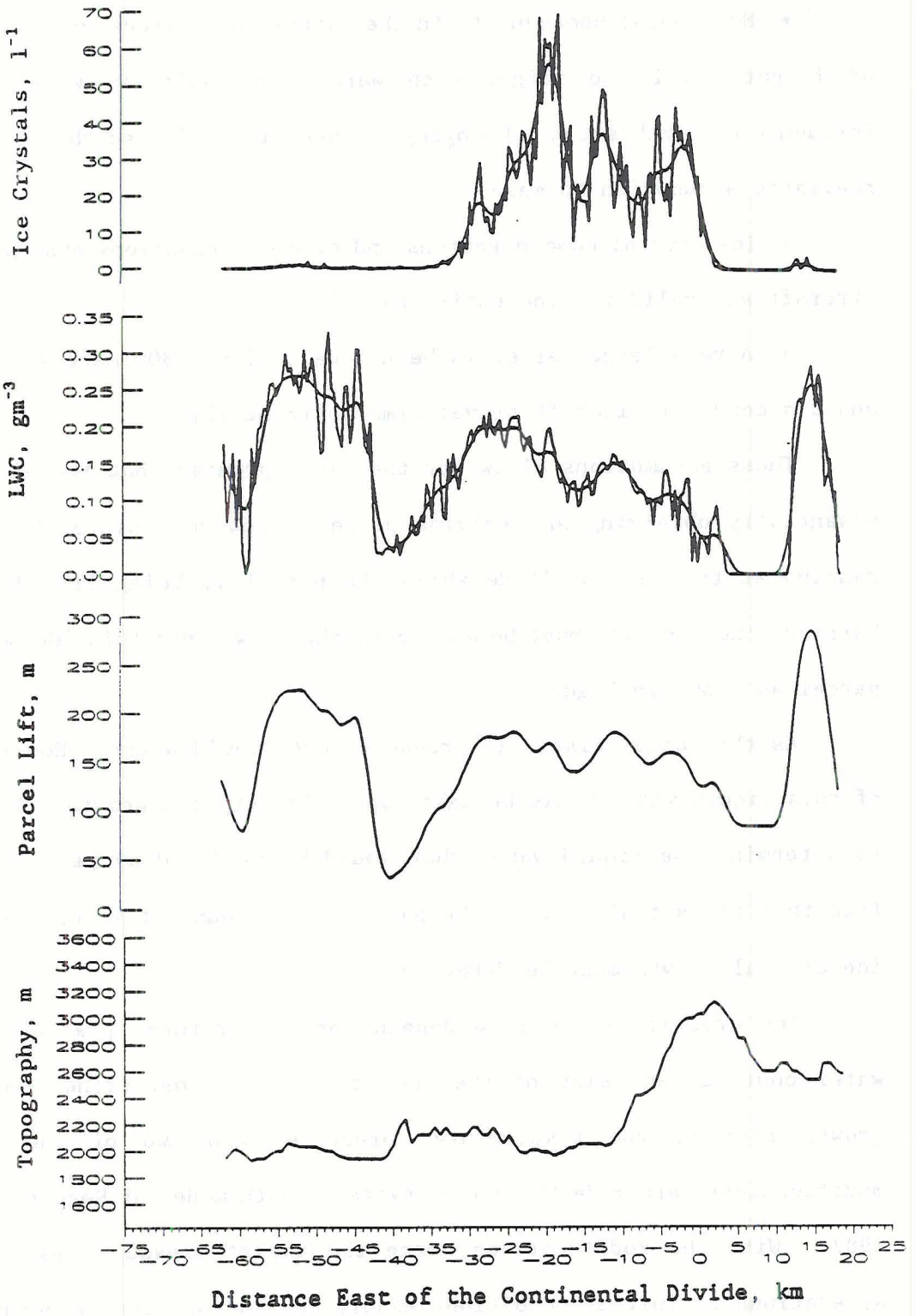

Figure 83. January 23, 1982 data from aircraft flight plotted along west to east coordinate. Top chart is ice crystal concentrations observed and filtered. Second from the top is cloud liquid water content observed and filtered. Third from the top is the calculated parcel lift. Bottom is the topography under flight track.

- Horizontal homogeneity in the north/south direction. Since winds at flight level and flight path were both basically west/east, the influence of north/south inhomogeneity would be small, so this is a fairly realistic assumption to make.

- Ice crystal concentrations and size distributions observed by the aircraft are valid for the entire parcel.

- A very large parcel is being dealt with: 300 meters vertically and 5 seconds of aircraft travel time horizontally.

These assumptions allow for the basic premise that the aircraft is essentially observing an evolving parcel. However, since the aircraft remains at the same altitude while the parcel is being lifted over the barrier, the aircraft must be moving farther down into this 300 meter deep parcel as shown in Figure 84.

As the parcel rises, it produces more liquid water. However, some of this liquid water would be taken up by ice crystal growth. Therefore to determine the liquid water that would be produced by parcel rise and from that the actual rise in the parcel, the amount of water taken up by ice crystal growth must be determined.

Ice crystal growth rate depends on temperature, pressure, liquid water content, and size of the ice crystal. To determine ice crystal growth rate at the temperature, pressure, and LWC of the parcels modifications were made to an ice crystal growth model of Rogers and Vali 1987. With the modifications, once the target pressure was reached - alterations of initial conditions enable the appropriate temperature and liquid water content to be present at the target pressure - the crystal size was reset down to 10 microns and the updraft was altered to equal the

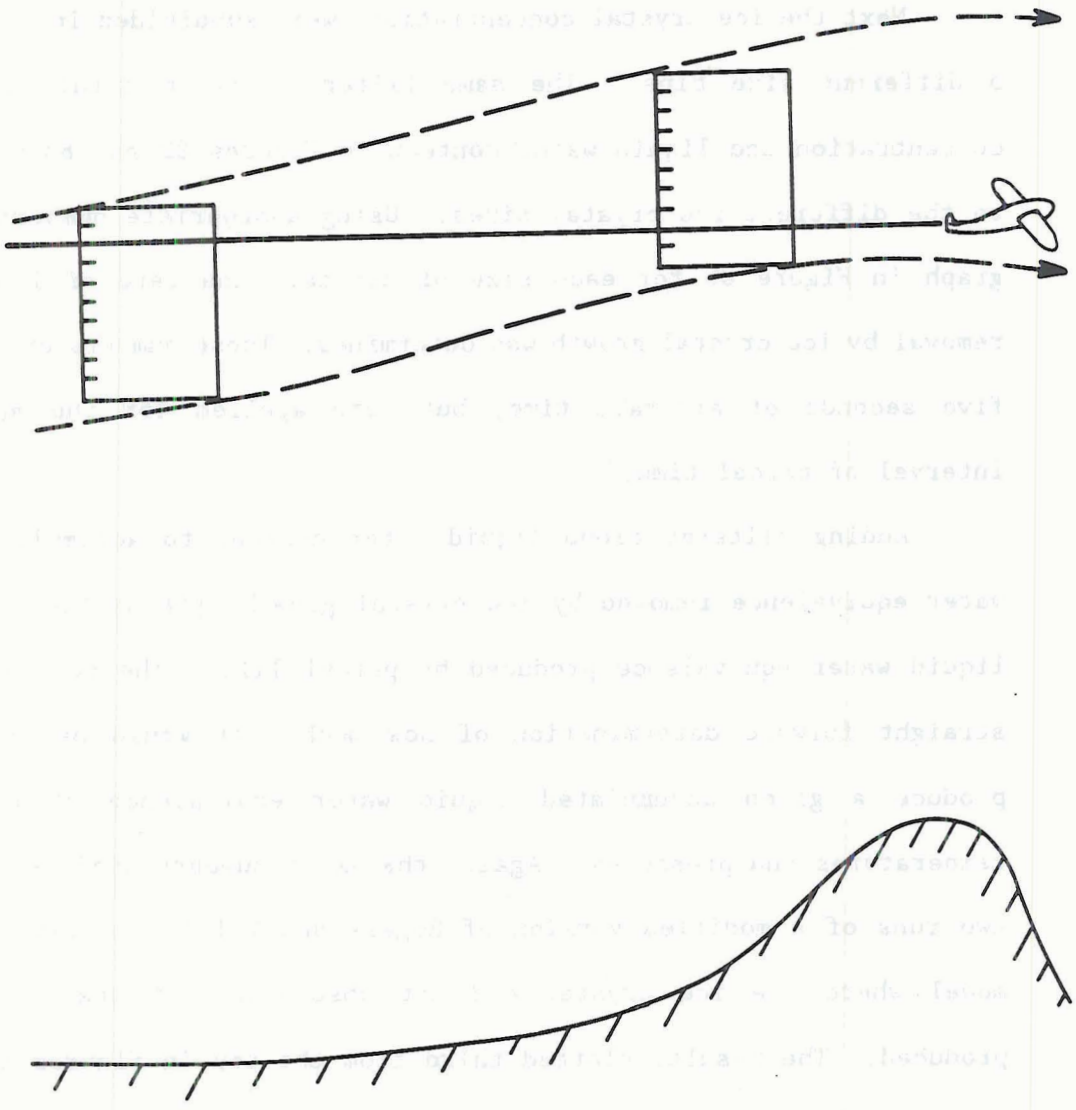

Figure 84. An evolving parcel following streamlines, shown as dashed lines, would be intersected by a level flight path at different depths in the parcel.

fall velocity so crystal growth rate at target pressure, temperature, and liquid water content could be determined as a function of crystal size. The model was run for appropriate conditions for both days with essentially the same results presented in Figure 85.

Next the ice crystal concentrations were subdivided into as many as 5 different size bins. The same filter shown on total ice crystal concentration and liquid water content in Figures 82 and 83 was applied to the different ice crystal sizes. Using appropriate numbers from the graph in Figure 85 for each size of crystal, the rate of liquid water removal by ice crystal growth was determined. These numbers changed every five seconds of aircraft time, but were applied for the appropriate interval of parcel time.

Adding filtered cloud liquid water content to accumulated liquid water equivalence removed by ice crystal growth, yields the accumulated liquid water equivalence produced by parcel lift. The next step was a straight forward determination of how much lift would be required to produce a given accumulated liquid water equivalence at case study temperatures and pressures. Again, the exact numbers used were based on two runs of a modified version of Rogers and Vali's ice crystal growth model where the ice crystal did not absorb any of the liquid water produced. The result, plotted third from the top in Figures 82 and 83, is parcel lift. This is how far the parcel would have to rise to produce the calculated accumulated liquid water equivalence. Or alternately, in keeping with the concept of examining one large evolving parcel, how deep into the parcel the aircraft was.

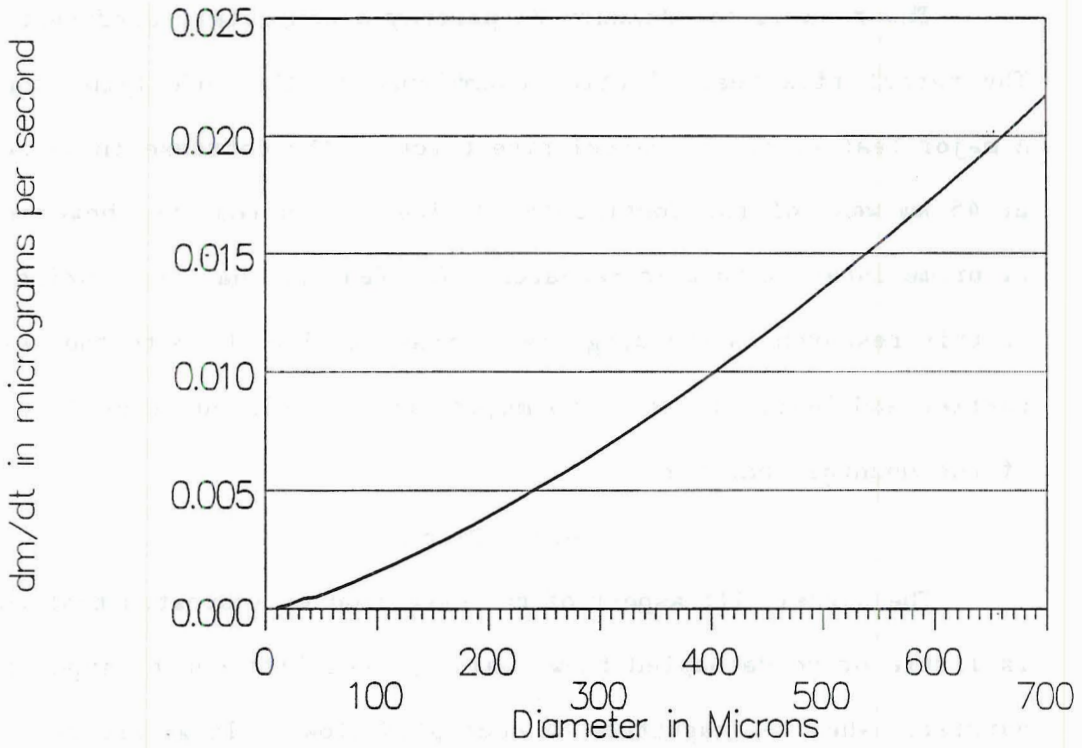

Figure 85. Ice crystal growth rate as a function of crystal size at 625 hPa pressure, -15 degrees C, and 0.1 gm^{-3} liquid water content.

For January 16, the result shown in Figure 82 indicates that parcel rise closely corresponds to the topography with a slight phase lead. There is a substantial rise at the barrier, and many smaller rises farther to the west.

The results for January 23 portray a completely different picture. The parcel rise bears little resemblance to the underlying topography. A major feature of the parcel rise trace is the decrease in parcel height at 45 km west of the Continental Divide. This feature, however, is not of prime interest to this research. The feature that is of prime interest to this research is the slightly decreasing rise 30 km to the west of the barrier and less. There is no major lift calculated at or just upstream of the mountain barrier.

6.5. Discussion

The parcel lift aspect of the case studies indicates that when there is little or no decoupled flow, major parcel lift can be expected at the barrier. When the magnitude of decoupled flow is large and deep, primary parcel lift is not experienced at the barrier. Since the lift is not experienced at the barrier, the parcel must rise farther upstream.

The precipitation analysis of the case study supports the earlier climatological analysis that precipitation during times of extensive decoupled flow tends to shift farther west. In Chapter 3's climatological analysis, the length of blocked flow was related to the Froude number, which in turn is related to the cross-barrier wind speed. The higher the cross-barrier wind velocity, the higher the Froude number and the smaller the blocked flow. The change in precipitation location found in Chapter 3 could not be proven to be related to differing locations of lift and

hence condensate production with different degrees of decoupled flow or simply related to different cross-barrier wind velocities altering crystal trajectories, with stronger winds blowing the crystals farther east. These case studies shed some light on this question since the case with little decoupled flow also had weaker cross-barrier winds. January 16's precipitation falling farther east would indicate that the changes in precipitation location with changes in extent of decoupled flow is not related to cross-barrier winds affecting crystal trajectories. It must therefore be related to changes in the location of lift and associated condensate production.

The January 23 parcel lift analysis indicates that with decoupled flow, parcels rise farther to the west. And with a deep and extensive layer of decoupled flow, the location of parcel rise is not associated directly with underlying topography. However, the location of regions of calculated parcel lift 65 to 25 km west of the barrier do not appear to be directly related to lift over regions of decoupled flow depicted in the cross section in Figure 83, either. So conclusive evidence that the parcel is indeed experiencing lift as it passes over the leading edge of the decoupled flow is not available from these case studies.

7. Modeling

7.1. Introduction

As found and reported in Chapter 6, parcels of air rising over the mountain barrier do indeed rise farther upstream during conditions with extensive low-level decoupled flow. However, it was not possible in the case studies reported in Chapter 6 to directly correlate the location of parcel lift with the location and depth of low-level decoupled flow. In an attempt to look more closely at such possible correlations two numerical simulations of orographic clouds were performed, one with extensive low-level decoupled flow and one with little or no decoupled flow.

7.2 Methods

The model used in this analysis was the Colorado State University's Regional Atmospheric Modelling System (RAMS). It was run in a two dimensional mode utilizing dynamics, thermodynamics, and microphysics with a horizontal grid spacing of 718 meters and a vertical grid spacing increasing from 250 meters near the surface to 500 meters in the upper atmosphere. The domain was 215 km in the horizontal and 14.8 km in the vertical. A 5 second time step was used in the calculations. RAMS was run in a nonhydrostatic mode with Klemp-Durran gravity wave radiation top boundary condition. Longwave and shortwave radiation were not included in these simulations. Since the model was used to simulate the Yampa Valley and the upper Yampa Valley has very high walls which impede North/South flow, the coriolis parameter was turned off.

The topography used was an east/west slice through the Yampa Valley from -108.76° longitude to -106.26° that was positioned to pass through the gap in the constricting ridges that divide the Upper Valley from the Middle Valley. This transect passed just north of Quarry Mountain. The latitude band used was 40.47° to 40.49°, which averaged three north/south 30 second resolution grid points to create the topography shown in Figure 86. This topography was then smoothed using a filter to create the topography shown in Figure 87 which was used in the model. During the actual model runs, however, the small hill in the far left and the far right on Figure 87 were leveled using the ZFLAT command.

A simple input sounding, shown in Table 6, was created from a composite of several soundings of winter orographic storms. The only variation in the sounding from the decoupled flow case to the no decoupled

Table VI. Input sounding.

PRES (hPa)	TEMP (°C)	RELH (%)	SPED (ms^{-1})	DRCT
70	-65	10	40	325
400	-28	10	35	310
542	-17	95	25	290
710	-11	98	15	270
825	-8 or -1	10	8	240

flow case was the surface temperature (though varying the surface temperature while using relative humidity in the sounding would vary the surface absolute humidity, the surface mixing ratio is very low either way, varying from 0.25 to 0.43 g kg^{-1}). The variation in the surface temperature from -8 to -1 was enough to change the input Froude numbers from 0.81 to 1.83, which are moderately more extreme than the case study Froude numbers of 0.94 and 1.43.

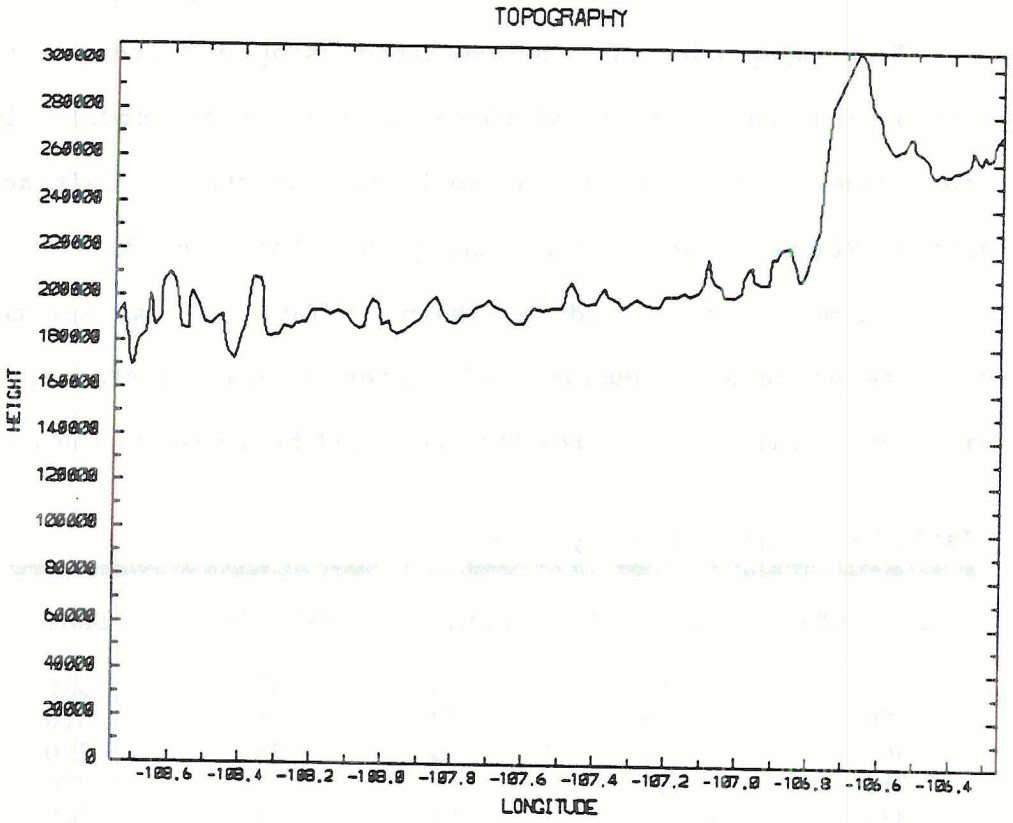

Figure 86. Actual COSE III topography from an West/East pass.

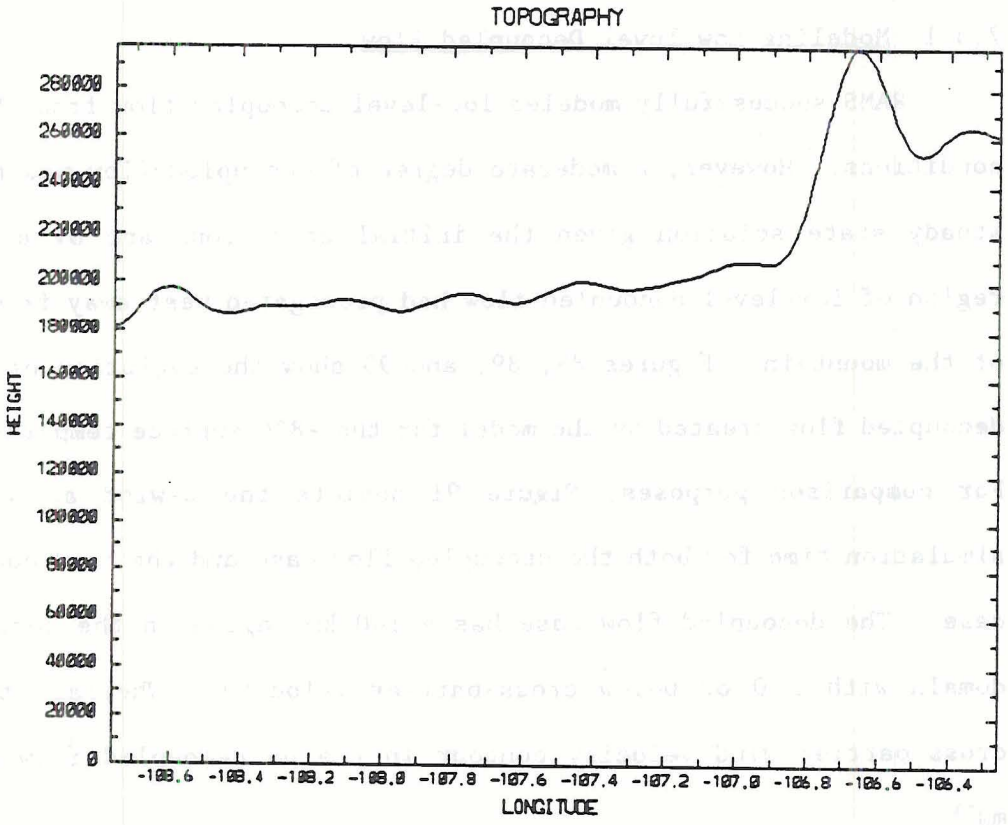

Figure 87. Filtered COSE III topography used in the numerical simulation.

Significant enough low-level decoupled flow developed within 2 hours in the -8° run to clearly differentiate the two runs. However, by 5 hours the westward extent of decoupled flow was passing westward out of the domain. Therefore, the model was run out for 2 hours dry with water only as a passive tracer followed by 2½ hours of full microphysics.

7.3 Results

7.3.1 Modeling Low-level Decoupled Flow

RAMS successfully modeled low-level decoupled flow from the initial conditions. However, a moderate degree of decoupled flow was not a true steady state solution given the initial conditions and by 6 hours the region of low-level decoupled flow had propagated west away from the base of the mountain. Figures 88, 89, and 90 show the evolution of low-level decoupled flow created by the model for the -8°C surface temperature case. For comparison purposes, Figure 91 depicts the u-wind at 4 hours of simulation time for both the decoupled flow case and the no decoupled flow case. The decoupled flow case has a 100 km region in the center of the domain with a 0 or below cross-barrier velocity. Whereas, the lowest cross-barrier wind velocity contour in the no decoupled flow case is 4 ms^{-1}.

7.3.2 Vertical Motion and Cloud Conditions

Vertical motion fields for the two cases, shown in Figure 92, have significant differences. In the no decoupled flow case, strong vertical velocities are experienced just upwind of the barrier crest, while over the valley, there is very little vertical motion. In contrast, the decoupled flow case has a small region of moderate vertical motion just

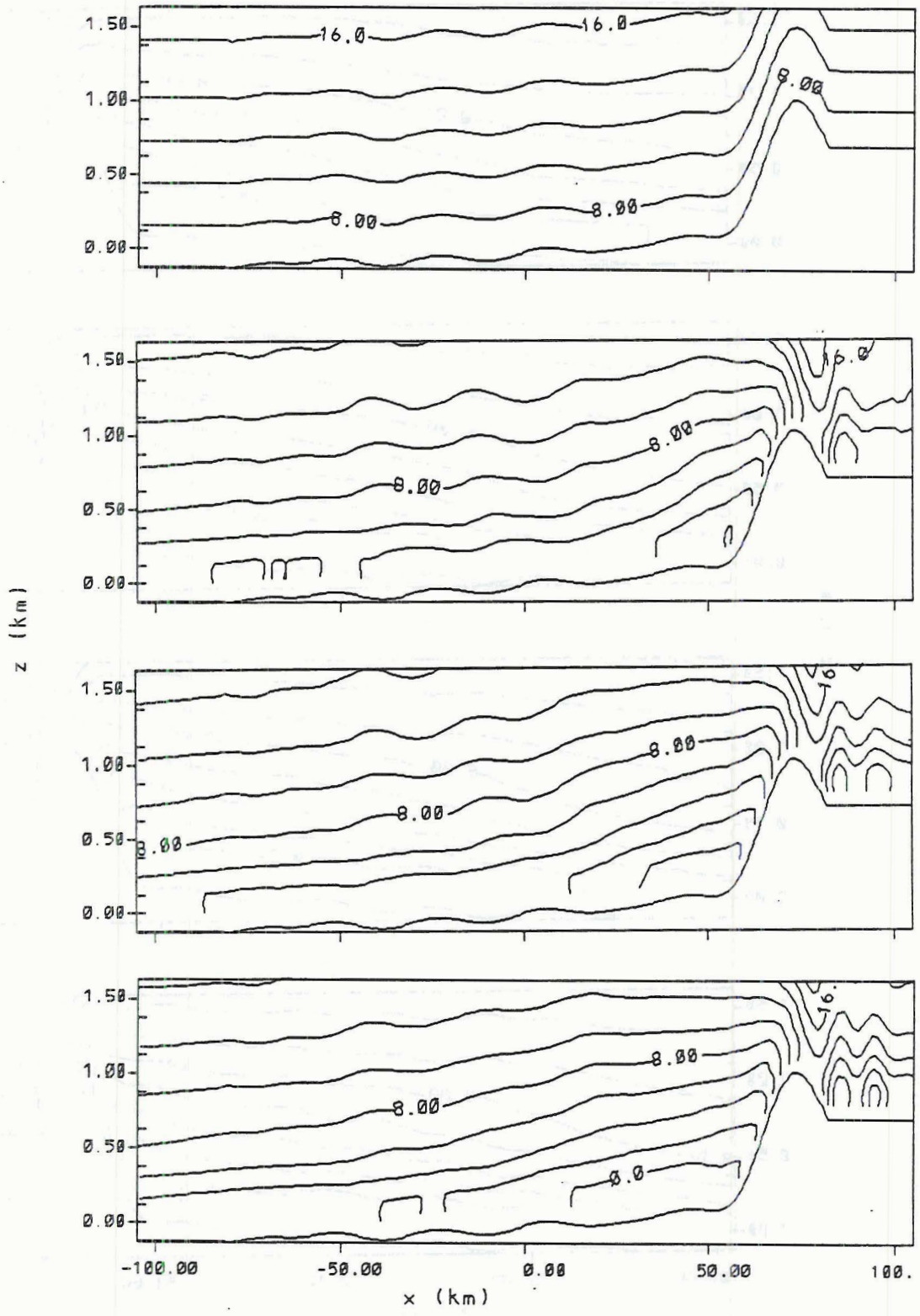

Figure 88. U-wind fields evolving with time for the decoupled flow case. From top to bottom, time equals 0, 1 hour, 1½ hours, and 2 hours. Contour increment is 2 ms^{-1}.

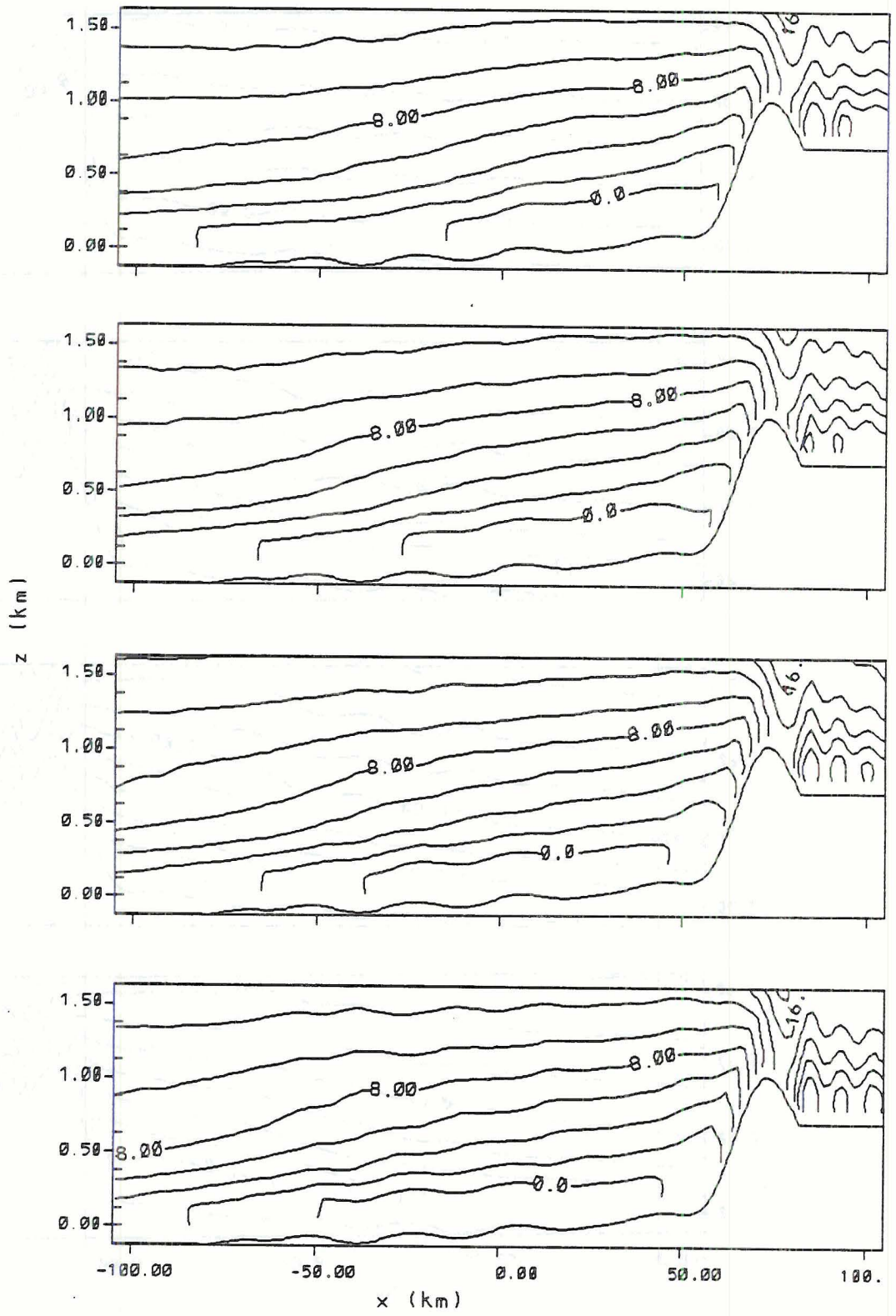

Figure 89. Continued evolution of the u-wind field in the decoupled flow case. From top to bottom, time equals 2½ hours, 3 hours, 3½ hours, and 4 hours. Contour increment is 2 ms^{-1}.

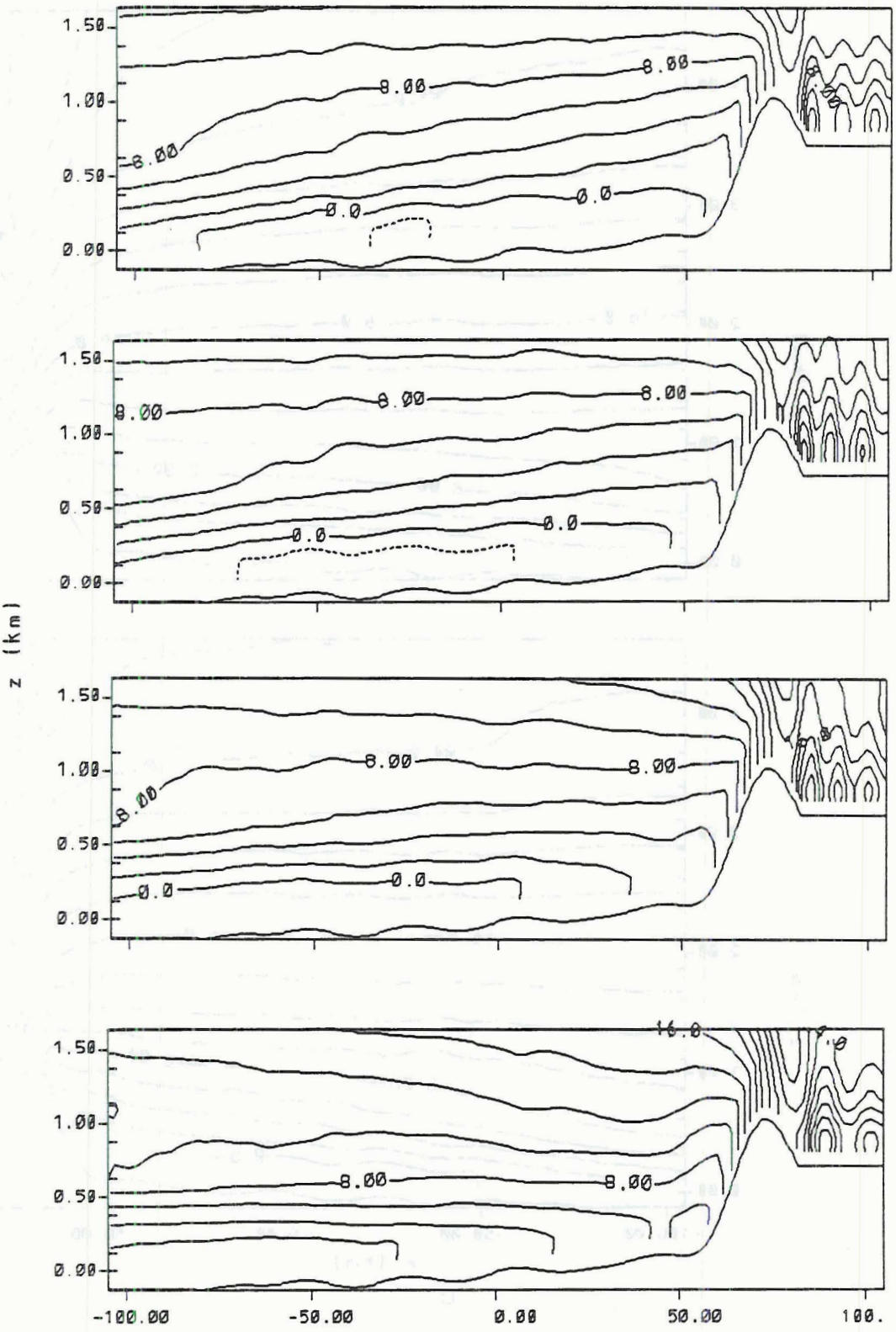

Figure 90. Continued evolution of the u-wind field in the decoupled flow case. From top to bottom, time equals 4½ hours, 5 hours, 5½ hours, and 6 hours. The contour increment is 2 ms^{-1}.

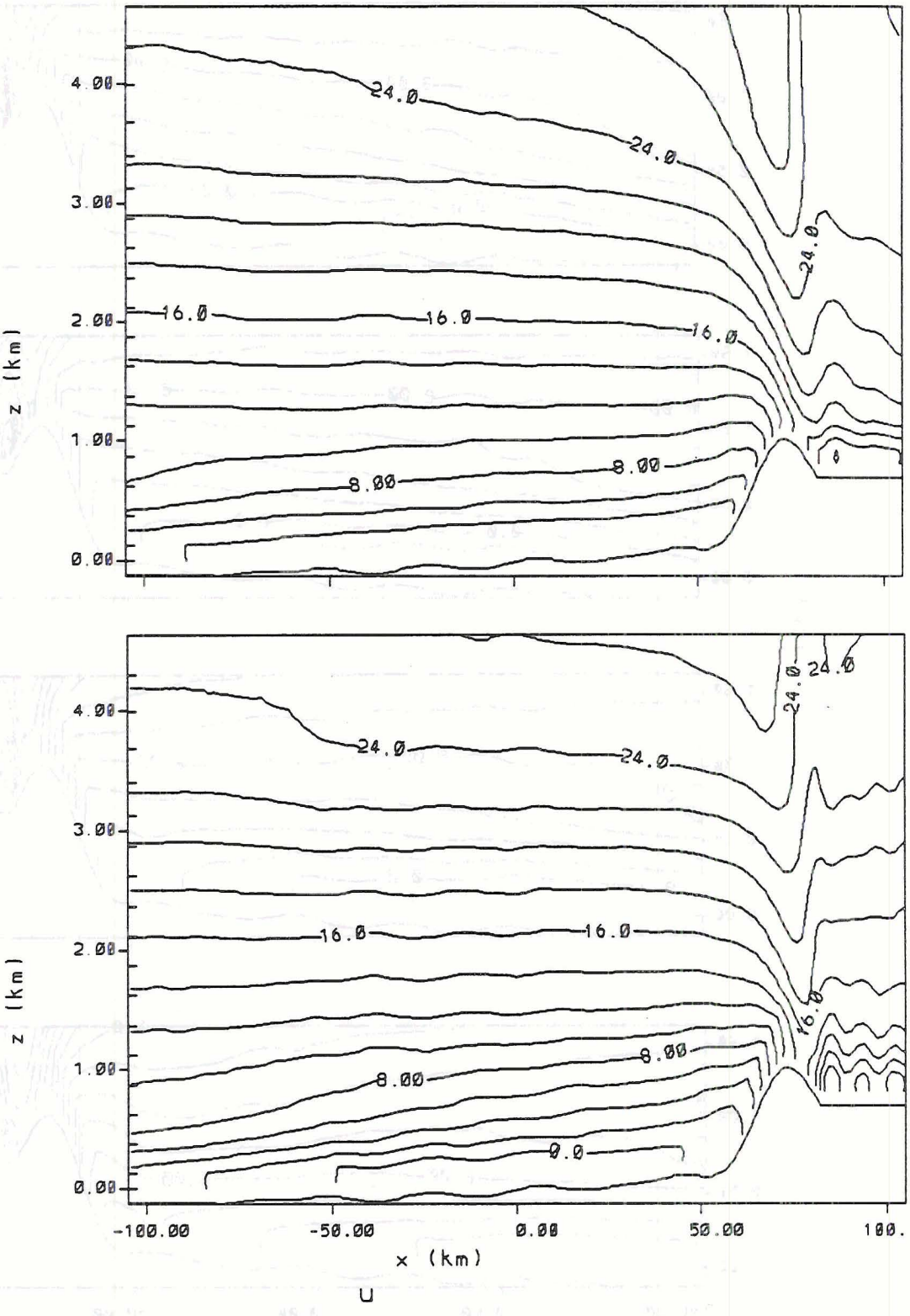

Figure 91. U-wind fields at 4 hours for the no decoupled flow case (top) and the decoupled flow case (bottom). Contour increment is 2 ms^{-1}.

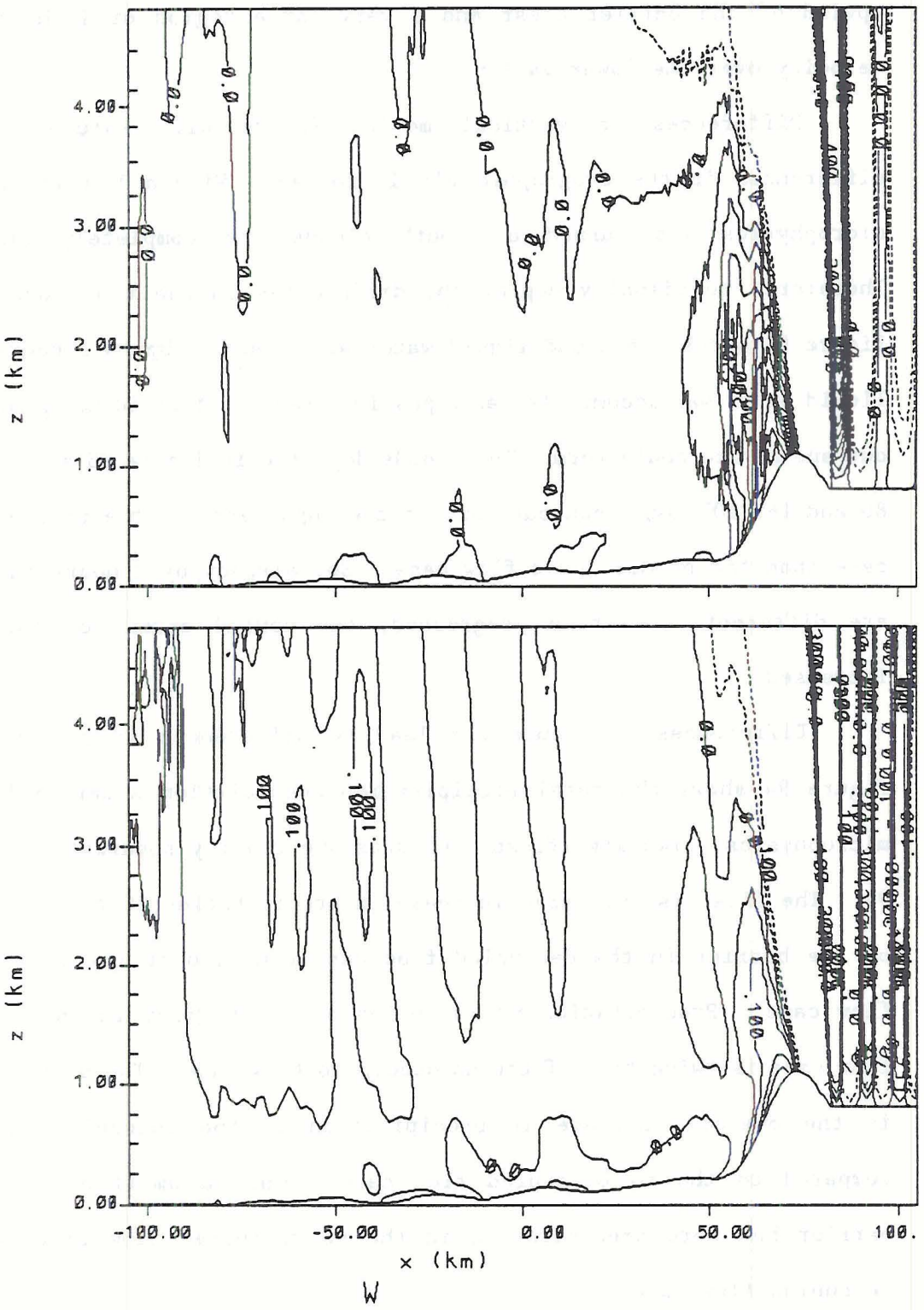

Figure 92. Vertical wind field at 4 hours for both the no decoupled flow case (top) and the decoupled flow case (bottom). The contour increment of 0.05 ms^{-1} was applied from -0.1 to 0.5 ms^{-1}.

upwind of the barrier crest and a very large region of light vertical velocity over the lower valley.

Differences in vertical motion fields will naturally create differences in the orographic clouds formed. Within 1 hour after the microphysics was turned on, both clouds had completely glaciated. Therefore, to visually depict the differences in the two cloud fields, Figure 93 shows the cloud liquid water at 2 hours. Up to 2 hours, cloud liquid water was accumulated as a passive tracer, it could not precipitate out and no ice could form. The clouds depicted in Figure 93 show that the 80 and 160 10^{-3} gkg^{-1} contours are farther upstream for the decoupled flow case than the no decoupled flow case. So, already by 2 hours the clouds are different. As time progressed, the upwind extent of the clouds increased.

Differences in clouds can lead to differences in precipitation. Figure 94 shows the total precipitation accumulation after 2½ hours of microphysics. Two significant features are readily apparent from Figure 94. The first is the large increase in precipitation 20 to 80 km upwind of the barrier in the decoupled flow case compared to the no decoupled flow case. Precipitation 60 km upwind of the barrier in the decoupled flow case is twice that of the no decoupled flow case. The second feature is the overall increase in precipitation in the decoupled flow case compared to the no decoupled flow case. Only a small area over the barrier had more precipitation in the no decoupled flow case than the decoupled flow case.

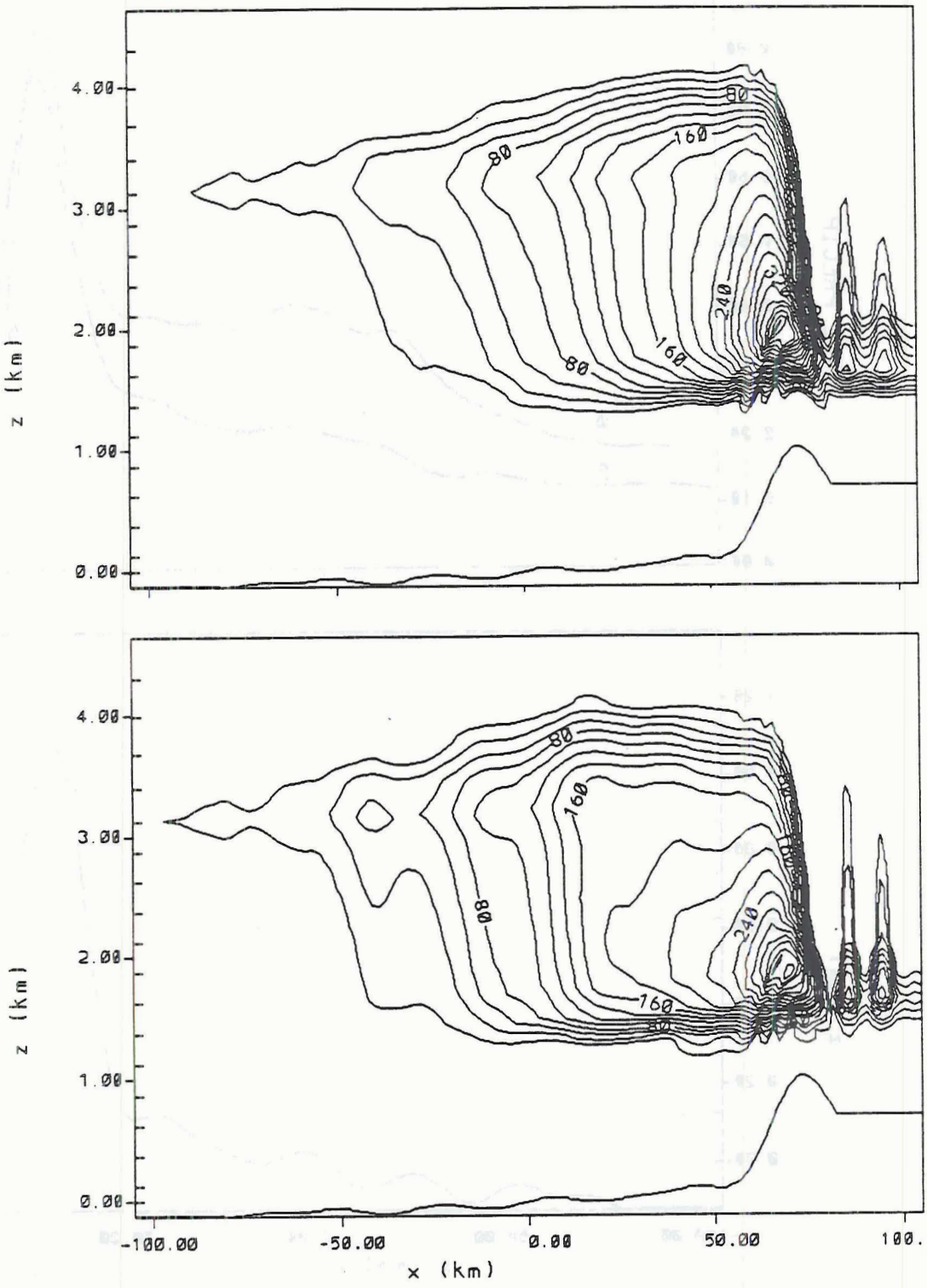

Figure 93. Cloud liquid water at 2 hours for both the no decoupled flow case (top) and the decoupled flow case (bottom). Microphysics and precipitation had not been turned on. Units are 10^{-3} g kg^{-1}.

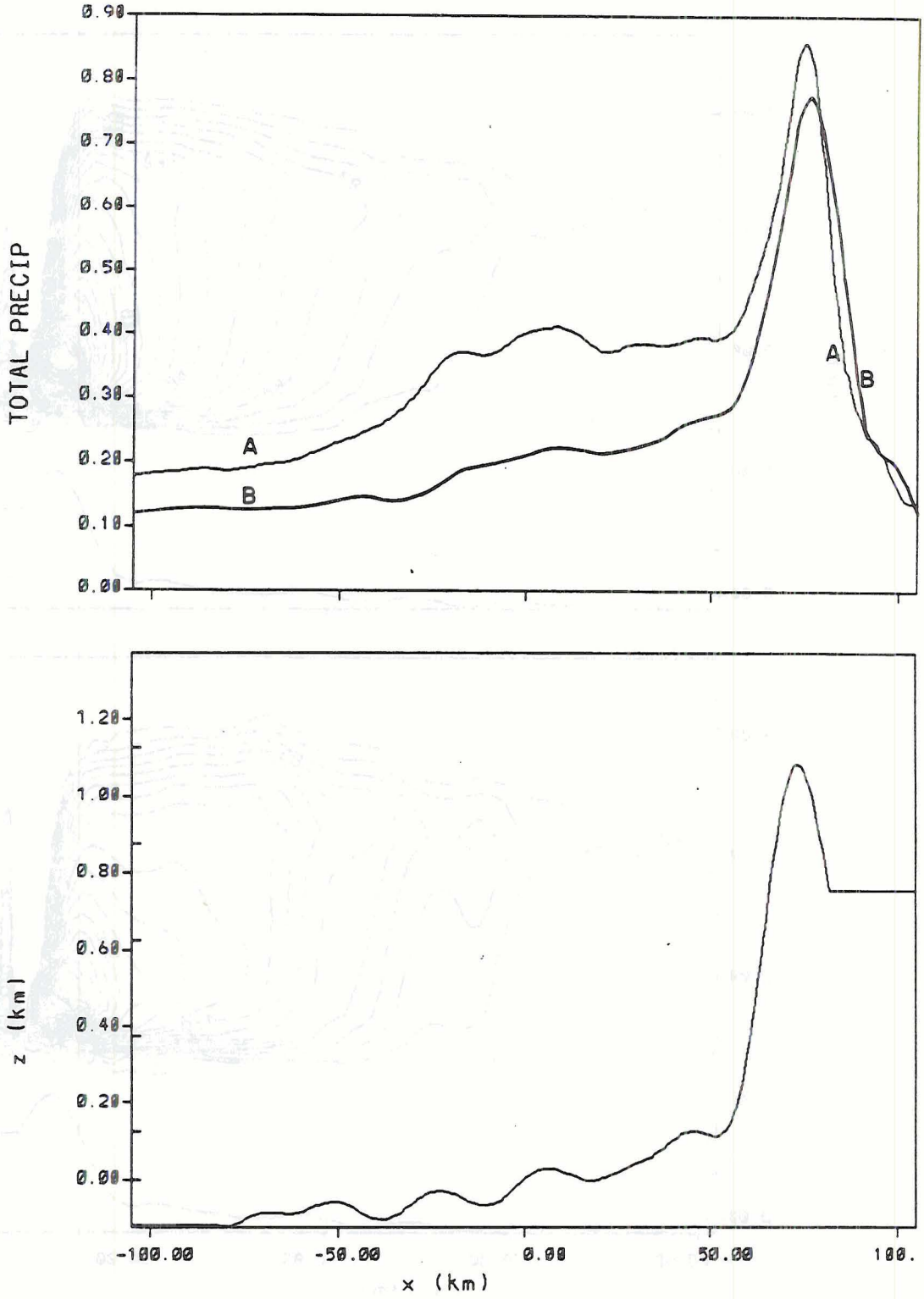

Figure 94. Total precipitation (top) at 4½ hours (2½ hours of full microphysics) for both the decoupled flow case (A) and the no decoupled flow case (B) in cm water equivalence. The bottom chart is the topography.

7.4 Discussion

It was shown in Chapter 6 that during extensive low-level decoupled flow, lift occurs farther upstream of the barrier and a higher percentage of precipitation is farther upstream of the barrier than would occur with little decoupled flow. The simulated features with the model agree with these observations. The results described in Chapter 6 could indicate that during conditions of extensive low-level decoupled flow, major orographic lift did not occur right at the barrier. However, these results could not correlate lift within the cloud with the westward length of decoupled flow. Here the model provides assistance.

The model results indicates that significant lift does occur above the upwind edge of region of decoupled flow using 0 to 2 ms^{-1} surface observations as a cutoff value for the definition of low-level decoupled flow. However, this lift is not confined to a small area as if the region of low-level decoupled flow was a solid extension of the mountain. Instead it is a large, diffuse area as the oncoming flow decelerates, converges, and is forced to rise.

Another significant feature of the model output is the increase in precipitation in the decoupled flow case over the no decoupled flow case. Since barrier height, cloud level winds, and moisture were the same for both cases, the increase in precipitation must have been caused by an increase in precipitation efficiency. The presence of low-level decoupled flow moving the location of condensate production farther upstream could increase the precipitation efficiency by increasing the time scale for particle growth.

8. Summary and Conclusions

The objective of this research was to examine the effect of low-level decoupled flow on winter orographic storms. This was accomplished by first examining 1½ months of precipitation and wind data from the 24 station PROBE mesonetwork, followed by case study analysis that supplemented PROBE data with data from cloud physics instrumented aircraft, and finally numerical simulations using a 2-D version of RAMS.

Analysis of 1½ months of PROBE data indicated that during this period precipitation was shifted upstream during events with large magnitudes of low-level decoupled flow. Other results include: precipitation was heaviest with shortest lengths of decoupled flow and lightest at the longest distances; precipitation intensity varied significantly with synoptic classifications and so did the degree of low-level decoupled flow with certain synoptic classifications producing small degrees of low-level decoupled flow while others favored production of large distances of decoupled flow; there was a 25% diurnal variation in precipitation which was much lower than that found in some other regions of Colorado by other researchers; and there was no significant diurnal variation in the length of decoupled flow during storm events probably because extensive cloud cover reduced surface radiative cooling.

Case study analysis also found the upwind shift in precipitation during conditions of large extents of low-level decoupled flow. Furthermore, during decoupled flow conditions, no significant lift

occurred just upwind of the barrier crest while this was the location of major lift in the case with a small region of low-level decoupled flow.

Numerical simulations also showed an upwind shift in precipitation in the decoupled flow case. In addition, the decoupled flow case showed a large region of light vertical velocity well upstream of the barrier which was not present in the no decoupled flow case while the no decoupled flow case had very strong vertical velocities right at the barrier which were not present in the decoupled flow case. The numerical simulation with low-level decoupled flow also showed significantly higher precipitation amounts than the no decoupled flow simulation which is consistent with greater time being available for particle growth.

The conclusions drawn from these results are that during conditions of extensive decoupled flow, part of the orographic lift is experienced well upstream of the mountain barrier as the oncoming flow decelerates into the region of low-level decoupled flow which causes convergence and lift. This results in an upwind shift in location of condensate formation which in turn shifts precipitation upstream. Though precipitation efficiency was examined only in the modeling part of this research, the results indicate that extensive low-level decoupled flow could increase precipitation efficiency and therefore be a criteria in a cloud seeding strategy. For example, less condensate production right at the barrier crest during cases with large extents of low-level decoupled flow may decrease the need for additional ice nuclei to absorb cloud liquid water produced there.

9. Suggestions for Future Research

As with many research projects, answering one question raises a couple more. Here are a few suggestions for future research:

- An observational study of the effect of low-level decoupled flow on precipitation efficiency. A good data source for this study would be the 29 rawinsondes launched downwind at Hebron during COSE III that were timed to correspond with an upwind rawinsonde launched at Craig.

- Examine the effect of low-level decoupled flow on other orographic phenomena. The two numerical simulations described in Chapter 7 indicated that the lee waves during the decoupled flow case were significantly different than the lee waves in the no decoupled flow case. If low-level decoupled flow upwind of a mountain barrier can change the trajectories of air parcels in a way which has an effect on lee waves, it might also have an effect on lee cyclogenesis. Both of which could be evaluated via numerical simulations.

- Examine the nature of cold frontal passage through a mountainous area. This could involve numerical simulations, case study analysis, and/or a climatological approach. Frontal passages were tracked through the COSE III research area on a real time basis with the PROBE mesonetwork. The PROBE data with temperature, pressure, relative humidity, and precipitation on a 15 minute basis over a broad range of elevations may provide interesting insights into the structure of cold fronts in mountains. A climatological approach could use a time ordinate with a 0 point when the front was right over a specific station.

10. References

Aerovironment, Inc.: Acoustic Radar... Applications and Interpretation of Records, An Information Booklet. Aerovironment, Inc., Pasadena, CA. 14 pp.

Aerovironment, Inc.: Monostatic Acoustic Radar. Aerovironment, Inc., Pasadena, CA. 66 pp.

Bader, David C., 1985: Mesoscale Boundary Layer Development over Mountainous Terrain. Colorado State University Atmospheric Science Paper #396, 251 pp.

Banta, Robert Mason, 1982: An Observational and Numerical Study of Mountain Boundary-Layer Flow. Colorado State University Atmospheric Science Paper #350, 203 pp.

Blumenstein, Rochelle, Robert M. Rauber, Lewis O. Grant and William G. Finnegan, 1987: Application of Ice Nucleation Kinetics in Orographic Clouds. Journal of Climate and Applied Meteorology, 26, 1363-1376.

Bolton, David, 1987: The Computation of Equivalent Potential Temperature. Monthly Weather Review, 108, 1046-1053.

Brown, Edmund H. and Freeman F. Hall, Jr., 1978: Advances in Atmospheric Acoustics. Review of Geophysics and Space Physics, 16:1, 47-110.

Cacciamani, C., S.C. Nanni, T. Paccagnella, C. Scarani, F. Tampieri, and F. Trombetti, 1984: Mesoscale Interaction of Stratified Flow and Topography in the Po Valley: A Diagnostic Study. Contributions to Atmospheric Physics. 57:3, 431-439.

Cerni, Todd A., 1983: Determination of the Size and Concentration of Cloud Drops with an FSSP. Journal of Climate and Applied Meteorology. 22:8, 1346-1355.

Cooper, William A. and Clive P. R. Saunders, 1980: Winter Storms over the San Juan Mountains. Part II: Microphysical Processes. Journal of Applied Meteorology. 19:8, 927-941.

Cooper, William A. and John D. Marwitz, 1980: Winter Storms over the San Juan Mountains. Part III: Seeding Potential. Journal of Applied Meteorology, 19:8, 942-949.

Defant, Friedrich, 1951: Local Winds. Compendium of Meteorology, T. M. Malone, Ed., Boston, American Meteorological Society, pp 655-672.

DeMott, Paul J., Robert M. Rauber and Lewis O. Grant, 1986: Inferences to Ice Nucleation Mechanisms in Wintertime Orographic Cloud Systems. Submitted to Journal of the Atmospheric Sciences.

Fraser, A. B., R. C. Easter and P. V. Hobbs, 1973: A Theoretical Study of the Flow of Air and Fallout of Solid Precipitation over Mountainous Terrain, Part I: Airflow Model. Journal Atmos. Sci, 30, 801-812.

Fujita, Tetsuya, 1967: Mesoscale Aspects of Orographic Influences on Flow and Precipitation Patterns. Proceedings of the Symposium on Mountain Meteorology, June 26, 1967. Colorado State University Atmospheric Science Paper #122, 131-146.

Garratt, J. R., 1984: Some Aspects of Mesoscale Pressure Field Analysis. Aust. Met. Mag. 32, 115-122.

Garratt, J. R., W. L. Physick, R. K. Smith, and A. J. Troup, 1985: The Australian Summertime Cool Change. Part II: Mesoscale Aspects. Monthly Weather Review, 113:2, 202-223.

Garratt, J. R., 1987: Personal communication.

Grant, Lewis O., ed., 1969: Weather Modification - A Pilot Project, Appendix A. Department of Atmospheric Science, Colorado State University, 98 pp.

Grant, L. O., 1986: A Program of Federal/State/Local Cooperative Weather Modification Research Design Considerations, Part II: Transport and Dispersion of Seeding Materials. Colorado State University Publication. 75 pp.

Grant, Lewis O., 1987: Hypotheses for the Climax Wintertime Orographic Cloud Seeding Experiments. Precipitation Enhancement -- A Scientific Challenge. AMS Meteor. Monograph, 21, 105-108.

Grant, Lewis O., 1987: Personal communication.

Graw, Richard, 1988: Wintertime Local Circulations in Northwestern Colorado. MS Thesis (second draft).

Grossman, Robert L. and Dale R. Durran, 1984: Interaction of Low-Level Flow with the Western Ghat Mountains and Offshore Convection in the Summer Monsoon. Monthly Weather Review, 112, 652-672.

Han, Y.-J., K. Ueyoshi and J.W. Deardorff, 1982: Numerical Study of Terrain-Induced Mesoscale Motions in a Mixed Layer. Journal of the Atmospheric Sciences, 39, 2464-2476.

Hindman, Edward E. II, 1973: Air Currents in a Mountainous Valley Deduced from the Breakup of a Stratus Deck. Monthly Weather Review, 101:3, 195-200.

Hindman, Edward E., 1986: An Atmospheric Water Balance over a Mountain

Barrier. Journal of Climate and Meteorology, 25:2, 180-183.

Hindman, Edward E., 1986: Characteristics of Supercooled Liquid Water in Clouds at Mountaintop Sites in the Colorado Rockies. Journal of Climate and Applied Meteorology, 25:9, 1271-1279.

Hobbs, Peter V., Richard C. Easter and Allistair B. Fraser, 1973: A Theoretical Study of the Flow of Air and Fallout of Solid Precipitation over Mountainous Terrain, Part II: Microphysics. Journal Atmos. Sci., 30, 813-823.

Hoinka, Klaus P., 1987: Personal communication.

King, Clark, 1988: Personal communication.

Koch, Steven E. and John McCarthy, 1982: The Evolution of an Oklahoma Dryline. Part II: Boundary-Layer Forcing of Mesoconvective Systems. Journal of the Atmospheric Sciences, 39, 237-257.

Lee, Robert, 1981: Wintertime Cloud Systems over the Colorado Rockies: Two Case Studies. Second Conference on Mountain Meteorology, Steamboat Springs, November 9-12, 1981, 368-370.

Lettau, Heinz H., 1967: Small to Large Scale Features of Boundary Layer Structure over Mountainous Slopes. Proceedings of the Symposium on Mountain Meteorology June 26, 1967. Colorado State University Atmospheric Science Paper #122, 1-74.

Manins, P. C. and B. L. Sawford, 1982: Mesoscale Observations of Upstream Blocking. Quart. J. R. Met. Soc., 108, 427-434.

Marwitz, John D. and August H. Auer, Jr., 1968: Ice Crystal Growth by Diffusion and Accretion. Proceedings of the International Conference on Cloud Physics, 249-254.

Marwitz, John D., 1980: Winter Storms over the San Juan Mountains. Part I: Dynamical Processes. Journal of Applied Meteorology, 19:8, 913-926.

Marwitz, John D., 1988: Personal communication.

McCarthy, John and Steven E. Koch, 1982: Evolution of an Oklahoma Dryline. Part I: A Meso- and Subsynoptic- Scale Analysis. Journal of the Atmospheric Sciences, 19, 225-236.

Neff, W. D. and C. W. King, 1985: Studies of Complex-Terrain Flows Using Acoustic Remote Sensors. NOAA Publication ASCOT 85-1, 131 pp.

Orgill, Monte M., 1971: Laboratory Simulation and Field Estimates of Atmospheric Transport-Dispersion over Mountainous Terrain. Colorado State University Dissertation, 302 pp.

Pierrehumbert, R. T., and B. Wyman, 1985: Upstream Effects of Mesoscale

Mountains. Journal of the Atmospheric Sciences, 42:10, 977-1003.

Rauber, Robert M. and Lewis O. Grant, 1982: COSE III Operation Log. Colorado State University Atmospheric Science Publication, 444 pp.

Rauber, Robert M., 1985: Physical Structure of Northern Colorado River Basin Cloud Systems. Colorado State University Atmospheric Science Paper #390. 362 pp.

Rauber, Robert M., Lewis O. Grant, and DaXiong Feng, 1986: The Characteristics and Distribution of Cloud Water over the Mountains of Northern Colorado during Wintertime Storms. Part I: Temporal Variations. Journal of Climate and Applied Meteorology, 25:4, 468-486.

Rauber, Robert M. and Lewis O. Grant, 1986: The Characteristics and Distribution of Cloud Water over the Mountains of Northern Colorado during Wintertime Storms. Part II: Spatial Distribution and Microphysical Characteristics. Journal of Climate and Applied Meteorology, 25:4, 489-504.

Rauber, Robert M., 1987: Characteristics of Cloud Ice and Precipitation during Wintertime Storms over the Mountains of Northern Colorado. Journal of Climate and Applied Meteorology, 26:4, 488-524.

Reid, John D., 1976: Dispersion in a Mountainous Environment. Colorado State University Atmospheric Science Paper #253, 150 pp.

Rilling, Robert, 1989: Personal communication.

Rogers, David C. and Gabor Vali, 1987: Ice Crystal Production by Mountain Surfaces. Journal of Climate and Applied Meteorology, 26:9, 1152-1168.

Rogers, David, 1987: Personal communication.

Ross, D. G., I. N. Smith, P. C. Manins, and D. G. Fox, 1988: Diagnostic Wind Field Modeling for Complex Terrain: Model Development and Testing. Journal of Applied Meteorology, 27, 785-796.

Schoenberg, Sally Ann, 1983. Regional Wind Patterns of the Inland Waters of Western Washington and Southern British Columbia. NOAA Technical Memorandum ERL PMEL-43, 61 pp.

Tan, Kapin and Verne Leverson, 1980: The Effect of Dynamic Blocking on the Formation of Stagnant Air in Mountain Terrain. Presented at the Second Joint Conference on Applications of Air Pollution Meteorology. 4 pp.

Tan, Kapin and Verne H. Leverson, 1981: Airflow and Plume Dispersion in Complex Terrain under Stable Atmospheric Condition. Fifth Symposium on Turbulence, Diffusion, and Air Pollution. Pp 234-235.

Uttal, Taneil, Robert Rauber, and Lewis O. Grant, 1985: Trajectories of Ice Crystals through the Upper Levels of an Orographic Cloud and Resulting Calculations of Ice Mass in the Cloud. Proceedings of the Fourth Scientific Conference on Weather Modification. 6 pp.

Uttal, Taneil, 1985: Distribution of Liquid, Vapor, and Ice in a Phase Budget of a Colorado Orographic Cloud Systems. Colorado State Atmospheric Science Paper #388, 97 pp.

Whiteman, C. David, 1980: Breakup of Temperature Inversions in Colorado Mountain Valleys. Colorado State University Atmospheric Science Paper #328. 250 pp.

Yu, Chang-Han and Roger Pielke, 1986: Mesoscale Air Quality under Stagnant Synoptic Cold Season Conditions in the Lake Powell Area. Atmospheric Environment, 20:9, 1751-1762.